Technical Report No. 174

# EXPERIMENTAL ERROR AND SIGNAL DATA FROM HIGH BIT RATE TACTICAL TROPOSCATTER DIGITAL COMMUNICATION LINK

by

M. P. Ristenbatt
E. P. Gould

COOLEY ELECTRONICS LABORATORY

Department of Electrical Engineering
The University of Michigan
Ann Arbor, Michigan

Contract No. DA-36-039-sc-89168
U. S. Army Electronics Command
Fort Monmouth, New Jersey 07703

April 1966

## ACKNOWLEDGEMENTS

The authors gratefully acknowledge the work of Mr. Alan Collins, who did the original computer programming for the data analysis. Also, credit is due Mr. Irvin Kullback and his associates at the Radio Relay and Tropospheric Equipment Group of USAEL for the operation of the link during these tests, and for supplying technical and calibration information about the link.

TABLE OF CONTENTS

TABLE OF CONTENTS (Cont.)

LIST OF ILLUSTRATIONS

LIST OF ILLUSTRATIONS (Cont.)

LIST OF ILLUSTRATIONS (Cont.)

## LIST OF TABLES

## ABSTRACT

This report describes experimental error and signal data from a 100 mile troposcatter digital communication link at a bit rate of 576 kc. A repetitive one-zero pattern with binary FM was used at 4.8 kMc. Data were taken in each of the four seasons, recording 10 to 15 six-minute tapes per season.

The objective was a detailed computer analysis of error behavior, including analysis of instantaneous signal behavior so as to describe system conditions during errors. Five signals were sampled and multiplexed directly onto a digital tape: AGC, Combiner, Channel A, Channel B, and local Error Count.

It was found that the single channel signal distributions were grossly Rayleigh, and that deviations from Rayleigh appear to be due to specular fading. Various statistical error results were derived. Without specular fading, the errors tend to occur in single bursts, associated with signal fades. With specular fading groups of error bursts tend to occur. For the data here 90 percent of the error-runs are less than 0.4 millisecond in length. Ninety percent of the intervening error-free runs were greater than 30 milliseconds for the poorest $P_E$ encountered. ($P_E = 1.39 \times 10^{-3}$). The probability of achieving a diversity fade 10 db below the median for a time greater than 100 milliseconds, in an interval of 8 hours, is about $1.4 \times 10^{-2}$. This indicates that fading margins of 10 to 15 db and equipment that can tolerate fade lengths of 100 milliseconds or more should yield successful synchronization.

From the equipment point of view, increases in tolerable fade length do not appear profitable until one exceeds 30 to 50 milliseconds. Further increases sharply reduce the probability of encountering such fades.

Finally, the results verified that there is little signal variation from season to season except varying median level.

In general, the data analyzed here permit determining the requirements for synchronization circuits of the fading link. In addition, the data here serve an indicator of what can be expected with 100 mile troposcatter links at a bit rate of 576 kc.

# I. INTRODUCTION

Because of the ever increasing demand for communication of digital information, troposcatter is being tested with digital signals at increasingly higher bit rates. As is well known, a troposcatter link provides a reliable link for distances between 50 and about 500 miles. Although a troposcatter link requires relatively high power, its transmission is usually more persistent and reliable than that of an ionospheric reflection link (Ref. 1).

In dealing with a digital communication system, it is necessary to determine two related but separate issues: (1) the probability of error assuming that the system is synchronized, and (2) the effect of the channel conditions on synchronization. Much of the classical theory dealing with the probability of error assumes that the system is synchronized. In a time multiplexed digital system there are two levels of synchronization: (1) the bit synchronization, and (2) the frame synchronization. Under poor channel circumstances (such as fading), the frame synchronization is the more difficult problem. If frame synchronization is temporarily lost, the search procedure necessary to re-establish frame sync amounts to an error extension of the original channel errors.

This error extension caused by frame sync "search" has been a source of difficulty during attempts to operate a time division multiplexed PCM train over an experimental troposcatter link (Ref. 2). It was, therefore, decided to make a detailed study of the error run characteristics of the experimental troposcatter link. A primary objective of this study is to ascertain the timing circuit requirements for successful handling of the frame sync (and bit sync) situation during signal fades. An additional, immediate motive is to contribute whatever possible to an understanding of the causes of the errors on a typical (tactical) high data-rate troposcatter link. For both of these reasons, then, experimental data were taken on the Tobyhanna, Pennsylvania-to-Fort Monmouth, New Jersey link.

Historically, troposcatter links have largely used analog modulations. A number of operational troposcatter links exist and typically use either FM modulation or single sideband (SSB). Although much is known about the use of the troposcatter link with analog signals (Refs. 3 and 4), relatively little information is available on the behavior of troposcatter links for digital signals.

Two recent theoretical studies of the digital troposcatter are reported in Refs. 5 and 15. A primary issue in both of these is to account for the selective fading, in addition to the flat Rayleigh fading, at the higher bit rates. These studies seek to establish the maximum rate at which digital signals can be sent over troposcatter, in terms of basic propagation properties. Reference 5 describes the limit in terms of linear delay distortion, whereas Ref. 15 expresses the limit in terms of the correlation bandwidth.

When digital communication links are tested, the signal measurements and the probability of error ($P_E$) measurements are often made separately because the signal data occur continuously while the error data occur only sporadically (and infrequently). However, to analyze the causes of the particular error behavior, it is necessary to interlock the signal and the error data. Data interlock was accomplished here by directly multiplexing the signal and error data on a digital tape. This interlock permits investigating the relation between the particular signal behavior and error behavior. The digital tape containing the multiplexed signals is analyzed directly on a digital computer without any intermediate signal processing.

The objective of this report is to present the results of the data taken on this link for the purpose described. The major features of the data have been plotted and curves will be shown herein. A predecessor report (Ref. 13) describes the data acquisition equipment and partial results from the first data run. It is hoped that the results here will be of interest to anyone studying the use of troposcatter links for digital communications. Although each link is somewhat unique, certain basic phenomena can be expected to be similar on all links.

The experimental results discussed in this report were taken from the experimental 100 mile digital troposcatter link which is operated by the Radio Relay Branch of USAEL. The 100 mile link is representative for tactical applications (a strategic link may be 300 to 500 miles long). The link has a bit rate of 576,000 bits per second and uses binary FM at a radio frequency of 4.8 kMc with space (dual) diversity. The data recorded consisted of multiplexing an amplitude sample from each of the two diversity receivers, an amplitude sample from either the combined signal or the AGC signal, and a sample indicating the instantaneous error count. These four signals were directly recorded on a digital tape and then analyzed on a digital computer.

The link being studied is unique in that it has the relatively high bit rate of 576,000 bits per second. Also, the RF frequency of 4.8 kMc is relatively high for tropo. In addition, the direct digital recording of the multiplexed data permits keeping the signal and error data related in time.

The data to be reported here were taken at four separate time intervals: April 1964, July-August 1964, November 1964 and February 1965. During each of these data periods the data were recorded, over a few days time, and in basic sections of 6-minute digital tapes. Our total data then consisted of about 10 tapes from each of the four data periods. We edited the total set of tapes and conducted some analysis on about 24 tapes. About one-half of these were subjected to detailed analysis, and these are the tapes that will be described in this report.

Before describing the results of the data, we will quickly review the data acquisition method. Basically this method entails the recording of the data directly on a digital tape for immediate access to the digital computer. This interlocks all the data so that various studies can be made on the computer.

Since the predecessor report (Ref. 13) describes the instrumentation in some detail, we will here synopsize, and only repeat that which appears necessary for convenience. Any further details can be found in the previous report.

## II. DESCRIPTION OF LINK AND DATA ACQUISITION EQUIPMENT

In this section we will describe the link over which the data were taken and the data acquisition equipment.

### 2. 1 Description of Link

The digital troposcatter link is operated between Tobyhanna, Pennsylvania and the Hexagon at Fort Monmouth, New Jersey by the U. S. Army Electronics Laboratory. The total distance is about 100 miles. The signal for these tests is a repetitive 1010-train[1] at 576,000 bits per second. Binary frequency modulation is used with a peak-to-peak deviation of 750 kc. Dual space diversity combining is accomplished with an equal gain predetection diversity combiner. The antennas are spaced 40 feet or 200 wavelengths apart (center-to-center) and consist of 15-foot parabolic dishes. The transmitter power is 1 kilowatt with an RF frequency of 4. 8 kMc. The receiver I. F. bandwidth is approximately 1 megacycle. A profile chart of this particular link is shown in Fig. 2. 1 (furnished by the Radio Relay Branch of USAEL). As noted, the transmitter site is on a mountain at an altitude of 2210 feet above sea level. The receiver is on the roof of the Hexagon Building at Fort Monmouth, at an altitude of 168 feet above sea level. There are two major obstructions in the path occurring at heights of 2000 and 1500 feet. The antenna beams are set to graze these obstructions for maximum received signal. The scattering angle is estimated to be 0. 674 degrees.

According to the Radio Relay Branch, the path loss on this link exceeds the predicted path loss figure (Ref. 6). This causes the link operation to be unsatisfactory at the poorer times in the year (winter).

---

[1] Using such a simple modulation has the advantage that the synchronization reduces to solely bit synchronization. When a more realistic digital modulation is used (such as a pseudo-random sequence) the performance of the synchronization circuits affect the error-behavior.

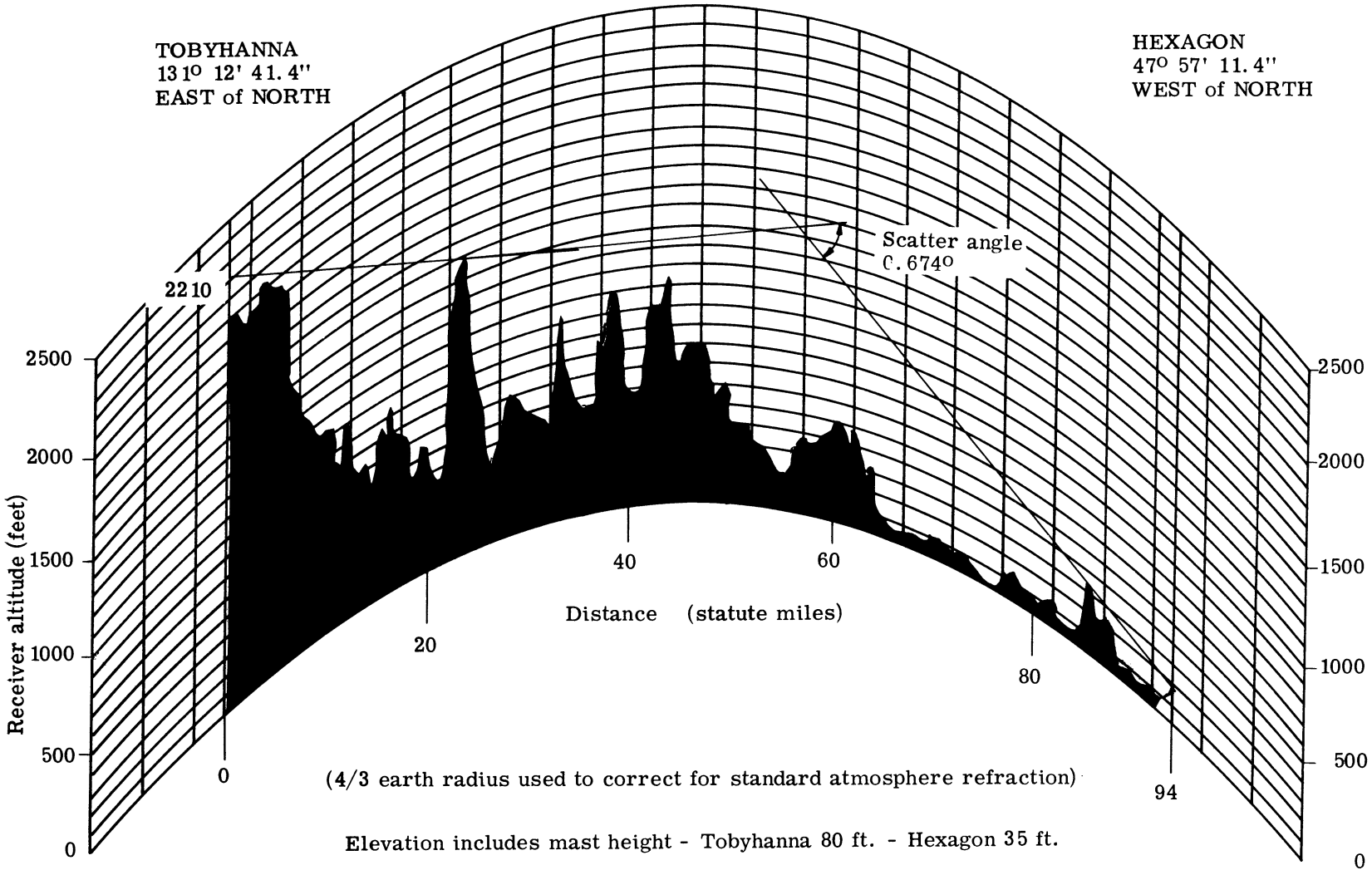


Fig. 2. 1. Profile chart.

## 2.2 Description of Data Acquisition Equipment

Figure 2.2 is a block diagram of the equipment used to acquire the data described below. The troposcatter link receiver detects the alternating 1010-modulation pattern with an FM discriminator and produces a (PCM) video signal. This video signal is sent to an error detection system supplied by USAEL and built by RCA (Ref. 7). The continuous signal strength measurements are obtained directly from the receiver by first using a log-linear amplifier (at IF) for a suitable compression characteristic and then detecting the output. In the April and July tests, the combiner signal was used to measure the effective power resulting from the two diversity channels. This "combiner" signal strength, measured by a linear amplifier, is obtained directly at the output of the combiner before entering the AGC amplifier. In the November and February data, we recorded both the combiner and the AGC signal, as measures of the total effective power.

In the first test (April) we used an error detection signal which was already available on the terminal receiver, called "bit error test point." While trying to calibrate the error-count (during "no signal") we noted three actions in the (terminal) error detection circuitry that needed improvement. It was determined that under poor S/N conditions, noise spikes were saturating the front end of the error detection circuitry. A silicon diode clipping circuit was installed to reduce these noise spikes.

The second change was made in the multivibrator circuit. It was determined that the multivibrator did not have a sufficient recovery time when changing from an error to a no error condition. A silicon diode was installed in the base circuit to provide a low resistance recovery path for the multivibrator circuit.

Although these changes probably had little effect on the overall average error rate, they should cause the error and error free run lengths to be more accurate than before.

Along with these changes, we took the error signal from an earlier point (TP3) on the terminal error detection chassis. We then processed this signal subsequently with digital equipment. This replaced analog operations, which permitted some distortion of error run statistics, between TP3 and the "bit error test point."

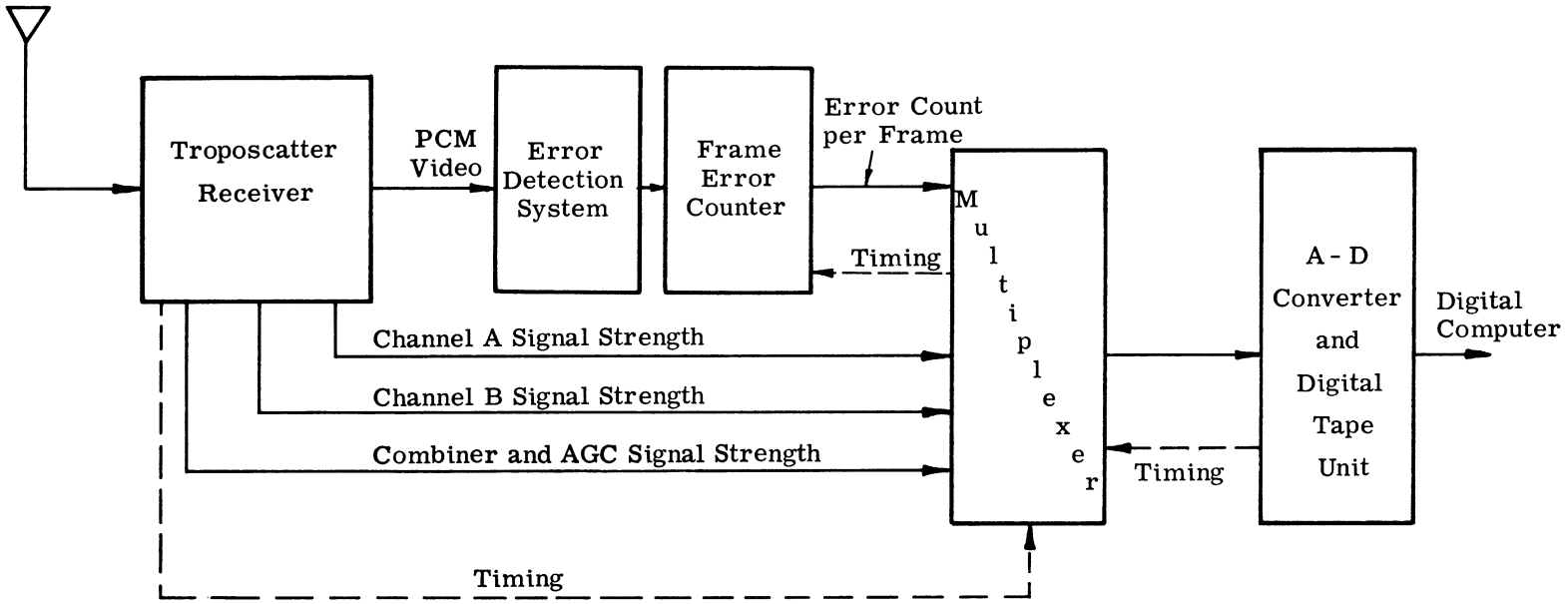


Fig. 2. 2. Block diagram of data acquisition equipment.

All of these changes were made before the July tests, so that only the April data were recorded without the changes. The operations of frame error counting, timing, multiplexing, and recording the four signals were performed with CEL specially-devised equipment (see Fig. 2. 2).

This equipment was described in the predecessor report (Ref. 13). The changes that were made since the previous report time (Ref. 13) are described in Appendix A. For convenience we will here synopsize the operation of this data acquisition equipment. Any detailed information is available in Appendix A or in the predecessor report (Ref. 13).

The basic timing is established by our digital recording rate of 41, 142 characters per second, with 6 lateral bits per character. We quantized each of the four signals into 64 levels (6 bit), and sampled each signal about 10, 285 samples per second.

Measurement of the signal strengths was achieved simply by sampling at the correct time. For the error measurement, we counted the errors during a "frame" corresponding to a sample time. At a 576, 000-signal bit rate, a frame time of about 0. 1 millisecond (10. 285 samples/second) specified 56 bits per frame. The error count within such contiguous frames was obtained by forming a shift-register counter, and feeding a D-A converter (labeled Frame Error Counter in Fig. 2. 2).

The timing for all these operations represented an intricate problem. The sampling times had to be coordinated with the frame error counting and resetting. The timing equipment and the frame error counting system were formed with commercial digital data blocks.

The multiplexer-A/D converter (with its internal timing) was accomplished with equipment built to our specifications by Raytheon Company. The digital tape unit is an IBM 729 II. This multiplexer, an A-D converter-tape recorder combination, is a general facility which we use to interface between various physical experiments and the digital computer. This entire complex represents a typical instrumentation which must be accomplished when using the A-D converter and digital tape unit with real-time physical experiments.

With the use of this direct recording technique, we are able to retain the time relation between instantaneous signal behavior and short-term error behavior. Also, this direct-access-to-computer method avoids some of the operational problems associated with usual data processing systems.

2.2.1 Timing Considerations. For some purposes, it is desirable to have a record of whether each particular transmitted bit is received correctly or is in error. This is not possible in real time since the bit rate of the troposcatter link is 576 kilobits per second, while the maximum tape writing speed of the A-D/tape unit is only 41.667 kc. This is the basic reason for dividing the data into "frames" of bits, and then noting the number of bit errors that occur in a particular frame.

In the four (data)-channel situation one is restricted to a character rate of 10,417 (41,667/4) with 6 bits per signal. Grouping the bits into 56 bit frames yields a character rate of 576 kc/56 or 10,285 characters (samples) per second per signal for a total of 41,142 characters per second. Although slightly different from the standard IBM clock rate, this bit rate is within the reading tolerance of the IBM unit.

For the two (data)-channel case,[2] where the number of errors per frame is recorded along with the signal strength of the only input channel, the frame size is 28 bits per frame. Further, it is possible to record only the number of bits in error per frame; then the frame size is reduced to the smallest frame size (14 bits) possible with this equipment.

2.2.2 Auxiliary Signals. As noted above, auxiliary information is recorded on the behavior of the troposcatter link at the time of the frame error count. With the link operating in a dual-diversity mode, the input signal strength of each input channel and the signal strength of the combined and AGC signal are recorded to provide the mose useful auxiliary data. In the single channel mode, the most useful auxiliary data are provided by recording the signal strength of the only operating channel.

The signal strength measurements were taken at test points within the troposcatter receiver. Figure 2.3 is a block diagram showing the points at which the test signals were taken. The signals which are tapped from the mixer preamplifier output are put through a log-linear amplifier which compresses (or compands) the output axis of the voltage. This is required on the single channel signals since there is a wide variation in the signal strength during the fading.

---

[2]The two channel case occurs when we eliminated the diversity, and operated the receiver as a single channel receiver. By recording a single channel case directly before (or after) a diversity case, one can estimate the error improvement afforded by the diversity.

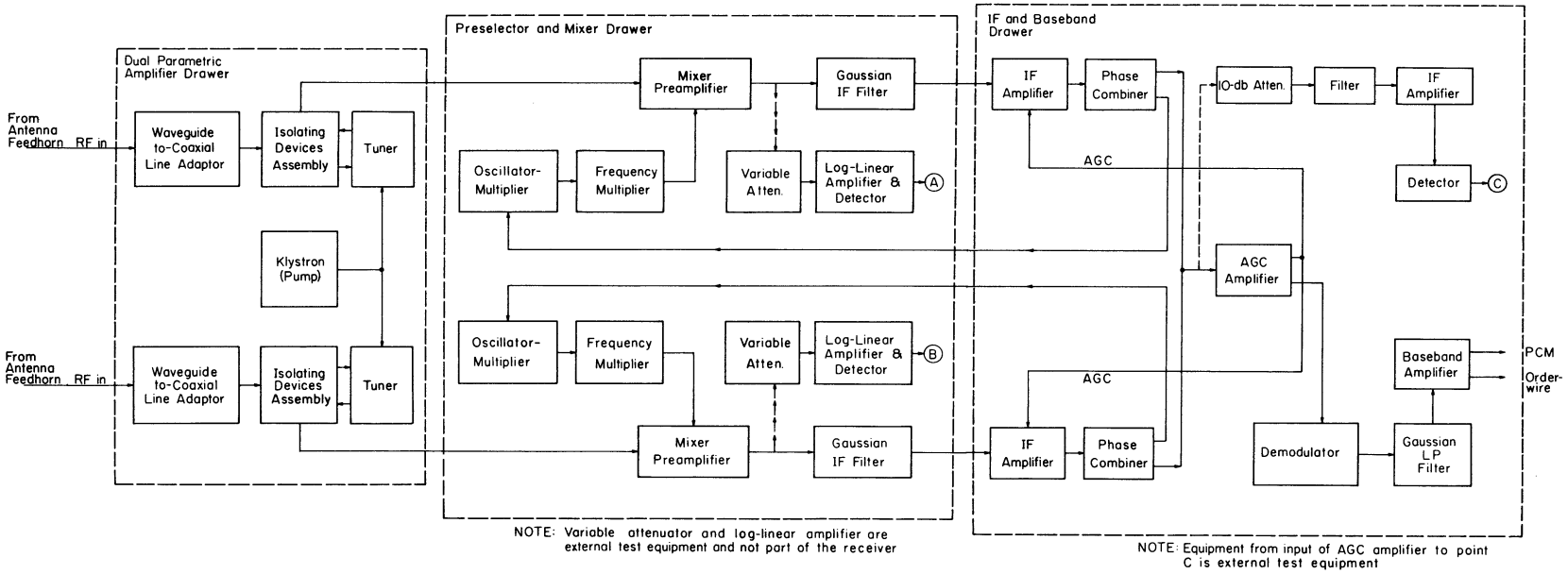


Fig. 2.3. Block diagram of troposcatter diversity receiver.

The combined signal output is taken from the output of the phase combiner as shown in Fig. 2.3. This test signal is put through an IF amplifier and then detected. The AGC signal is taken at the output of the AGC amplifier.

Using calibration curves for the outputs of the log-linear amplifiers, we can relate the signal strength to the analog sample value which is sampled by the multiplexer of Fig. 2.2. The only remaining processing needed on these signals is a variable gain analog amplifier which adjusts the signals so that they use the total range of the A-D converter. We used operational amplifiers for this function and achieved the variable gain by changing the ratio of feedback resistance to input resistance (see Appendix A and Ref. 13).

2.2.3 Frame Error Counter. Since all measured auxiliary signals could be placed directly into the multiplexer of the A-D/tape equipment, we decided to process the number of errors per frame so that it also could be placed directly into a channel of the multiplexer. A method was devised that would convert the number of incoming bit error pulses per frame to an analog voltage level directly proportional to the number of bit errors per frame.

The way in which the error count is formed, and the timing with which this error count is sampled along with the other signals are indicated in Fig. A.1 of Appendix A. The reader is referred to Appendix A for any further description of the equipment.

## III. DESCRIPTION OF DATA AND DATA ANALYSIS

In this section we will describe the range of data that was taken, followed by a description of the data analysis which was performed on the digital computer. We will present a table summarizing the crucial aspects of all the data which were analyzed.

### 3.1 Overall Data Conditions

As mentioned, we took data over a period of a few days at four separate times. The data sessions were chosen to obtain data in each of the four seasons. The data were taken early in April 1964 (called TPA data), the first few days in August, 1964 (which we call TPJ data, and generally, refer to as July data), mid-November, 1964 (called TPN data) and mid-February, 1965 (called TPF data). It was a desired objective to see if the four data from the different seasons were sufficiently different so as to affect the synchronization requirements.

The use of four separate testing periods also permitted us to solve some initial problems, both in the terminal equipment and in our data acquisition equipment. In general, every effort was made to take advantage of any new knowledge gained as we went along. Thus, we effected improvements in the terminal error detection circuitry after the April tests (as noted in the previous chapter). Other improvements, especially in the area of calibration techniques and suppression of severe ground loop noise, were effected.

For these reasons, it should be emphasized that the conditions under which the data were taken improved as the series proceeded. We will, therefore, rely heavily on the last two test series (November-TPN and February-TPF), especially for the quantitative fade results.

Two areas warrant discussion here: the calibration procedure and the ground loop noise. In the calibration issue, we at first had difficulty getting accurate measures of the "effective" power from the diversity (two-channel) receiver. Initially, we considered using either the AGC signal or the direct combiner signal. The AGC signal saturates at low input power, so that this measure looses accuracy during the deep fades (where the errors occur

and where our main interest lies). The direct combiner signal, on the other hand, has in series with it the varying gain of the IF amplifier (controlled by the AGC signal). Thus, its sensitivity to varying input effective power is reduced by the changing IF gain. When the IF gain saturates, however, at the very low powers, the combiner signal should then be sensitive to varying power.

We initially reasoned that the low power area was of most interest, and after a discussion with the USAEL people, we used the combiner signal for the diversity-power measurement in both the April 1964 and July 1964 tests. When it became apparent that we could not get accurate mean (or median) signal levels using the combiner signal (because of the reduced sensitivity in the normal signal range), we recorded both the AGC signal and the combiner signal in the November 1964 and February 1965 tests. When using the AGC signal calibration we got good agreement between the single channel means and the diversity-receiver mean.

Also, during the first two tests it became apparent that there was sufficient drift in the various terminal equipment to require taking a calibration during each half-day of testing. We, therefore, did this during the November (TPN) and February (TPF) tests.

Another change effected in the November (TPN) and February (TPF) tests was to add a 60 cps notch filter (and a low-pass filter) to the three analog signals. We found that there was severe ground loop noise (which changed with time) in the room in which the data were recorded. It is primarily for this reason that we rely on the TPN and TPF data for the fade data.

In addition to recording "normal operation" data, we recorded some data under single channel operation. This permits obtaining an experimental value of the diversity improvement, by comparing the error-behavior in the single channel case at a given mean with the behavior of the diversity case at the same mean.

We also recorded some data at reduced power; however we did not analyze in detail any of these tapes because of the lack of time. Initially, we recorded some data with the receiver parametric amplifiers turned off; we later decided that the proper way to obtain a reduced signal-to-noise situation was to reduce the transmitter power (as above).

We will now summarize the data situation for each of the test periods. Pictures of the multiplexed signals will show how the signals tended to behave, especially when causing errors.

3.1.1 April, 1964 Data (TPA). The first attempt at taking data was made on April 2 and 3, 1964. Because of difficulty in getting agreement between the error count from the computer run and the error count taken at test site, we returned on April 10 and recorded another set of data.

The data recorded in this TPA series showed moderate power levels. The 6 minute probability of error varied from a high of $1.46 \times 10^{-4}$ to a low of $3.5 \times 10^{-5}$. Pictures of the multiplexed signals are shown in Figs. 3.1 and 3.2. Table 3.1 shows the averaged error data for four separate (6 minute) tapes. The average $P_E$ for the four tapes is $5.5 \times 10^{-4}$. This value is commensurate with the previous error experience for an April afternoon (Ref. 14).

| Label | $P_E$ | Time | Estimated % Airplane Interference |
|---|---|---|---|
| TPA 4 | $3.5 \times 10^{-5}$ | Friday Afternoon | 28 % |
| TPA 6 | $4.46 \times 10^{-4}$ | Thursday Morning | --- |
| TPA 8 | $2.68 \times 10^{-4}$ | Thursday Afternoon 2:20 p. m. | 7.4 % |
| TPA10 | $1.46 \times 10^{-4}$ | Thursday Afternoon 4:45 p. m. | 16 % |

Table 3.1. Average Error Rate April 9 or 10, 1964.

We will see throughout this report that the specular fading caused by airplanes is a major factor in determining the error behavior. The specular fading has two contradictory roles: 1) it increases the mean signal level during the time that the reflector is within the common volume, and 2) it causes severe fading during the time that the reflector either passes near or enters (or leaves) the common volume.

TPA8, Thursday afternoon

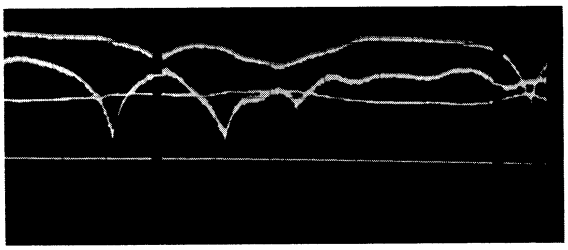

a) (105) Typical signal behavior

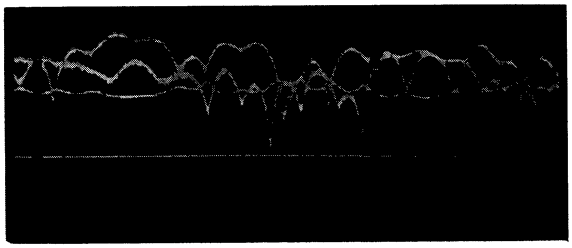

b) (268) Fast moving signal

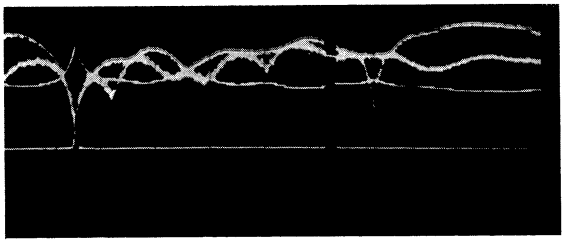

c) (53) Errors at deep fade

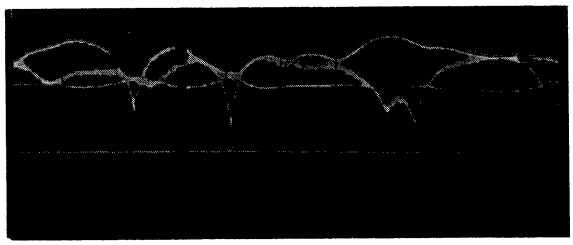

d) (180) Errors at a fade

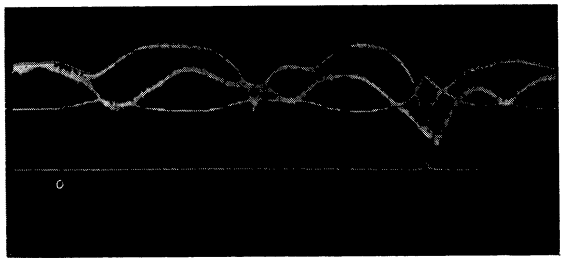

e) (209) Errors at a fade

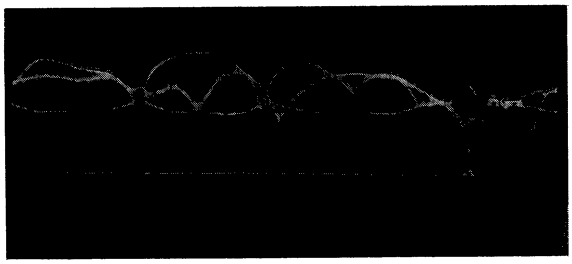

f) (472) Errors at a fade

*Time axis is 0. 1 second per centimeter.

Fig. 3. 1. Selected samples from TPA8, August Thursday afternoon tape.

TPA4, Friday afternoon

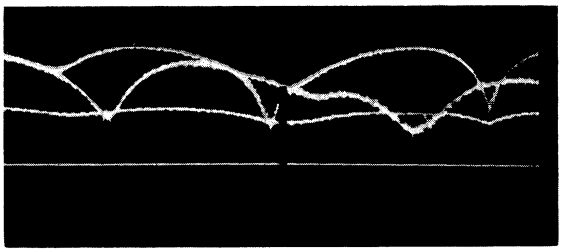

a) Record 182 - normal fading

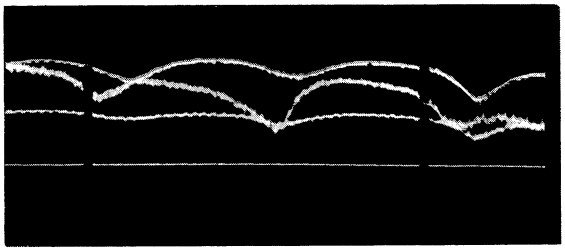

b) Record 488 - normal fading

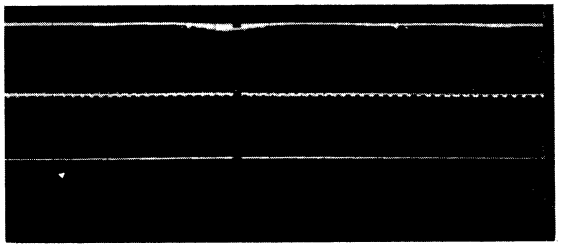

c) (273) - Signal saturation with airplane in common volume

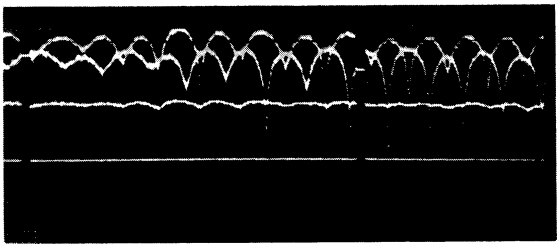

d) (288) - Airplane leaving common volume

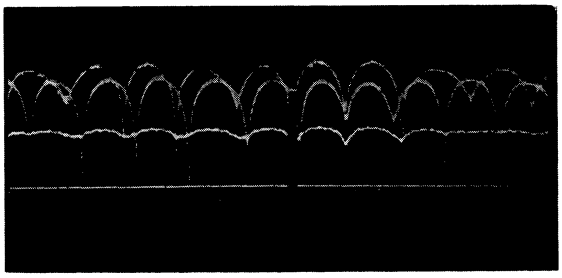

e) (7) - Additional spectral fading

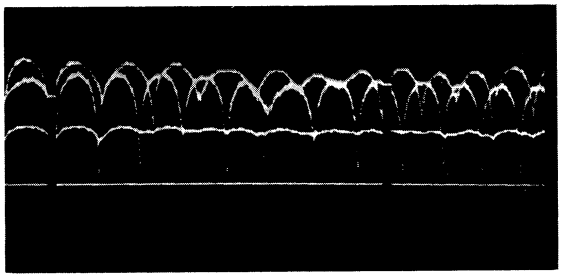

f) (377) - Additional spectral behavior

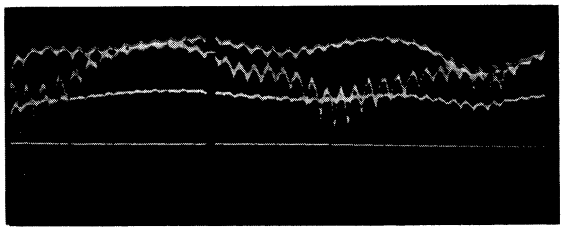

g) (104) - Spectral behavior when airplane is distant

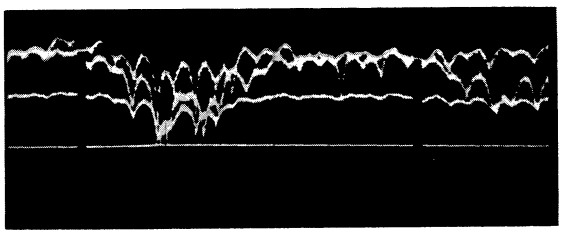

h) (305) - Errors occurring with airplane in distance

Fig. 3.2. Selected samples from TPA4, August Friday afternoon tape.

If the signal level is low, then, the presence of the airplanes may not appreciably alter the total $P_E$, but it will alter the pattern of errors. A substantial number of the errors will occur during the severe specular fading--while no errors will occur while the reflector is within the common volume.

Figure 3. 1 shows selected signal samples from a Thursday afternoon tape, while Fig. 3. 2 shows samples from a Friday afternoon tape. In Fig. 3. 1 the relatively rapid graphs are channel A and channel B, while the relatively constant (lower) graph is the AGC signal. We used the AGC for a few tapes in April; usually the combiner was used. The error counts appear as vertical samples above the lower line. A high sample means a high error count (out of 56). From Fig. 3. 1 e) and f), it can be seen that the errors usually form a triangular-type pattern. At first the count is low, then it increases as the fade deepens. The reverse occurs as the signal recovers from the fade.

Figure 3. 2 is especially interesting for its depiction of the specular fading caused by airplanes. The typical action is similar to g), when the airplane is distant. As it nears the common volume, it causes signals such as in d), e), and f). While in the common volume, the signal level is increased, because of the reflection (as in c), where the signals are saturated). When leaving the common volume the action is similar to that on entering.

In the absence of specular fading, the April data were characterized by long, relatively slow, fading and movements.

Although the trend for all of the signal strengths can be seen from Fig. 3. 1, it is seen that the noise is appreciable on these signals. The ripple was of two types. First of all, the 60 cycle ripple, apparently because of lack of adequate grounding of the ground cable in the USAEL tropo room; and also a 1500 cycle per second ripple which was apparently coming from a characteristic of the return transmitter in that room. In any event, this ripple on the signal strength caused us to avoid extensive level crossing analysis with either the April or the July data. The error data, however, are accurate and will be reported in the later sections.

Note that the effective diversity power in this TPA series (Fig. 3. 1) was measured by the combiner voltage. This moves in phase with the linear sum of the single channel strengths. The combiner signal is small (compared to the AGC) and we, therefore, used an

amplification of about 20 db before recording. As was noted before, the sensitivity of the combiner signal is low (in the normal signal region) because of the role of the varying IF gain.

3.1.2 July, 1964 Data (TPJ). The July data were taken on Monday and Tuesday, August 3 and 4, 1964. Although technically recorded in August, we had planned this test series for July. Since we missed July by only a few days, we continue to refer to it as July data. Since the data occurred at the juncture of July and August, we could consider them as either July or August data.

The most outstanding feature is that the signal level is so high during this period that the errors are practically insignificant. When the errors are so infrequent, one must measure over a long period of time to obtain reasonable statistics. Therefore, from the point of view of our major interest in the signal behavior that affected errors, this TPA series served mainly to confirm that any errors will only infrequently be caused by natural signal fading. Errors caused by specular fading will also be reduced, but will occasionally occur.

These July tests did serve to uncover a previously unknown feature of the particular equipment used in this link. During the TPA analysis, it became apparent that there was a random source of errors that appeared even when the diversity signal was quite high. It was later found[1] that the source of these fictitious errors was the oven control circuit. Whenever the oven control circuit turned on, it caused a few isolated errors to appear in the error detection circuit. This, in effect, meant that there was (and is) a limit of about $10^{-7}$ on the error rate as seen by this equipment, no matter what the power level.

A table showing the $P_E$ value for various 6 minute tapes is shown below (Table 3.2). The average $P_E$, averaged over all these tapes, is $1.59 \times 10^{-\upsilon}$. This again is better than the averaged values measured earlier on this link (Ref. 14).

Figures 3.3 and 3.4 show pictures of the July data. Figure 3.3 shows samples from a morning tape, while Fig. 3.4 uses an afternoon tape. The rapidly moving signals are channel A and channel B. The diversity power is measured by the combiner signal in these tapes. In Fig. 3.3 the combiner signal is extremely noisy.

[1] These same fictitious errors were seen by the DAIS personnel from Bell Telephone Laboratories. They traced the errors to the actual cause.

| Label | Corrected $P_E$ | Time |
|---|---|---|
| TPJ 2 | $3.48 \times 10^{-6}$ | Monday Afternoon, 4:00 p. m. |
| TPJ 3 | $1.87 \times 10^{-7}$ | Monday Afternoon, 4:10 p. m. |
| TPJ 4 | $3.22 \times 10^{-6}$ | Monday Afternoon, 4:25 p. m. |
| TPJ 7 | $3.48 \times 10^{-6}$ | Tuesday Morning, 10:30 a. m. |
| TPJ 8 | $5.35 \times 10^{-7}$ | Tuesday Morning, 10:50 a. m. |
| TPJ12 | $1.16 \times 10^{-7}$ | Tuesday Morning, 12:20 a. m. |
| TPJ13 | $1.16 \times 10^{-7}$ | Tuesday Afternoon, 1:00 p. m. |

Table 3. 2. August 3 and 4 data.

The typical action (without specular fading) was long looped signals, such as seen in Fig. 3. 3 a) to d). The specular activity caused very rapid (about 30 cps) activity on the single channel signals, as can be seen in Fig. 3. 3 e) to h).

In Fig. 3. 4 the combiner signal was quieted down. Again the spectral fading is very rapid and deep. Figure 3. 4 d) shows the signal when an airplane is entering the area; e) shows the signals while in the common volume; and f) shows the signal upon leaving the common volume.

From Fig. 3. 2, it can be seen that the signals at this point still contained appreciable noise. We did take calibration curves of the tropo equipment at the time the data were taken. We dealt with this in terms of voltages and our computer routines went through these curves in terms of the voltages. (For the TPN and TPF series, we measured the calibration curves directly in terms of power.)

The pictures will also confirm that we used the combiner signal as the measure of diversity power in this TPJ series.

In one TPJ test (TPJ15), we turned the parametric amplifiers off. The $P_E$ was $6.06 \times 10^{-6}$. Hence, this is additional evidence that during the high-signal seasons additional power is, of course, not crucial. The role of intersymbol influence because of the selective fading also places a limit on the error improvement with additional power.

TPJ7, Tuesday morning

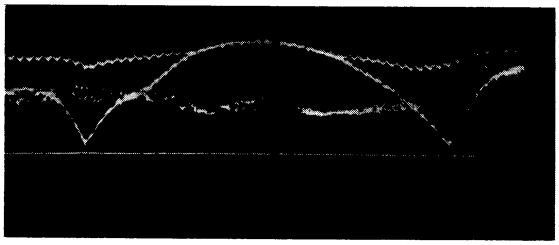

a) (237) Typical fade behavior

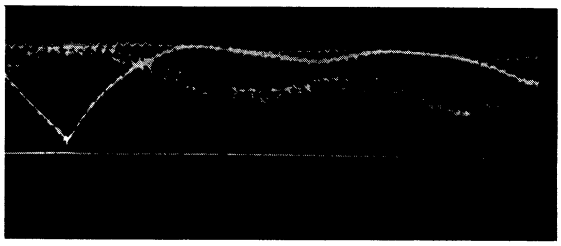

b) (336) Typical fade behavior

c) (413) Typical fade behavior

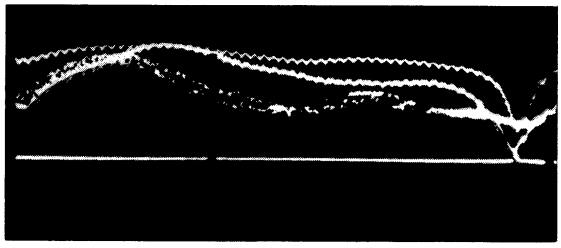

d) (110) Errors during typical fade

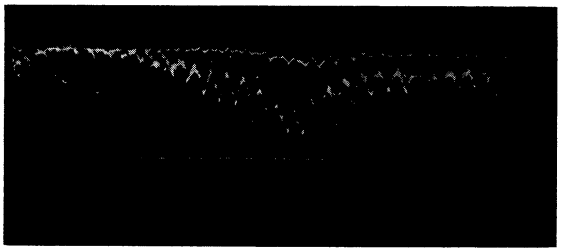

e) (448) Airplane entering area

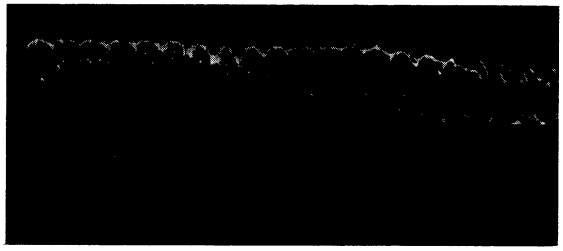

f) (476) Saturation and then airplane leaving area

g) (545) Beginning of another airplane fade

h) (558) Airplane leaving area

Fig. 3. 3. Selected samples from TPJ7, August Tuesday morning tape.

TPJ4, Monday afternoon

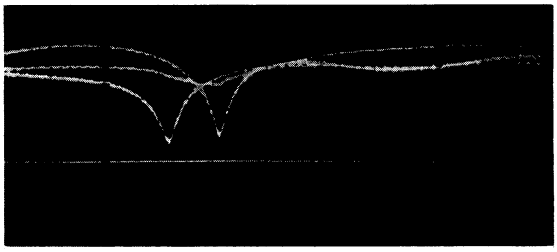

a) (171) Typical fading

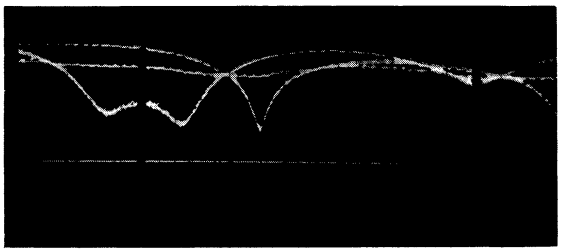

b) (125) Typical fading

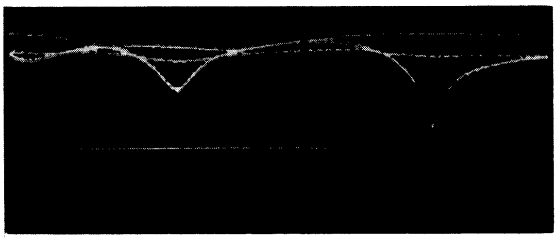

c) (333) Typical fade

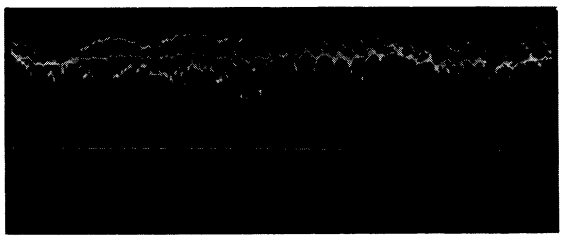

d) (508) Airplane entering area

e) (515) Middle of airplane-affected area

f) (535) Airplane leaving area

Fig. 3.4. Selected samples from TPJ4, August Monday afternoon tape.

3.1.3 November, 1964 Data (TPN). The November data are in the beginning of the poor season (winter) for the error behavior. Our data are characterized by a great range of $P_E$ in the tapes that we took. The gross $P_E$ data are shown in Table 3.3. The average $P_E$ for the seven tapes is $1.45 \times 10^{-3}$. This probably is poorer than would be expected. This is accounted for by the unusually poor error rate on the Thursday morning data. This is probably because of the weather, since it was raining at the receiving terminal (Fort Monmouth). In each of these Thursday morning tapes, channel B goes off scale at times. At these times the AGC signal reacts as though it is single channel operation.

| Label | Corrected $P_E$ | Time of Day | |
|---|---|---|---|
| TPN 4 | $1.53 \times 10^{-5}$ | Wednesday Morning, 11:00 a. m. | |
| TPN 6 | $1.98 \times 10^{-4}$ | Wednesday Afternoon, 2:00 p. m. | |
| TPN 7 | $1.72 \times 10^{-4}$ | Wednesday Afternoon, 2:15 p. m. | |
| TPN10 | $1.48 \times 10^{-3}$ | Wednesday Afternoon, 3:20 p. m. | |
| TPN11 | $9.22 \times 10^{-4}$ | Thursday Morning, 9:45 a. m. | rain at receiver |
| TPN12 | $1.74 \times 10^{-3}$ | Thursday Morning, 10:20 a. m. | rain at receiver |
| TPN 3 | $4.07 \times 10^{-3}$ | Thursday Morning, 10:40 a. m. | rain at receiver |

Table 3.3. November 18 and 19 Data (TPN).

Since channel B acted differently than channel A, we think there is some possibility that the rain was affecting the actual receiving equipment.

Another item of interest is that the power was reduced by 3 db (500 watts) for one tape (TPN5) on Wednesday morning. This reduced the error rate to $2.5 \times 10^{-4}$, compared to the previous Wednesday morning (TPN4) rate of $1.53 \times 10^{-5}$. Clearly the power is sufficiently marginal now that any reduction seriously affects the errors.

Pictures of the November multiplexed signals are shown in Figs. 3.5 and 3.6. It can be seen in Figs. 3.5 and 3.6 that the signal behavior in November is more gentle and rolling, rather than peaked. This is partly because of the filters, but also partly because of the change signal. The fading bandwidth appears to be lower in November than in April or July.

TPN4, Wednesday morning 11:00 A. M. tape

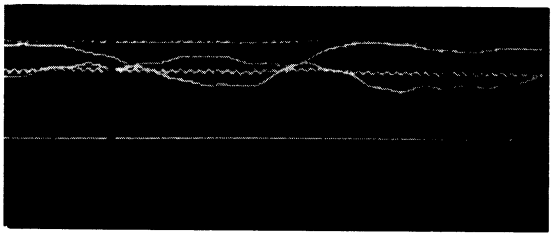

a) (353) Normal signal behavior

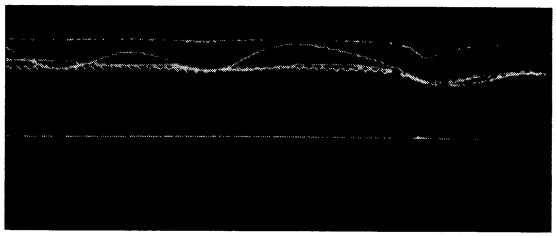

b) (389) Short error burst

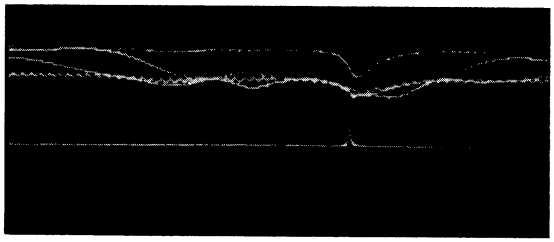

c) (413) Error burst due to signal fade

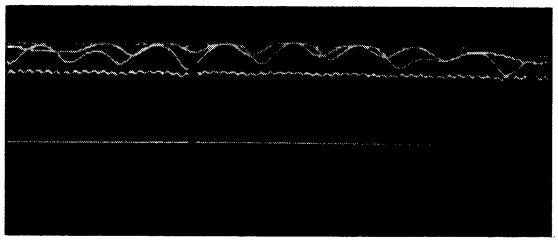

d) (303) Airplane action

TPN12, Thursday morning (rain at receiver)

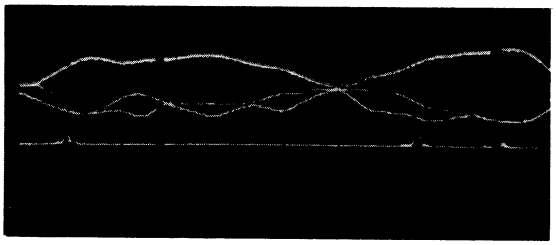

e) (84) Severe error bursts

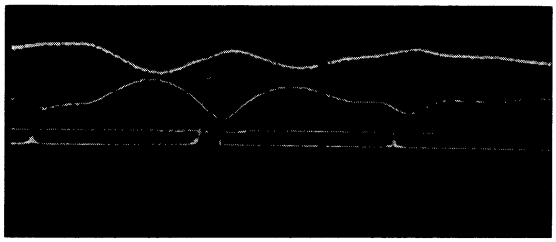

f) (247) Severe error bursts

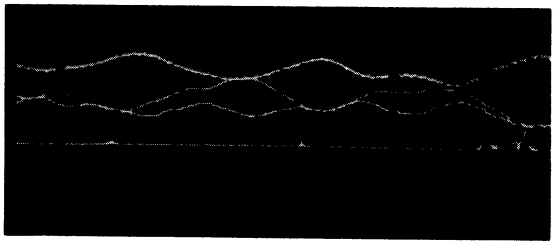

g) (178) Error bursts

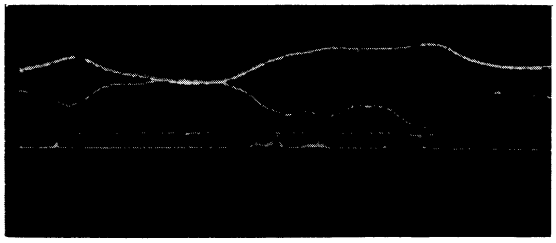

h) (21) Severe error bursts

Fig. 3.5. Selected samples from TPN4 and TPN12, November Wednesday and Thursday morning tapes.

TPN 10, Wednesday afternoon

a) (146) Errors due to typical fading

b) (188) Errors due to typical fading

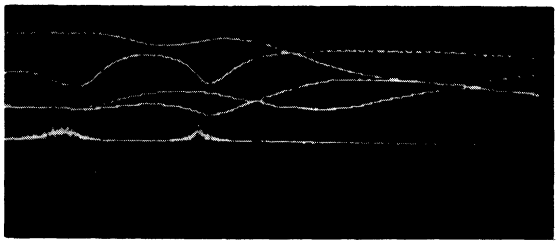

c) (282) Long error run

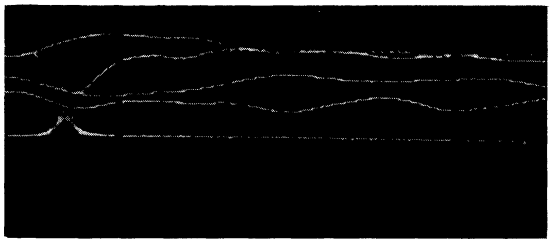

d) (580) Errors from typical fade

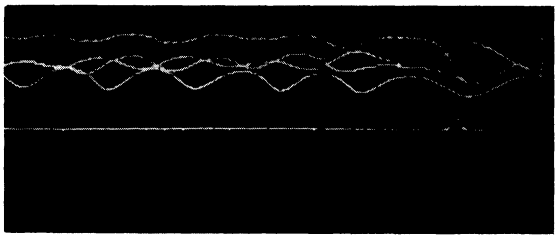

e) (349) Errors due to entering airplane

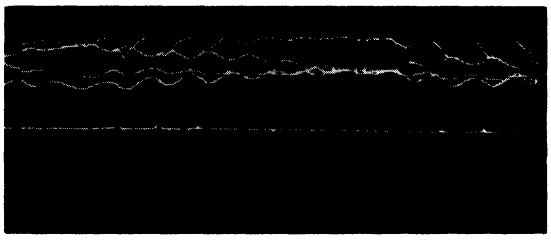

f) (383) Errors due to leaving airplane

Fig. 3.6. Selected samples from TPN10, November Wednesday afternoon, 3:20 p. m. tape.

On Fig. 3.5 a) to d) (TPN4) both an AGC and a combiner signal were recorded. The combiner is the top signal. Again the "morning" signals are channel A and channel B. The intermediate line is an inverted AGC signal. (This is one of two AGC signals; the other AGC signal was used most of the time.) As can be seen, the error bursts in Fig. 3.5 b) and c) correspond to the drops in combiner signal. Note that the errors slightly lead the combiner signal. The effect of the filtering of our signals can be gauged by comparing the specular fading of Fig. 3.5 d) to the specular fading in Figs. 3.1 through 3.4.

Serious error bursts are shown in Fig. 3.5 e) through h). For this tape the channel A, channel B, and (preferable) AGC signal were recorded. The AGC signal is the uppermost one in Fig. 3.5 e) through g). Also, it moves oppositely to the A and B signals. The very serious errors are a somewhat special case since it was raining at the receiver. Note that in Fig. 3.5 f) and h) the channel B signal has gone off-scale. At such times the receiver is practically single channel.

Figure 3.6 shows a November afternoon tape. The signals are (starting from top in a): combiner, AGC, channel A, and channel B. Again it is consistently true that the error runs slightly lead the combiner drop, and even more lead the AGC peaking. This is entirely a function of the equipment.

From the pictures it can be seen that the noise has been suppressed on the multiplexed signals. We used a 60 cycle per second notched filter for the channel A, the channel B, the AGC and the combiner signals. In addition, we converted the variable gain operational (analog) amplifier into an integrator (low pass). This suppressed the 1500 cps ripple and gave us a fairly clean signal. Although these filters slightly altered the shape of the signal (mostly deep fades during airplane fading) we are confident that they have not altered the crucial statistics of the signal.

We took calibration curves each half day for this data. The curves were taken directly in terms of the input power of an individual channel.

3.1.4 February Data (TPF). The data that we encountered in February showed an unusually high signal level for that time of year. The average $P_E$ encountered, over our seven diversity tapes, was $1.11 \times 10^{-4}$.

In this February data, the morning signals moved about a good deal more than the afternoon signals. Also, the $P_E$ for the morning was about the same as in the afternoon; usually the morning tapes have a better $P_E$ than the afternoon ones. Table 3. 4 below shows the gross $P_E$ for the February diversity tapes.

| Label | $P_E$ | Time |
|---|---|---|
| TPF 1 | $3.71 \times 10^{-5}$ | Wednesday Afternoon, 2:35 p. m. |
| TPF 5 | $1.96 \times 10^{-4}$ | Thursday Morning, 10:45 a. m. |
| TPF 6 | $1.14 \times 10^{-4}$ | Thursday Morning, 11:00 a. m. |
| TPF 7 | $3.81 \times 10^{-5}$ | Friday Morning, 11:00 a. m. |
| TPF 9 | $2.26 \times 10^{-5}$ | Friday Morning, 10:05 a. m. |
| TPF 8 | $1.03 \times 10^{-4}$ | Friday Morning, 11:20 a. m. |
| TPF12 | $2.72 \times 10^{-4}$ | Friday Afternoon, 2:00 p. m. |

Table 3. 4. February 24 to 26, 1965 data.

The signal was sufficiently strong on Wednesday afternoon that two reduced power tests were made. When the transmitted power was reduced by 3 db (to 500 watts) the $P_E$ was $2.58 \times 10^{-7}$ (TPF2). This is startling. Either an unusual phenomenon can occur (such as ducting) or the issue of intersymbol influence because of selective fading can help explain this. Certainly reduced power tests should be given priority in any future work.

When the power was further reduced to 100 watts (TPF3), the $P_E$ observed was $2.46 \times 10^{-5}$. This is about the same as the earlier full-power tape (TPF1).

Pictures of the multiplexed February signals are shown in Figs. 3. 7 and 3. 8. The signals recorded are, as in TPN10: combiner, channel A, channel B, and AGC. The order stated here is the order of the signals at the left side of Fig. 3. 7 a). Again the typical signal behavior can be seen from these curves. As seen, the error runs lead the combiner slightly, and the AGC signal even more. Figure 3. 7 a) and b) are excellent illustrations of the relation between the errors and the various signals.

Figure 3. 8 shows similar signals for a February Friday afternoon tape.

TPF9, Friday morning

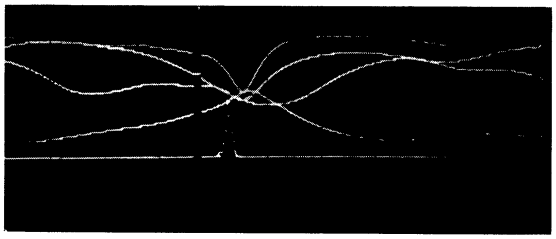

a) (27) Errors due to fade

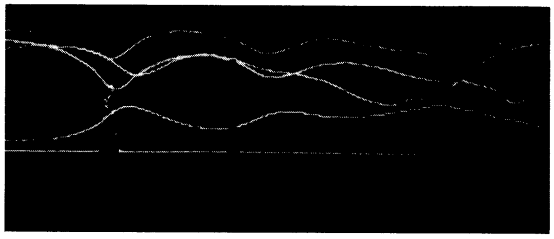

b) (138) Errors due to fade

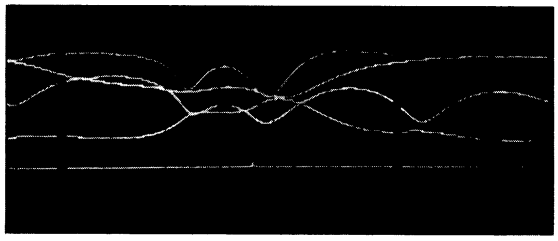

c) (226) Typical fade activity

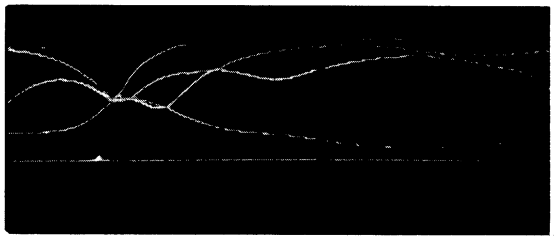

d) (528) Typical fade activity

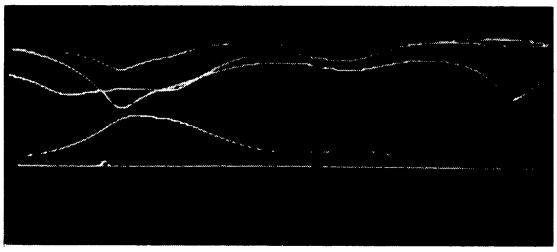

f) (206) Errors and fade activity

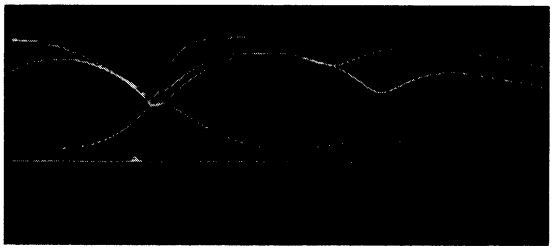

e) (103) Errors and fade activity

Fig. 3.7. Selected samples from TPF8 and TPF9, February Friday morning tapes.

TPF12, Friday afternoon

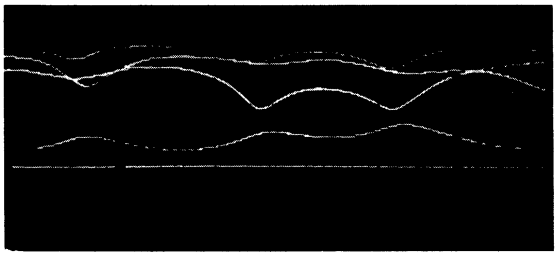

a) (481) Typical signal activity

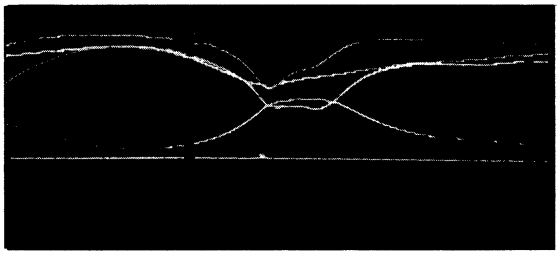

b) (193) Typical face activity with errors

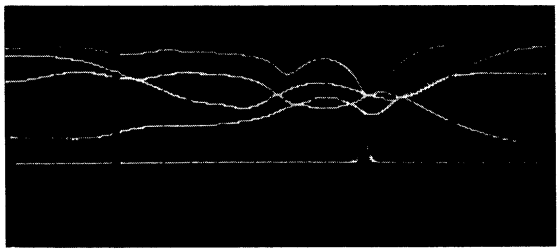

c) (316) Errors during a fade

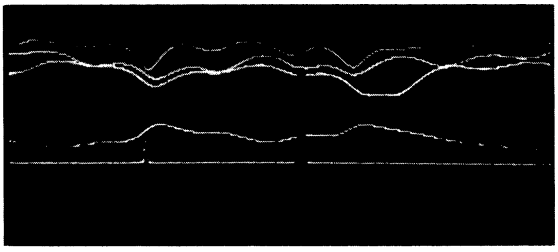

d) (509) Errors during a fade

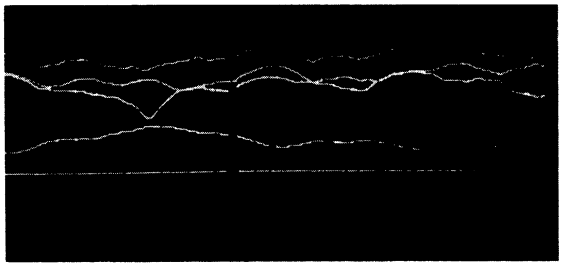

e) (71) Typical signal activity

Fig. 3.8. Selected samples from TPF12, February Friday afternoon tape.

The data taking situation in February was similar to that in November. We used the notch-noise filter and roll-off filter; later on we found that we didn't need them. Between November and February the noise conditions in the tropo room were considerably improved. Since the filters were already in our system, we did not notice the change, and consequently kept the filters in for this TPF data.

## 3.2 Description of Computer Analysis

In this section we will describe the gross data analyses conducted by the computer on the data that were described in the previous section. The computer programs that were written are of two types: 1) a signal analysis program, and 2) a level crossing program.

The major items in the signal analysis program are the probability of bit error per signal level, probability of frame error per signal level, the error-free and error-run tabulations, and the distributions of the various signals.

The major items in the level crossing analysis are the cumulative distributions for the various signals at different power levels.

During the first attempts at data analysis we put the signal analysis and level crossing in the same computer run. This meant that we had to compute a signal mean on only an early portion of the tape, and the fade levels had to be chosen without knowing the signal behavior. For these reasons we separated the two programs. Thus, we could choose the fade levels sensibly by referring to the computer output from the signal analysis portion.

We will now describe briefly the major calculations in both programs.

3.2.1 Probability of Error Versus Signal Level. The probability bit error and the frame error rate for each of the signal levels were computed. This probability is formed at a given signal level, by taking the ratio of the number of bits in error at that level to the total bits which occurred at that level. The equivalent is done for the frame error. In conjunction with this plot we have a table printout which, for each signal level, shows the number of times a given error count occurred while at that level. This printout in effect shows how the $P_E$ occurred at the given level. In another printout, we show the sequential error-run--error-free run sample count for the entire six minute sample. This retains the time-ordered run behavior, in case subsequent analysis requires this feature.

3.2.2 Error-Free and Error-Run Tabulations. The computer computed the run-length tally and the corresponding cumulative tally for the error runs. An error run is simply the number of contiguous frames (56 bits) during which at least one error occurred.

A similar tabulation was made for the error-free runs. An error-free run is simply the length (in 56 bit frames) between error runs (or frames).

3.2.3 Distribution of Signal Levels. The computer plotted both the discrete density function and the cumulative function of all the signal levels recorded in the tests. This was done for channel A, channel B, combiner signal, AGC signal, and A + B. The density function is formed by the ratio of the number of times the signal was at the given level out of the total number of sample points. The cumulative then was calculated by a cumulative tally of the density tally.

A comment on the A + B situation is warranted. To gain additional evidence as to the diversity behavior a linear sum A + B signal was generated by processing the individual channel signals on a digital computer. This signal was generated by converting samples from the magnetic tape to true input voltages using the log-linear calibration curves. The time interlocked sample voltages from the A and B channels were then added together to form the new linear sum signal. The mean of this special signal was compared to the means of the AGC and combiner signals. The linear sum addition accomplished by the computer corresponds to the action of an ideal predetection combining of input power. A distinct advantage of this signal over the true physical combiner signal and AGC signal is that this signal is not influenced by the varying gain of the IF amplifier. The probability distribution of the signal amplitudes for this A + B signal should follow closely a convoluted Rayleigh distribution. Also, it is possible to compare the statistics of this A + B signal with theoretical results known for convoluted Rayleigh distributions.

Each of these distributions was also formed for all the signals "when errors occurred." In the beginning we found it instructive to compare the signal distribution when errors occurred to the overall distribution. The two distributions are analogous to the classical "noise alone" and "signal-plus-noise" distributions in signal detectability descriptions.

Another table printout showed the scatter diagram of the A and B signal when errors occurred. Although it is difficult to plot the results of such printouts, they are immensely helpful in pursuing the cause of any action that becomes apparent during the analysis.

3.2.4 Level Crossing Program. The level crossing analysis found the density function and the cumulative function for the length of level crossings for each of the signals. For channel A and channel B, the analysis was done only at the mean. For the AGC, the combiner signal, and A + B, the analysis was done at any level inserted as input data.

## 3.3 Summary of Analyzed Data

In Section 3.1 we described the total range of recorded data when the receiver was in its normal diversity mode. As mentioned there, we also recorded data when the receiver was operated single channel, and diversity with the parametrics off.

Because of a time and economic limitation we could not, of course, pursue all possible aspects of all these data. We, therefore, determined priorities as the test program unfolded. First of all, we eliminated for consideration those tapes in which the parametrics were off. Next we decided not to pursue the single channel versus diversity comparison, since it is not essential to our main concern--the synchronization issue. Therefore, we did not analyze the single channel tapes.

After editing the total list of diversity tapes (discussed in Section 3.1) we chose about twenty tapes for detailed computer analysis. A further editing occurred when we obtained the first signal analysis results from the computer. Our objective was to obtain about a dozen tapes in which both the error count check and the signal-mean check indicated that the data were reliable. In the cases in which these did not check, either the terminal equipment or our data acquisition equipment malfunctioned during that tape.

The error-count test refers to comparing the error count noted at the site during the data recording with the total error count noted by the computer. One legitimate course of error in this comparison is the record-gap time of the digital tape.

The other aspect which we checked on was the agreement of means between the various signals. We recorded three separate signal strengths (channel A, channel B and AGC), and the means of these should be reasonably close to each other. Although channel A

and channel B are instantaneously uncorrelated, the strength averaged over minutes is highly correlated. Thus, the compatibility of channel A and channel B, and the compatibility of these with the AGC (diversity) strength gave us confidence that the calibration procedures were reasonably accurate.

For convenience, Table 3.5 shows the crucial signal parameters for all of the data that will be reported on in the next sections. It will be useful to return to this table when studying various curves in the following sections. This table then should be referred to, to get the gross aspect when reading the various curves which follow.

| Tape Description | Experimental Error Count | Computer Totalized Error Count | Mean Strength of Channel A in dbm | Mean Strength of Channel B in dbm | Mean AGC Signal Strength in dbm | Median AGC Signal in dbm | $P_E$ Bit Error | $P_F$ Frame Error Rate | Fading Bandwidth Channel A in cps | Fading Bandwidth Channel B in cps | Number of Error Runs | Maximum Length of Error Run in msec (Quantized) | Remarks |
|---|---|---|---|---|---|---|---|---|---|---|---|---|---|
| TPA 4 | 7,000 | 6,739 | -81.0 | -83.0 | -82 | (-82.1) | $3.4 \times 10^{-5}$ | | 1.32 | 2.1 | 141 | 19.5 | Characteristic action is fairly slow, peaked, dip in signal. Contains specular fading. |
| TPJ 4 | 639 | 606 | -71.6 | -71.5 | | | $3.05 \times 10^{-6}$ | | | | 17 | 4.86 | Relatively slow fading. |
| TPJ 7 | 687 | 348 | -79.5 | (-78.2) corrected | | | $1.76 \times 10^{-6}$ | | | | 48 | 1.95 | Faster fading than in previous. |
| TPN 6 | 39,254 | 36,426 | -82.7 | -84.5 | -83.1 | -84.0 | $1.84 \times 10^{-4}$ | $3.112 \times 10^{-3}$ | 2.68 | 2.065 | 4,390 | 48.6 | Signals now have notch and roll filter in series (see Fig. A.6 of Appendix A) - airplane through common volume. |
| TPN 7 | 34,100 | 34,275 | -83.9 | -85.8 | -83.9 | | $1.73 \times 10^{-4}$ | $3.4 \times 10^{-3}$ | | | 4,663 | 48.6 | Signal moves around a good deal. |
| TPN10 | 292,975 | 275,669 | -89.6 | -91.2 | -89.8 | -90.8 | $1.39 \times 10^{-3}$ | $2.26 \times 10^{-2}$ | 2.24 | 2.36 | 30,036 | 100 | Much specular fading in this tape. 1 airplane goes through common volume (signal saturation) |
| TPN11 | 182,654 | 177,917 | -83.8 | -87.8 | -85.2 | | $8.97 \times 10^{-4}$ | $5.65 \times 10^{-3}$ | | | 4,732 | 100 | Channel B went off-scale at a few places - rain at receiver site. |
| TPN12 | 344,800 | 339,590 | -86.74 | -90.89 | -89.21 | -89.3 | $1.714 \times 10^{-3}$ | $1.5 \times 10^{-2}$ | 1.96 | 1.2 | 13,646 | 100 | Channel B still seems "sluggish". Rain at receiver site. |
| TPF 7 | 7,536 | 6,939 | -80.7 | -82.3 | -82.1 | -82.5 | $3.5 \times 10^{-3}$ | $4.6 \times 10^{-4}$ | | | 3,636 | 10 | Filters still in. Considerable specular fading. |
| TPF 8 | 20,481 | 20,472 | -82.7 | -84.0 | -83.8 | -84.0 | $1.03 \times 10^{-4}$ | $6.69 \times 10^{-4}$ | 3.03 | 1.772 | 654 | 48.6 | Little specular fading. |
| TPF 9 | 4,464 | --- | -80.7 | -81.4 | -81.7 | -81.9 | $2.24 \times 10^{-5}$ | $1.9 \times 10^{-4}$ | 3.64 | 1.915 | 210 | 10 | |

Table 3.5. Summary of data analyzed in this report.

## IV. STATISTICAL BEHAVIOR OF SIGNALS

Before presenting the error and fade data, in this section we will note the behavior of the signals for the data considered here. This behavior can be considered as the cause for the error behavior and the signal sync behavior to follow.

The first curves of interest here will be curves of the single channel behavior (during diversity operation). These are the signals with which the combined signal is formed as represented by the combiner or AGC. We will then note the distributions of the AGC signals, which represent the effective diversity power. Finally, we will plot and compare the single channel curves with the AGC and with the A + B data for given tapes.

### 4. 1 Single Channel Distributions

It has been found that for most tapes the single channel signal agrees quite well with a Rayleigh distribution. The November 1964 test series deviates the most from the theoretical Rayleigh distribution. Signals for the other three data sets (April 1964, July 1964, and February 1965) are roughly comparable in the degree of closeness to a Rayleigh distribution.

A series of curves is shown in Figs. 4. 1 to 4. 4 which shows the behavior of the single channel curves for the tapes from each of the recording test periods. Each graph contains the theoretical Rayleigh distribution, the best (or closest) experimental distribution found in that series of analyzed tapes, and the worst experimental distribution from that series of analyzed tapes. In every case, the experimental and theoretical curves are matched at the median. We will now comment on each series.

#### April Tests (Fig. 4. 1)

Figure 4. 1 shows the bounds for the April tapes that we analyzed. In general (as will be remembered from Ref. 13), the April data are characterized by the presence of airplanes (approximately 20 to 30 percent of the time) which caused very deep and fast fades.

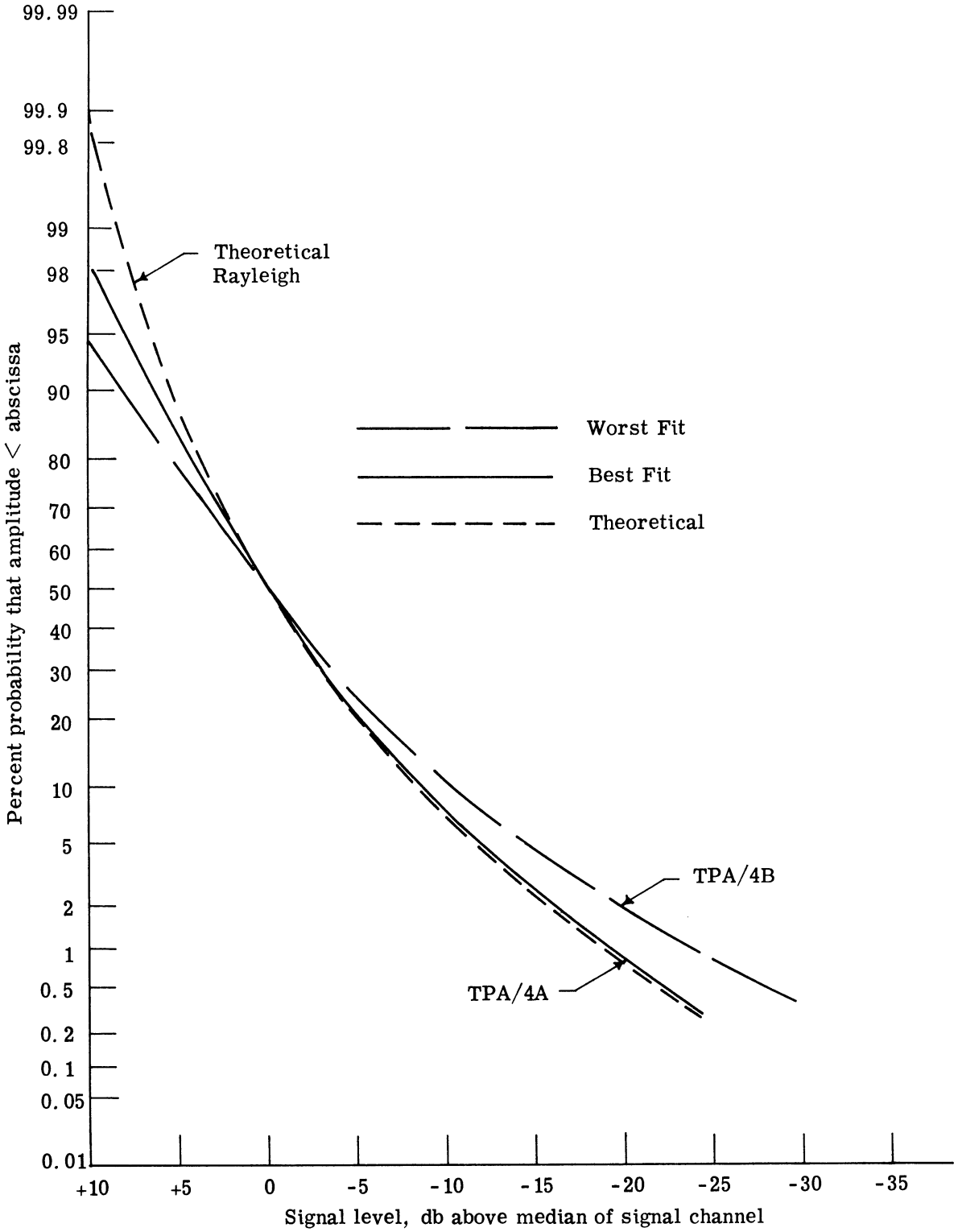


Fig. 4. 1. Comparison of fading signals with Rayleigh distribution for TPA series.

During these airplane periods the fade rate can reach as high as 30 to 50 cycles per second. It appears that the presence of this airplane effect provides the very deep fades which make the April curves rise above the theoretical Rayleigh at the very low signal levels.

July Series (Fig. 4.2)

In the July curves, it is again true that the signal tended to be above the theoretical Rayleigh distribution at the low signal levels. The typical fade behavior for this July data was about 1 to 2 cycle per second fades, based on looking at the signal versus time behavior. Although there was some hash on top of this July data, this did not particularly affect these signal distributions.

November Data (Fig. 4.3)

In the November series, the signal (of the tapes analyzed) departs more from the Rayleigh distribution than any of the other tapes. The signal behavior here was characterized generally by that of a slowly varying level, upon which there was a significant oscillatory tape signal behavior. For the periods of these two tests the signal distribution was quite non-Rayleigh. It is usually expected that a troposcatter signal distribution will most closely approximate a true Rayleigh distribution when the fade rates exceed something like 12 to 15 per minute. In the November case we are seeing a signal which is somewhat of a different type. An important question is whether or not this is a typical signal for this period of the year.

Two aspects affect these November data: (1) the inserted filters to reduce the 60 cycle ripple, and (2) the increased lower noise level in the calibration curves. The insertion of the filters will alter the signal only if the frequencies of change appear in the notch, 30 - 80 cps (see Fig. A.5 of Appendix A). This would affect low level signals, since the higher frequencies occur when the signal is in the lower regions. Therefore, both the February and November data will exhibit a tendency to roll-off from the true Rayleigh curve at the low signal end, because of the 60 cps filters.

In addition, the system appeared more noisy in November, characterized by the fact that we could not get the calibration curves to reach the low signal values that were recorded when taking our July calibration curves.

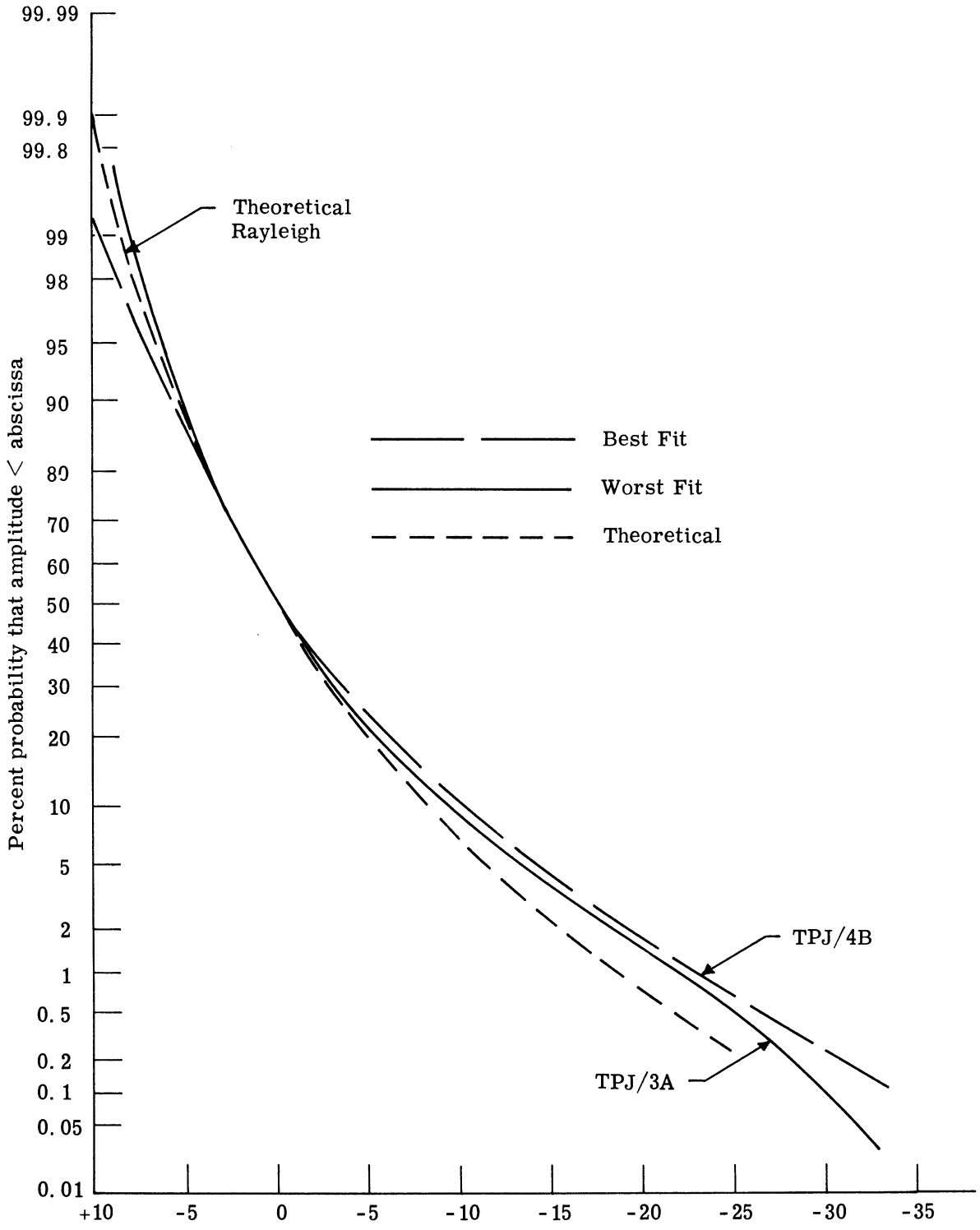


Fig. 4. 2. Comparison of fading signals with Rayleigh distribution for TPJ series.

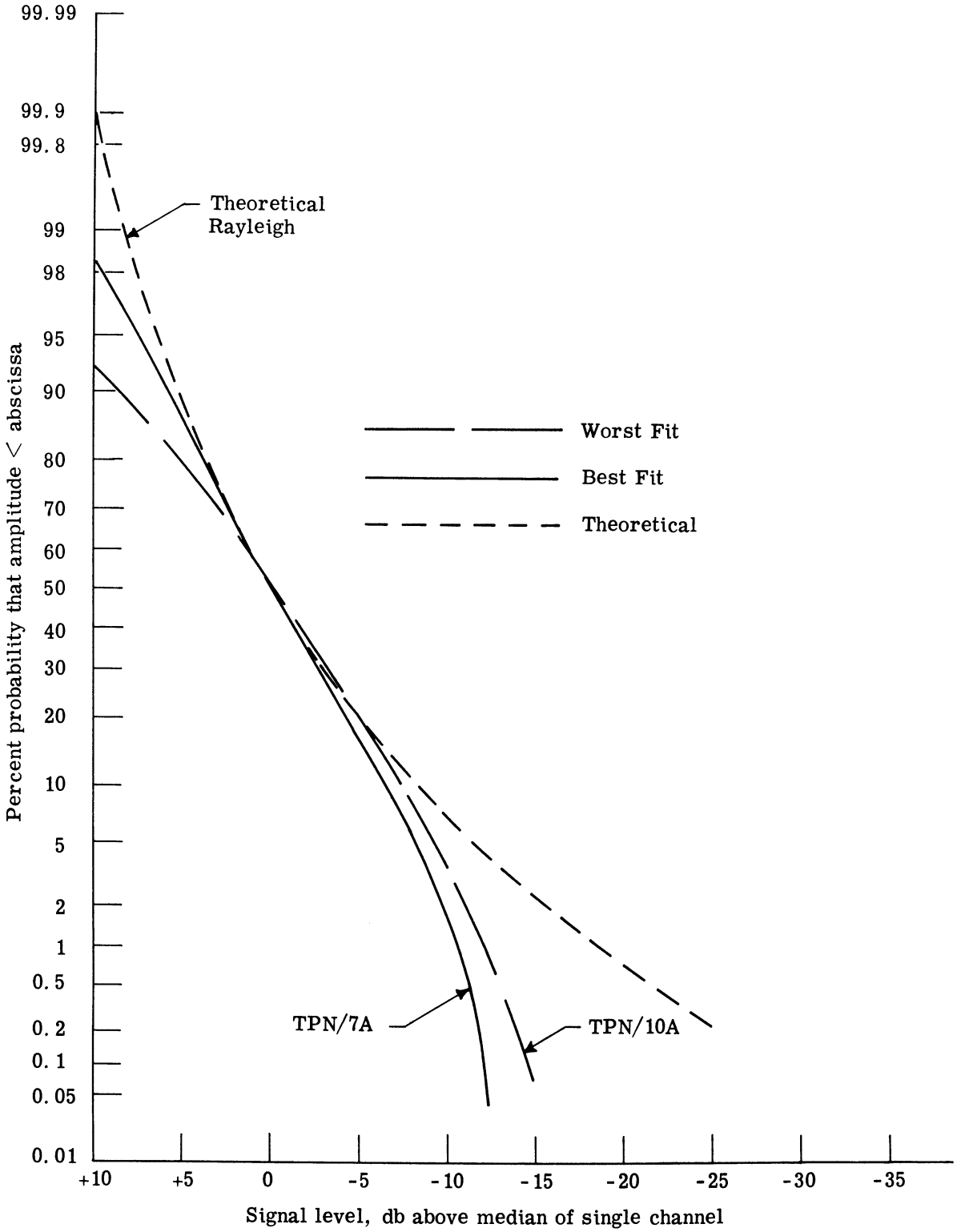


Fig. 4.3. Comparison of fading signals with Rayleigh distribution for TPN series.

February Tests (Fig. 4.4)

In the February tests (Fig. 4.4), the signals follow the Rayleigh at the high end but again dropped off at the low end. We attribute this mainly to the filter action. The time behavior of the signals here appeared to be normal fading signals, with about a 1 to 2 cycle per second fading rate.

We have reached the following conclusions for these single channel distributions: the signal levels for the single channel cases observed on our tests are essentially Rayleigh. The excessive rise of the April data at the low end is presumably because of airplane fading.[1] The slight similar rise in the July data suggests calibration curves may be offset. In both the November and February data, we have a drop-off at the lower signal end. We believe that this is because of the combination of the filter and the noisier system input at these test times. It does appear that 6 minute averages are reasonable for ascertaining the degree to which a signal is Rayleigh.

## 4.2 Comparison of the Linear Sum of Channel A and Channel B Signals, AGC to a Combined Rayleigh Distribution

The calculation of the linear sum of channel A plus channel B signal was added to the computer program after the TPJ (July) data series. Thus, this linear sum signal is available only for the TPN (November) and TPF (February) test series.

The significance of the A plus B signal is that it is an ideal linear addition of two individual fading signals. The A plus B curve is related to the median of the (averaged) single channel level. The single channel median is chosen by taking the average of the experimental channel A with that of channel B. The curve resulting from A plus B is then plotted with respect to the averaged single channel median. As seen in both Figs. 4.5 and 4.6, the resulting curve follows very closely that of the theoretical diversity-combined Rayleigh. The excellent agreement between A plus B and the theoretical combined Rayleigh distribution indicates that the individual signals do indeed have independent Rayleigh distributions with approximately equal medians. This indicates that it should be possible with this link to closely achieve the theoretical advantage of an equal gain diversity system over a single channel system.

---

[1] The deviation from the Rayleigh distribution is similar to the curve presented in Ref. 13.

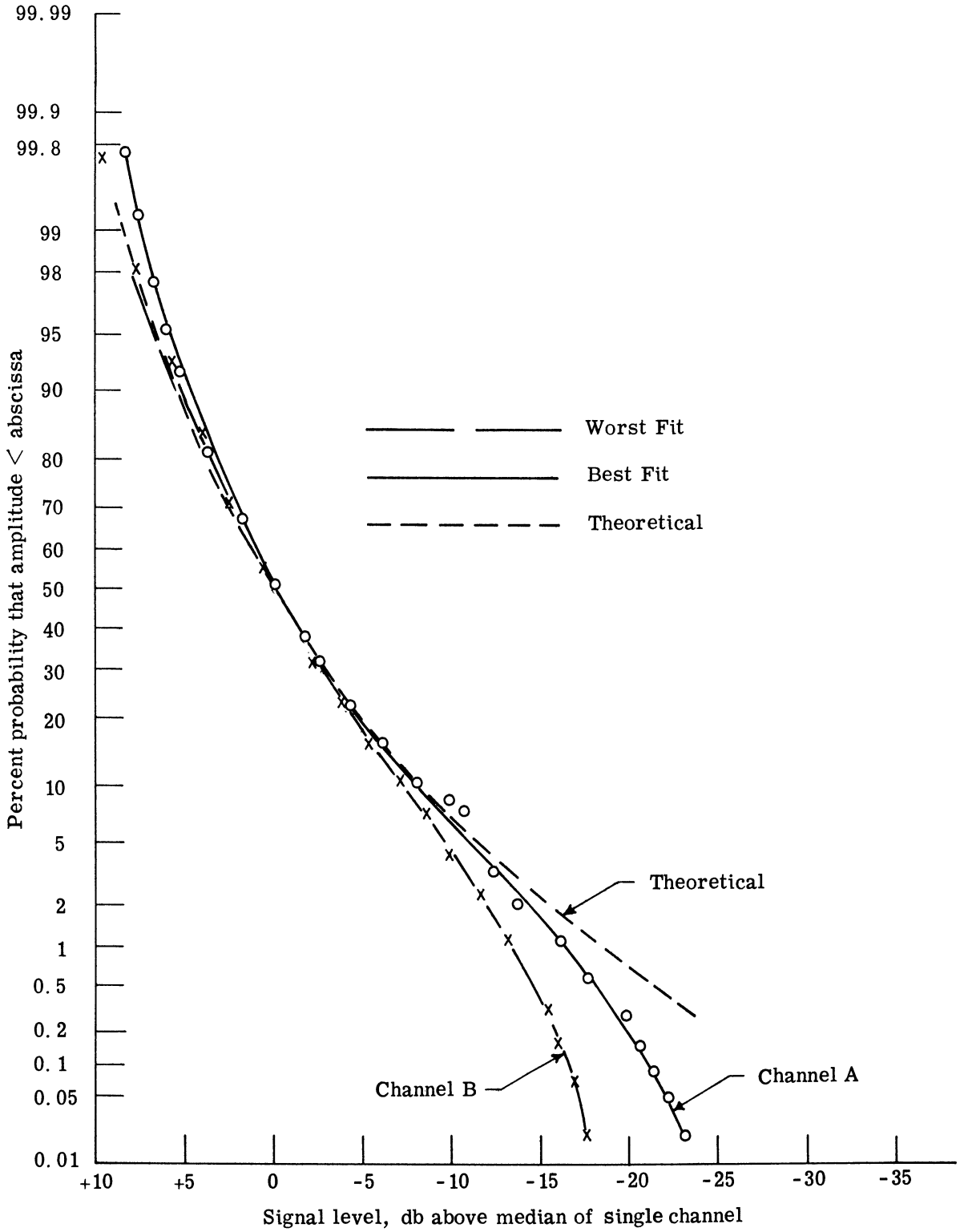


Fig. 4.4. Comparison of TPF/8 single channels to Rayleigh distribution.

In plotting the AGC curve, we again normalized to the (averaged) median of the single channel. The AGC then appears as shown in Figs. 4.5 and 4.6. We feel that this curve shows how the combiner is "adjusted." The evidence here shows that, the "combined power" characteristic catches up with the theoretical at a high signal level. The combiner does well at the low signals (where it is most critical) but apparently loses out in the intermediate range (compare the AGC to the theoretical curve between -5 and +5 db).

The actual combiner signal is behaving roughly as expected. At the high signal regions, it is affected by the varying IF gain and, therefore, the curve is flattened (relative to theoretical Rayleigh). However, at the low values it should reasonably reflect the correct combined power. It does this for the TPF/8 (Fig. 4.6) case but not as well for the TPF/7 (Fig. 4.5). We cannot account, at this time, for any reasons why the combiner should differ that significantly for the two cases.

In general, then the treatment of this action of the AGC and the combiner is useful in describing how the system is working.

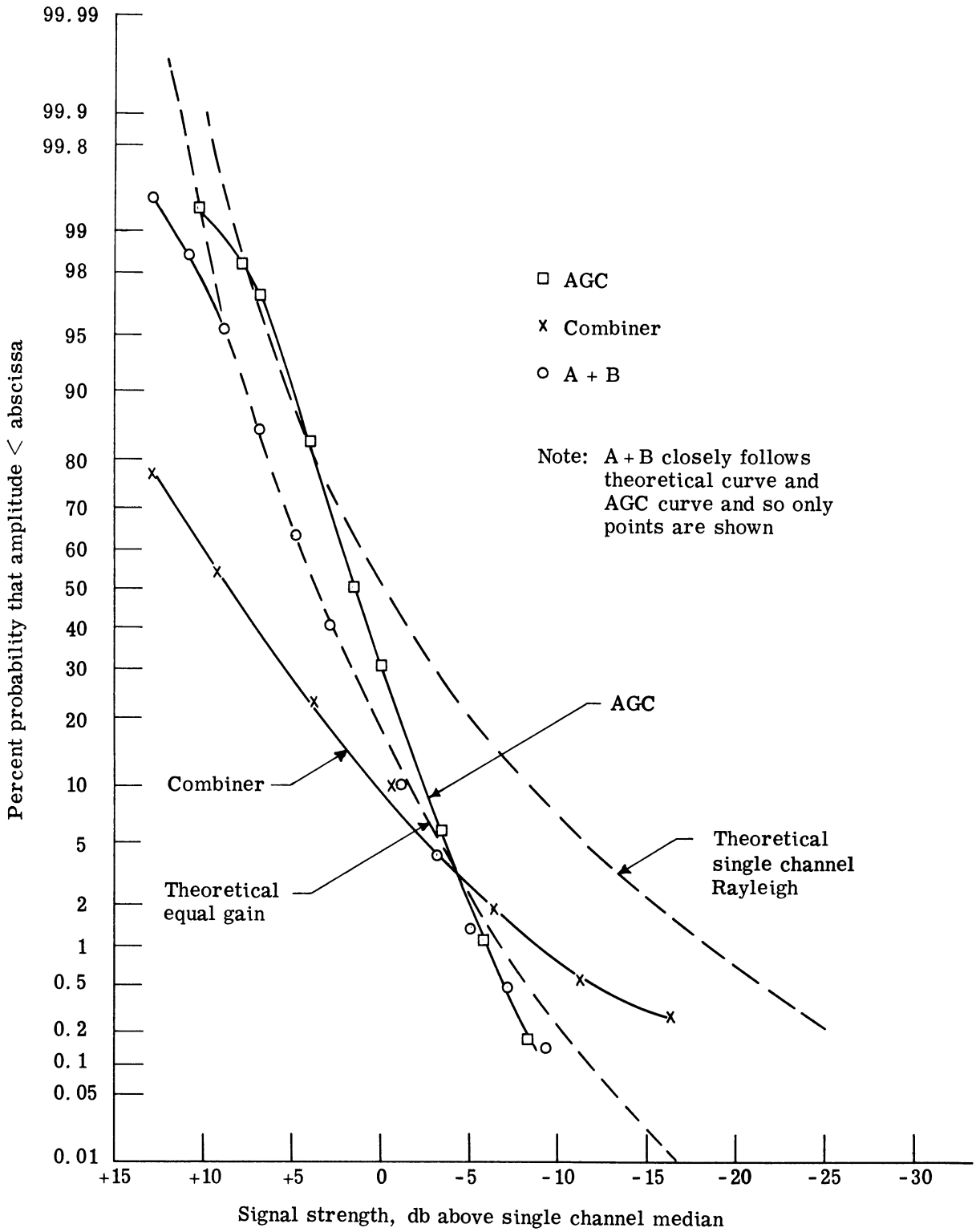


Fig. 4.5. Comparison of A + B, AGC, combiner curves of TPF/7 to theoretical Rayleigh distributions.

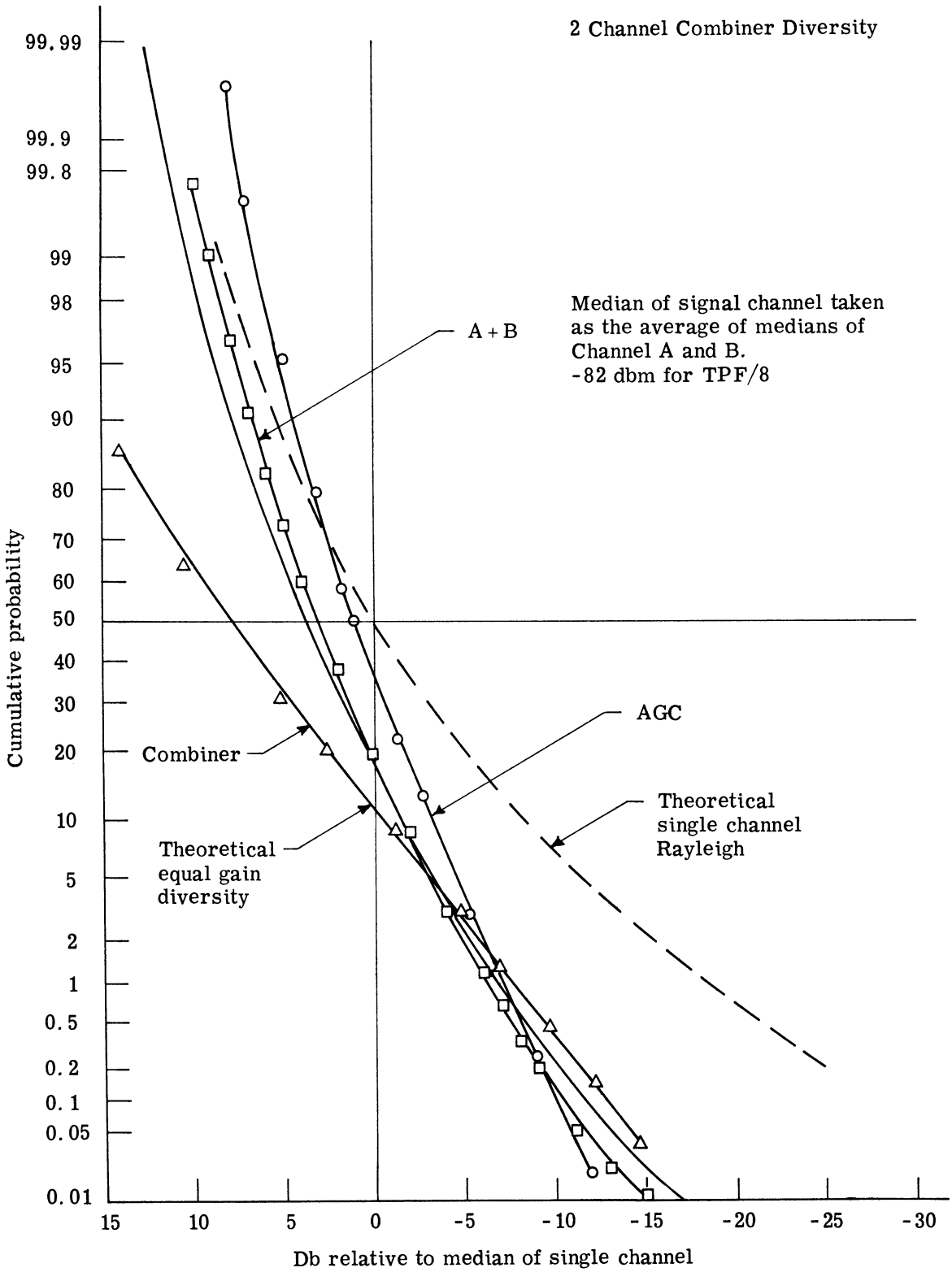


Fig. 4.6. Cumulative probability signal less than or equal to abscissa for A + B signal, AGC, and combiner for TPF/8.

## V. STATISTICAL ERROR RESULTS

In this section we present the statistical error results for the data taken during this series. The particular tapes analyzed are summarized in Table 3.5. Reference should be made to that table as these curves are studied.

In general, we shall be interested to see: 1) if the error behavior is discernibly different in the different seasons, 2) what parameter the behavior is highly correlated with, and 3) what are the quantitative percentages of time which bound the error behavior.

The material here is best treated by referring to the various graphs. Consequently, the discussion and subsections will be keyed on the various figures.

### 5.1 Average $P_E$ Versus Average Signal Level

Figure 5.1 shows the bit probability of error ($P_E$) averaged over the entire 6 minute sample versus the mean signal level for all the tapes which were analyzed in detail. Note that this is the most frequently used form of measuring and plotting $P_E$ characteristics: one usually averages the $P_E$ over an interval very long compared to a bit time and plots that versus the signal averaged over the same period of time. $P_E$ plots like this are gross indicators of the equipment performance (in response to the varying signals).

Note that in Fig. 5.1 we have ignored the "J" points (July - August data). There are two crucial reasons for doing this: 1) there were so few errors in these tests that the variance will be quite high, and 2) those errors that did occur were later found to be caused by the oven control circuit (see Section 3.1).

An interesting item in Fig. 5.1 is that the TPN/10 point lies to the left of TPN/12. The significance is that the TPN/10 data used the combiner signal for their diversity power measure while TPN/12 used the AGC. Thus, the combiner measure gives a lower power, for the same $P_E$, than does the AGC. This agrees with the results to be seen on Fig. 5.2.

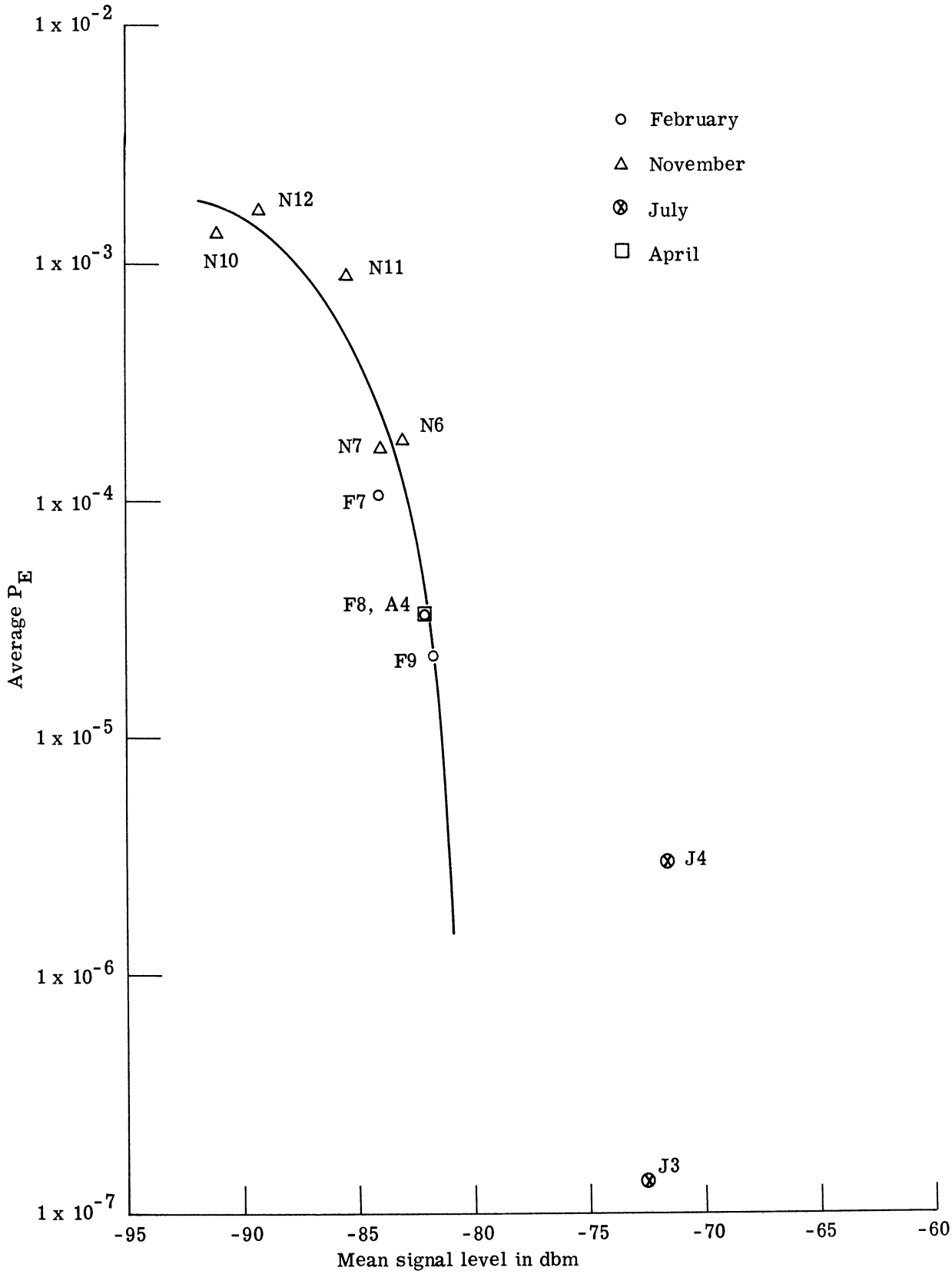


Fig. 5. 1. Average $P_E$ versus average signal level for all analyzed tapes.

## 5.2 $P_E$ Versus Signal Level

Figure 5.2 shows the entire set of points which resulted from plotting the $P_E$ at a given signal level versus the signal level (in dbm) for each of the tapes that we analyzed. The scattering of the points on this figure is because of the variance from the relatively small sample size (especially near both extremes of the curves). The $P_E$ is calculated by taking the ratio, at each signal level, of the number of bits which were in error at that given signal level divided by the total number of bits that occurred at the signal level. This curve yields information about how the equipment operates. The information here is more direct than that of Fig. 5.1 since here the $P_E$ is calculated separately for each signal level. Thus, this information is especially meaningful in showing the consistency of equipment operation. If the calibration curves were ideal, and if there were no sample variance, these curves would directly show any changes in equipment performance.

On Fig. 5.2 the two matched-dashed lines show the nominal bounds for the $P_E$ curves of those tapes which used the AGC for their diversity measurement. The left-most curve shows the $P_E$ curve when the combiner signal was as the diversity signal measure, for a November and an August tape. Note that other tapes using the combiner measure appear to the right of the AGC group. Thus, the combiner curves do not appear very consistent in their placement with respect to the AGC curves.

From Fig. 5.2 we can see that those tapes using the AGC as a diversity power measure show a good deal of consistency--they are all within a 3 db bound. The combiner curves, on the other hand, appear more inconsistent. The fact that the AGC curves are within a 3 db range is a gross indication of the equipment consistency (between the November and February tests).

The action in Fig. 5.2 suggests that, for a given actual diversity power the combiner will give a lower reading than the AGC calibration. This was corroborated in our fade analysis data, which are described in Section 4.

Another item affecting Fig. 5.2 is the fact that the error runs lead the combiner signal decrease, and even more lead the AGC signal. One evidence of this is that nearly all curves in Fig. 5.2 actually experience either a complete or a partial "S" type behavior (around -90 dbm).

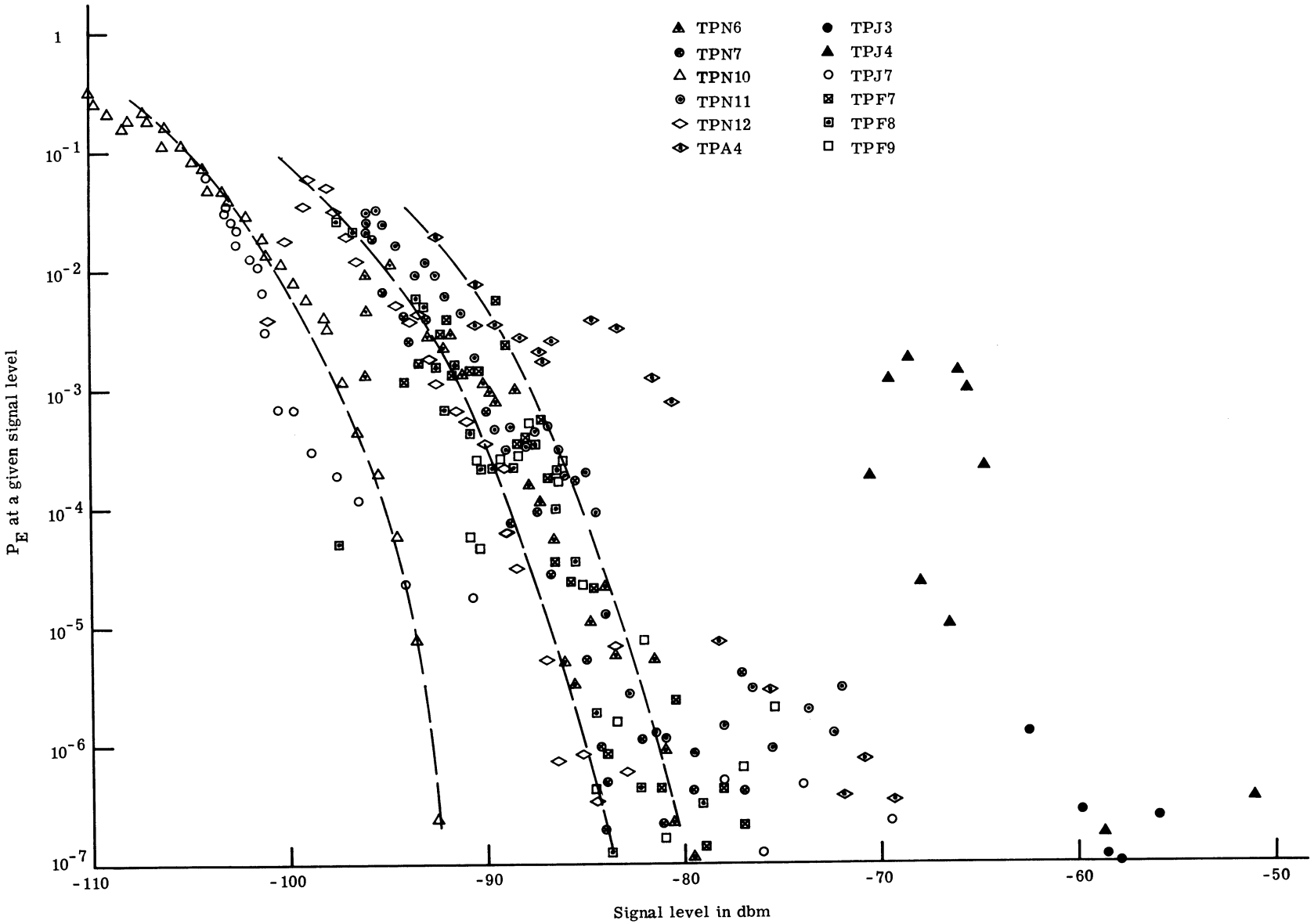


Fig. 5. 2. $P_E$ at a given signal level versus signal level.

## 5.3 Fraction of Time Spent in Error Runs $\geq$ Abscissa

A basic feature of the error behavior is depicted in Fig. 5.3a. This shows the cumulative distribution of the fraction of time in error run versus run length. This is the same as the fraction of total (data) time that the error run length was greater than or equal to the abscissa value (in milliseconds). These curves are reasonably consistent (for the different seasons). They suggest that one can estimate the cumulative error behavior by knowing the overall $P_E$. Although also well correlated with the signal mean, it appears (and seems plausible) that the $P_E$ is a better parameter for this set of curves.

Knowing the $P_E$, one can estimate the total time that error runs will exceed a given length with the information of Fig. 5.3a. This is useful and necessary information when considering error-extension of encoding techniques and when devising and evaluating synchronization circuits.

The information in Fig. 5.3a can be shown in different form by the cumulative information in Fig. 5.3b. This plots the percent of error runs $\leq$ the abscissa run length. It is seen that the curves are all close to each other. From this curve we can see that 90 percent of all error runs (over all seasons) are less than about 0.4 msec.

## 5.4 Error-Free Run Distribution

Another basic indication of the error performance is shown in Fig. 5.4. This shows the percent of samples that occurred in error-free intervals of length greater than or equal to the abscissa value. Again the basic character of the curves is consistent between November and February, and the $P_E$ is a good locator for the curves.

The values for these curves were found using the computer-derived tally table of error-free runs. We modified the error-free tallies to include the error frame. This could be done by starting at the "1-long" end and consecutively subtracting the previous number of error-free runs.

For the link situations encountered, the longest error-free runs lie between 3 seconds and 10 seconds. Consider the 50 percent point: if the $P_E$ is about $1 \times 10^{-3}$, 50 percent of the error-free runs are at greater than 1 second. For a $P_E$ about $3 \times 10^{-5}$, 50 percent are greater than 8 seconds.

In general, the curves of Fig. 5.4 indicate the "burstiness" of the data. Clearly

the better the $P_E$, the more bursty are the errors (indicated by the steepness of the cumulative curves). From the signal pictures in Section 3 we note that there are two levels of burstiness. First, a clump of errors occurs when the signal momentarily experiences a deep fade. Second, such deep fades themselves tend to be grouped; i. e., the clumps of errors tend to occur in groups. This latter action is especially pertinent when specular fading is the cause of the errors.

5.5 Cumulative Distribution of Error Rate

Still another useful form of the error data is shown in Fig. 5.5. This shows the percent of the time that the error rate was as good as the abscissa for various tapes. This, too, is useful in devising sync circuits. It specifies the total time during which the error rate will be above a certain value, but it does not say how the errors are distributed. Again it appears that this behavior is relatively insensitive to the particular season of the year and can be estimated by knowing the overall $P_E$.

When considering Fig. 5.5, it should be remembered that the "oven" errors (see Section 3. 1) provided an artificial (equipment malfunction) error limitation of about $1 \times 10^{-7}$. Therefore, the curves in Fig. 5.5 should not be considered accurate above $10^{-6}$.

Consider the 90 percent point. If the $P_E$ is about $1.7 \times 10^{-3}$, the error rate will be as good as $5 \times 10^{-3}$ for 90 percent of the time. If the $P_E$ is about $3 \times 10^{-5}$, the error rate will be as good as $3 \times 10^{-5}$ for 90 percent of the time. From the data here it appears that, given a $P_E$, the error rate will be as good as that $P_E$ about 90 percent of the time.

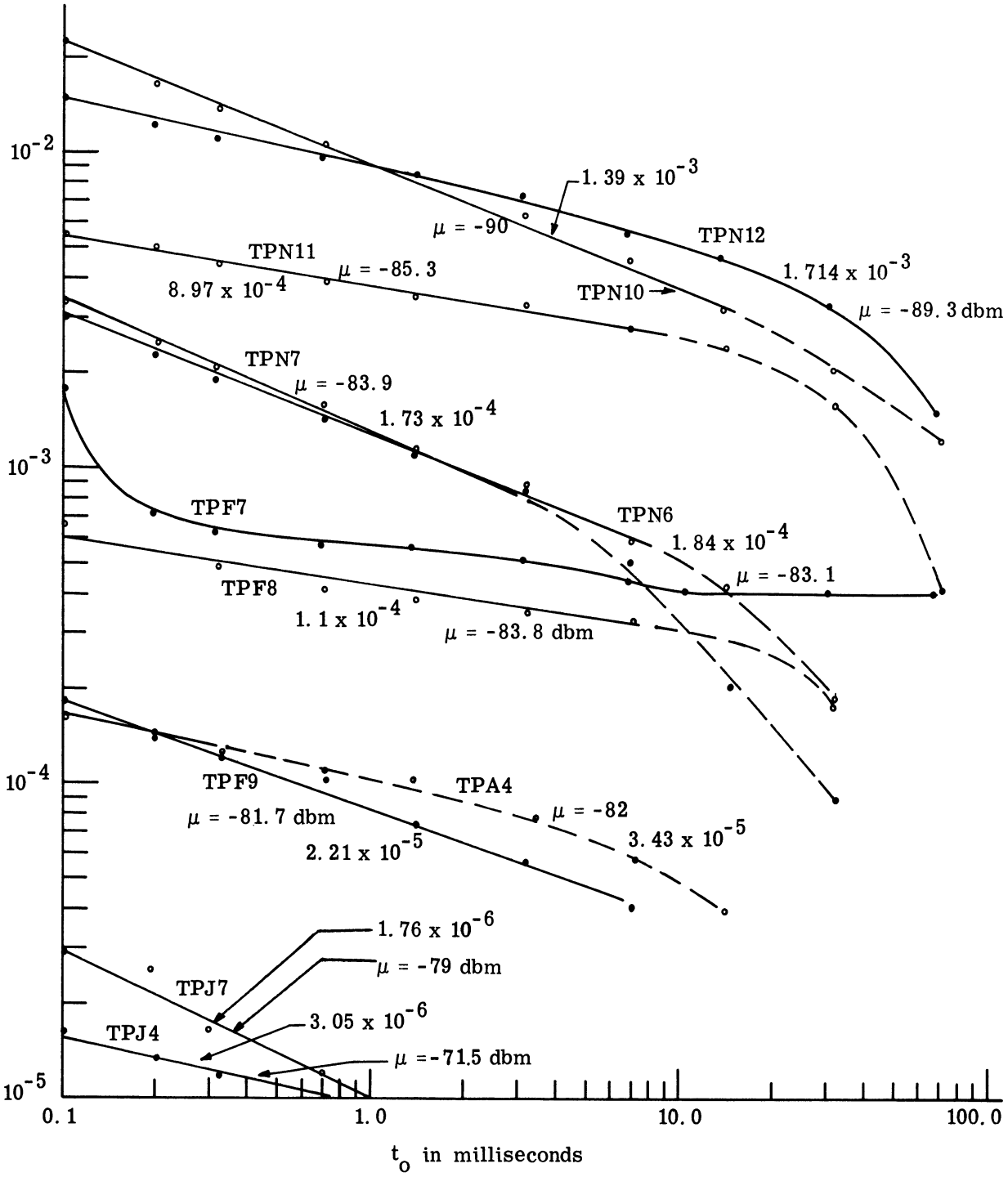


Fig. 5.3a. Fraction of time spent in error runs $\geq$ abscissa.

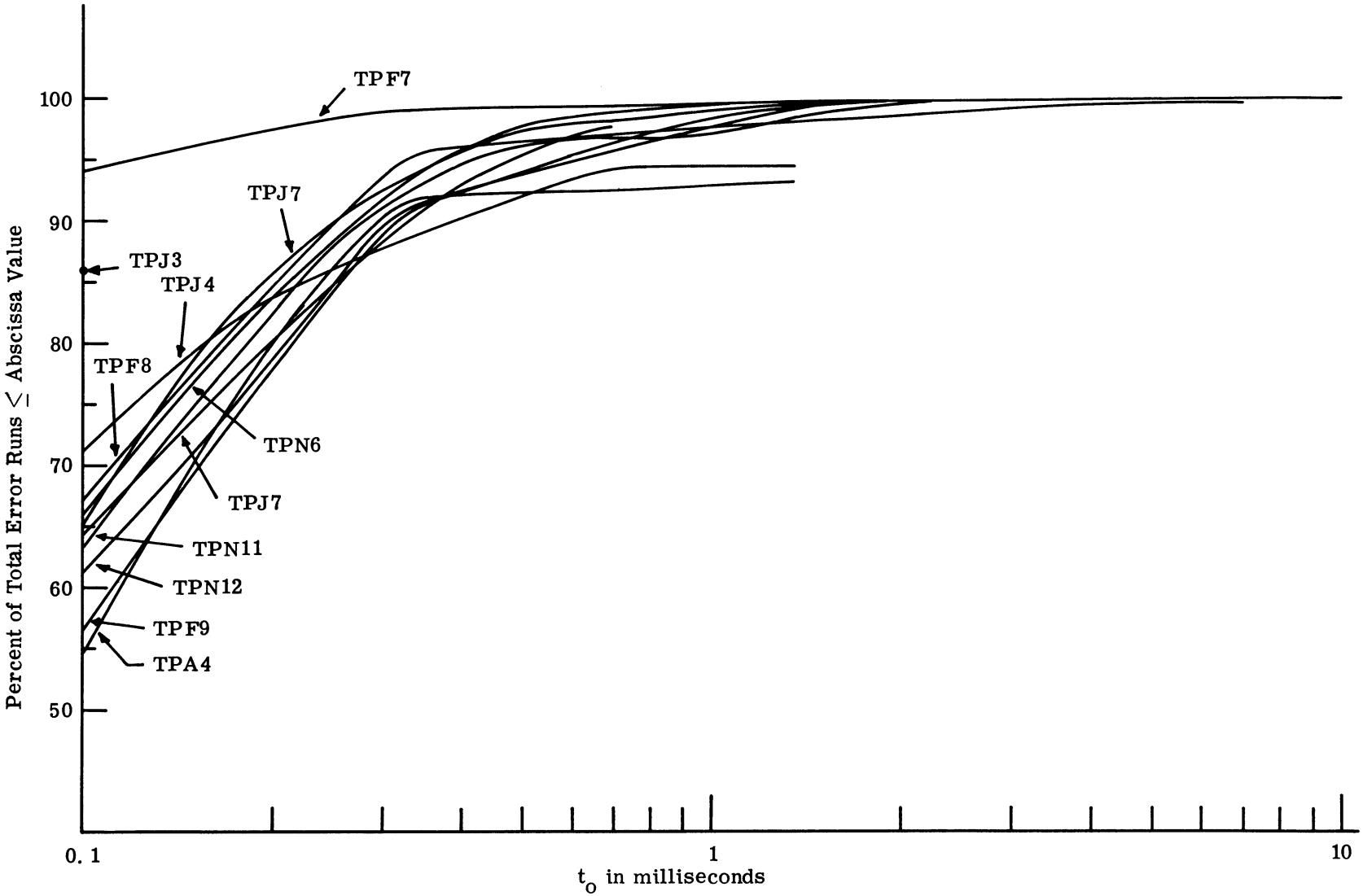


Fig. 5.3b. Percent of error runs $\leq$ abscissa value.

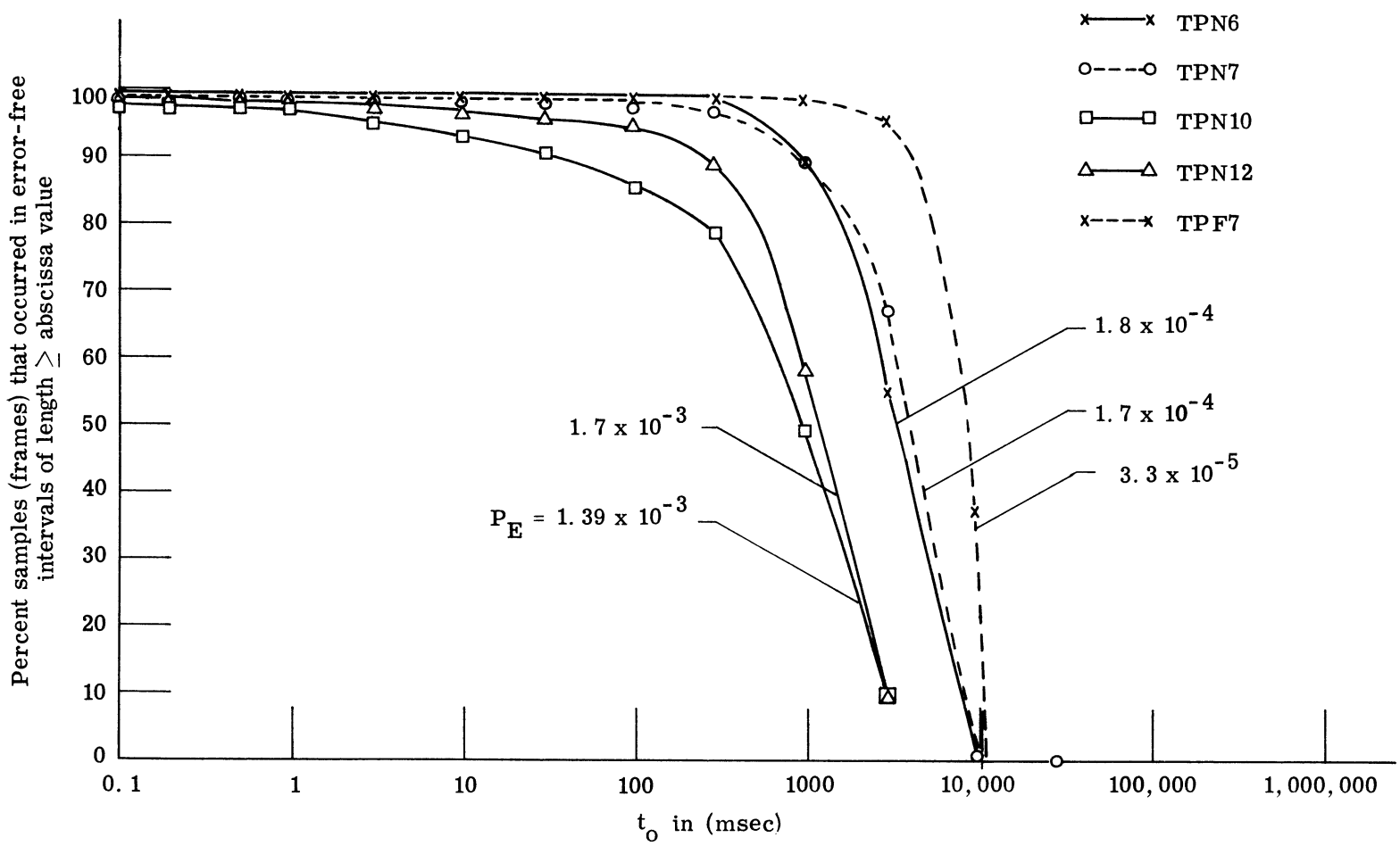


Fig. 5.4. Cumulative distribution of error-free runs.

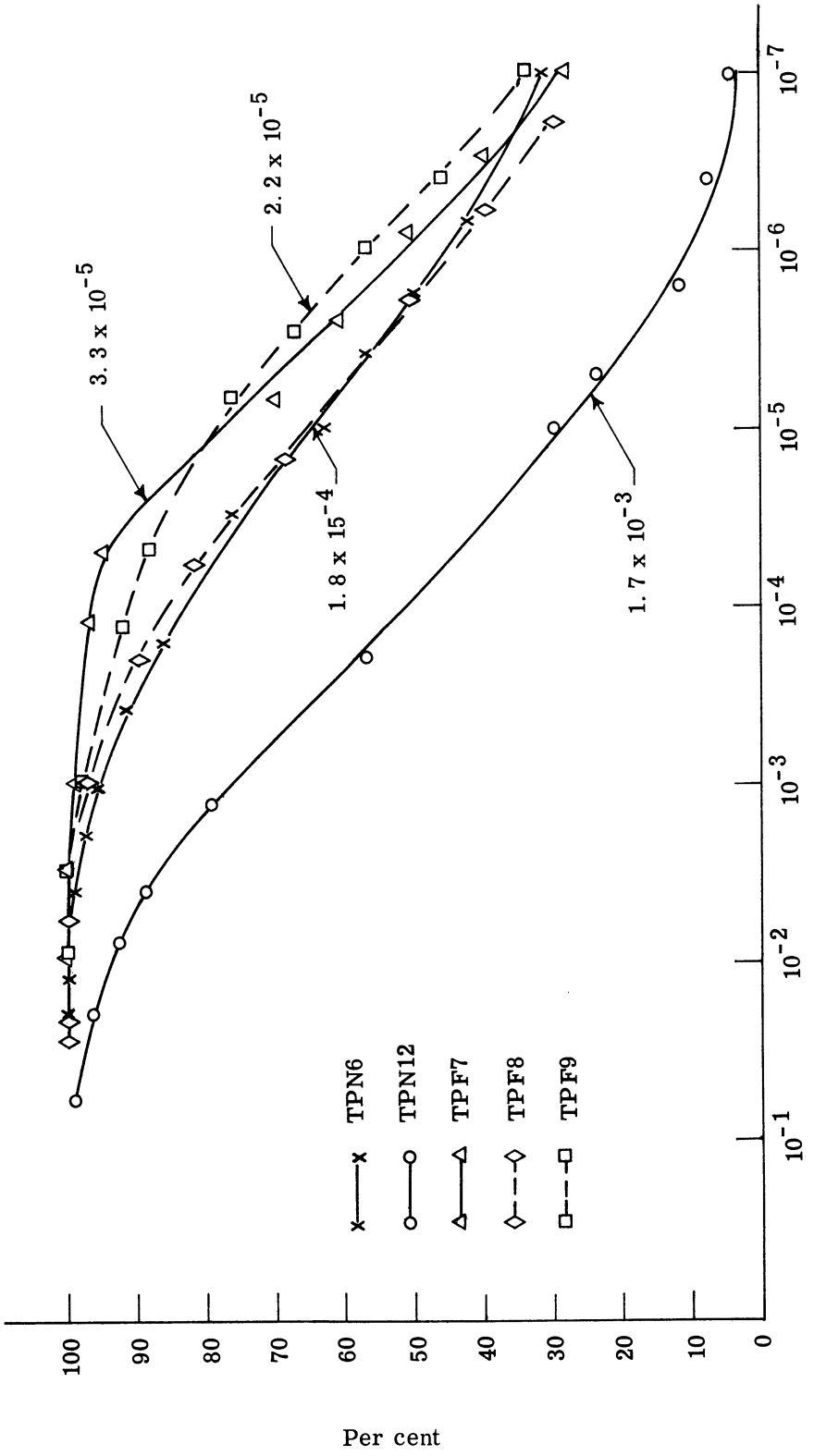


Fig. 5.5. Percent time that the error rate was as good as the abscissa.

## VI. LEVEL CROSSING PROBABILITIES OF DIVERSITY SIGNAL

As was noted in the introduction there are two problems concerned with operating digital systems in the presence of fading. One concerns the probability of error assuming that synchronization is achieved and is successful. The other concerns the effect of the fading on the ability to maintain the synchronism. It will be the purpose in this section to investigate the experimental data in light of the second issue: the effect of the fading on the ability to retain the bit and frame synchronization of the equipment. Assuming that the errors are directly related to signal fades, the crucial problem in assuring successful synchronization is then concerned with the "level crossing" aspects of the fading signal.

In many cases, the synchronization problem can be simplified to guarantee that the sync equipment can tolerate a faded (or loss of) signal for a given amount of time. In such a case, one is interested in the probability of the diversity signal fading below a threshold for a time greater than (or equal to) the tolerable time.

As an example of where it is necessary to deal with such probabilities, consider the frame synchronization in a time-multiplexed PCM system. The basic problem is that there is an ambiguity between the following two states:

(1) The system is still frame synchronized, but the signal is sufficiently bad so that the "decision making" device contains many errors.

(2) The system has lost frame sync, so that whether or not there is a good signal present is not pertinent.

It is clear that here one must know the probabilities of being below thresholds for various times to be able to sensibly design the sync time constants. For this reason, the central problem here is the probability of incurring fade lengths greater than a given length at various fade levels. This was a primary objective for collecting and analyzing the data.

We may note that the error results of the previous section are also directly related to the level crossing probabilities. For example, the curves of Fig. 5.3a give the fraction

of time in error runs greater than or equal to the abscissa. If one assumed a sharp threshold, with no errors when above the threshold and 50 percent errors when below, one could find the level crossing probabilities from such error information. However, the threshold action is actually gradual. Therefore, it is necessary to know the level crossing probabilities in addition to the error performance.

In the past (Refs. 2 and 13), we performed a theoretical estimate of the level crossing probabilities of the diversity signal by extending some known single channel probabilities (Ref. 9). The essentials of these previous analytical attempts are as follows.

In Ref. 9, an analog computer was used to evaluate the level crossing probabilities of a Rayleigh distributed random signal (equivalent to a single channel part of a diversity signal). In this work, the Rayleigh signal was generated by linear envelope detection of a narrowband Gaussian noise. It is well known that the envelope of a band of normally distributed noise approaches a true Rayleigh distribution as the bandwidth approaches zero. Essentially the experiment is run for intervals of length T; the level crossing probability is obtained by repeatedly running these experiments and by counting the number of times in which a fade greater than a length $t_o$ occurs.

To use these level crossing results, the following are required as input parameters:

$f_b$ = fading bandwidth (approximately the average fading rate)

T = observation time over which one observes the waveform

k = fading level (threshold), expressed as fraction of voltage mean.

In terms of these parameters, the precise level crossing probability measured in Ref. 9 is $P(f_bT, f_bt_o, k)$, and is defined as follows:

$P(f_bT, f_bt_o, k) \equiv$ the probability that there are one or more fades of length greater than or equal to $t_o$ during an observation period T.

When measuring the level crossing situation for a Rayleigh distributed waveform (under the given conditions), Favreau (Ref. 9) found that an expression which fits the data quite well is:

$$P(f_b T,\ f_b t_o,\ k) \cong 1 - e^{-P'(0)\, f_b T} \tag{6.1}$$

where P'(0) = average time density of occurrence of events (fades exceeding or equal to $t_o$).

Since Eq. 6.1 is in the form of the cumulative distribution for an event whose probability P'(0) in an independent sample time $\frac{1}{f_b}$ is small, one result of the measurements is as follows: the level crossing situation in a Rayleigh case can be considered as taking independent samples at time intervals $T = \frac{1}{f_b}$. As noted before, $f_b$ is the bandwidth of the Rayleigh signal. Note that we can now interpret P'(0) as being the probability of a fade in the interval $\frac{1}{f_b}$. This result simplifies the level crossing analysis.

Furthermore, the experimental measurements mentioned found the value of P'(0) versus k. P'(0) can be expressed as:

$$P'(0) = I(k)\, e^{-f_b t_o / r(k)} \tag{6.2}$$

where:

I(k) = intercept of Eq. 6.2 at $f_b t_o = 0$

r(k) = reciprocal of slope of Eq. 6.2 on log-log paper.

Using the resulting functions I(k) and r(k), we can find values of P'(0) for any combination of the parameters $f_b$ and $t_o$.

Given that Eq. 6.1 is the level crossing probability (versus fade length $t_o$) for a single channel signal, we then extended this concept to the diversity signal (Ref. 2). This was done by assuming that an equation analogous to (6.1) holds approximate for the diversity signal also. That is, let:

$$P'(f_b T,\ f_b t_o,\ k) \approx 1 - e^{-P'_{1,2}(0)\, f_b T} \equiv P'(t_o) \tag{6.3}$$

where:

$P'(f_b T,\ f_b t_o,\ k)$ = the probability that there are one or more fades of length greater than or equal to $t_o$ during an observation period T, <u>in the diversity signal</u>

$P'_{1,2}(0)$ = average time density of occurrence of fades exceeding or equal to $t_o$, <u>in the diversity signal</u>.

Assuming that the single channel crossing model approximately describes the diversity case, then the issue remained to evaluate $P'_{1,2}(0)$ for the equal-gain diversity case. This was done (Ref. 13), and values of $P'(f_bT, f_bt_o, k)$ were plotted versus observation times T. This was the theoretical estimate of the level-crossing probabilities of the diversity signal mentioned before.

Using measured fade data of the diversity signal, we will now apply the model implied by Eq. 6.3 to these data. Consider again the implications of this model. As for the single channel (Rayleigh) case, one can think of the fading situation as follows. The average fading ($f_b$) can be visualized roughly as providing the "opportunity" for a fade of a certain length. In other words, the average number of times in which the signal is "down" is given by this average $f_b$. Then, in evaluating P', one is in effect evaluating the joint probability of both being down and of staying below a certain level for a given amount of time. As would be expected such a result is dependent on the fine detail of the spectrum.

Another way to express this is as follows: We are assuming that at a given level $k_o$, the frequency of successful fades ($\geq t_o$) is given by the exponential distribution. Since the exponential distribution is the approximation to the binomial distribution (if N is large and p small) this certainly seems intuitively plausible, at least at those levels where fades occur only infrequently.

In applying Eq. 6.3 to our data, the first step is to plot the cumulative distribution of the time spent in fade below a given level. This plot was calculated in our level-crossing computer program (see Section 3.2) by calculating the fraction of time in fade for a time greater than the abscissa value. We will label these values $P'(f_bT, f_bt_o, k)$, or $P'(t_o)$ as a shortened form. With this interpretation the T is the 6-minute data recording period and the $f_b$ is the extant fading bandwidth for that tape.

Figures 6.1 through 6.5 show plots of $P'(t_o)$ versus $t_o$ for various fade levels, for five analyzed tapes. Two sets of curves are on each graph: one set is plotted from an AGC measure of the diversity signal while the other is plotted from a combiner measure of the diversity signal. The AGC ones are marked (A) while the combiner ones are marked (C). The diversity power level obtained directly from the calibration procedure is also shown on each curve. Also, in the box, the numbers show the "db below AGC mean" for each of the levels.

As could be expected from the past discussion (Fig. 5. 2), the AGC set forms a consistent pattern, and the combiner set forms a consistent pattern. Comparing the two, however, shows that the combiner set "looks" more like a lower diversity signal level than the AGC set. This is entirely commensurate with the results of Fig. 5. 2. We had to choose one set as correct to proceed with this issue. The AGC set was chosen because: 1) the AGC consistently shows a good agreement among the single channel versus diversity signal, and 2) using this set gives the conservative results.

Therefore the AGC set was used to "calibrate" the levels for the combiner set. The values shown circled in Figs. 6. 1 through 6. 5 give the estimated levels in db below median[1] for the combiner-derived curves. These estimated combiner curves were used to pursue this issue; they were used instead of the AGC set because they had more sensitivity at the lower signal level. The AGC saturates at the very low signal level.

As additional information, the plots of $P'(t_o)$ using the linear sum signal A + B (see Section 3. 2. 3) are shown in Appendix C, for the same tapes as covered by Figs. 6. 1 through 6. 5. These curves generally corroborate the fade levels determined by the method just described.

Referring to Figs. 6. 1 through 6. 5, it can be seen that all of the graphs, of course, have the same general form on the log-log plots. They are nearly flat and then incur a steep dropoff around 100 milliseconds. These curves can sensibly be compared to those of Fig. 5. 2. The cumulative error run curve of Fig. 5. 2 for TPN6 (Fig. 6. 1) would lie around - 12. 5 db below the mean on Fig. 6. 1. Therefore, in an approximate fashion, the equipment appears to have a threshold at -83. 1 - 12 = -95. 1 dbm. In comparing the other curves (Figs. 6. 2 - 6. 5) with their respective counterparts on Fig. 5. 2, it appears that the equipment can be considered as having a simple threshold about -95 to -97 dbm.

By comparing the curves of Figs. 6. 1, 6. 2, and 6. 3 with those of Figs. 6. 4 and 6. 5 we can note the season-to-season aspect. The November plots are all consistent, and so are the February plots. However, these data suggest that the November signals move deeper from the mean than do the February ones.

---

[1]Note that the mean and median of the diversity signals are fairly close (see Table 3. 5).

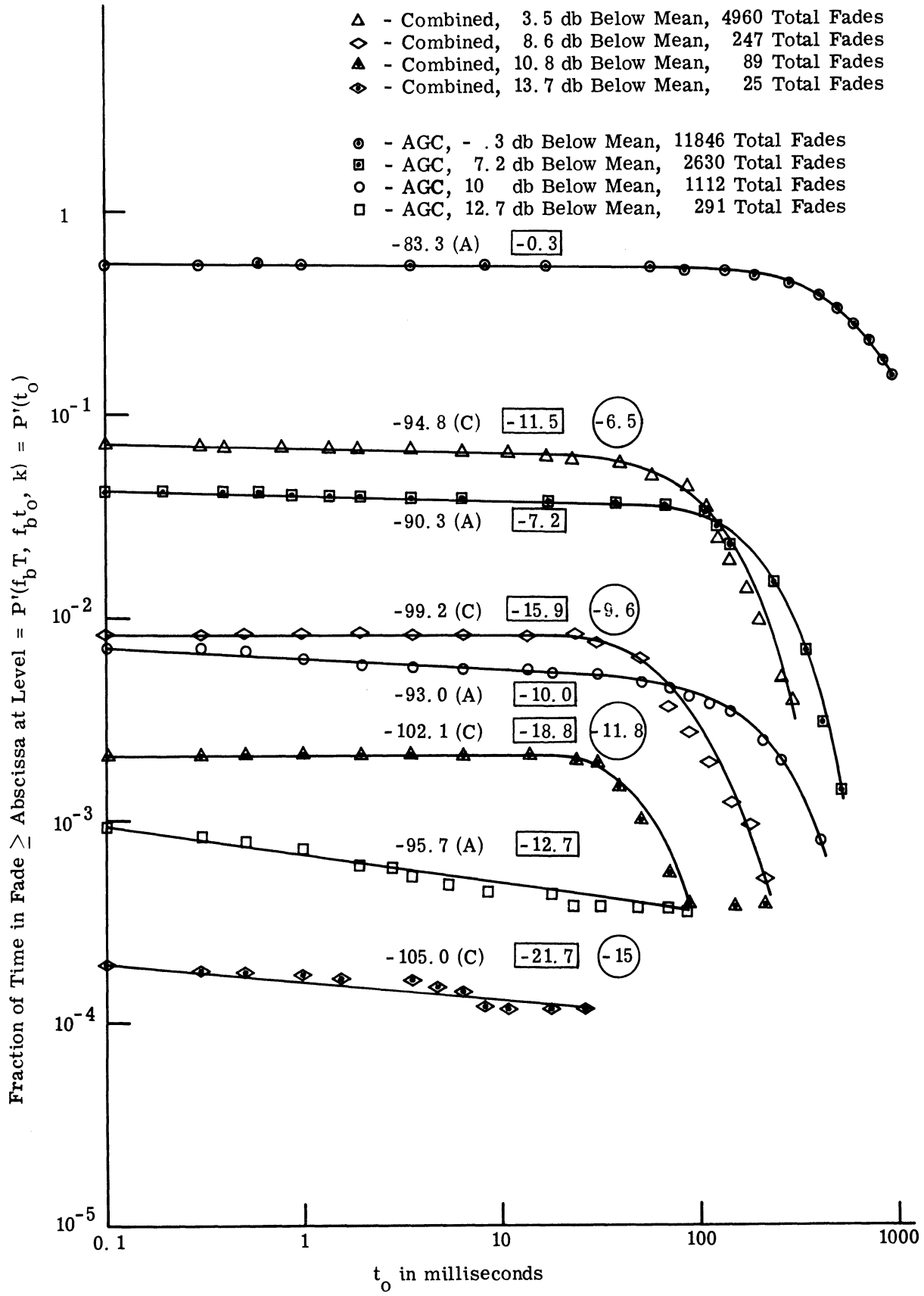


Fig. 6.1. Probability of one or more fades of length greater than or equal to the abscissa, during a period (T) of 6 minutes, for TPN6.

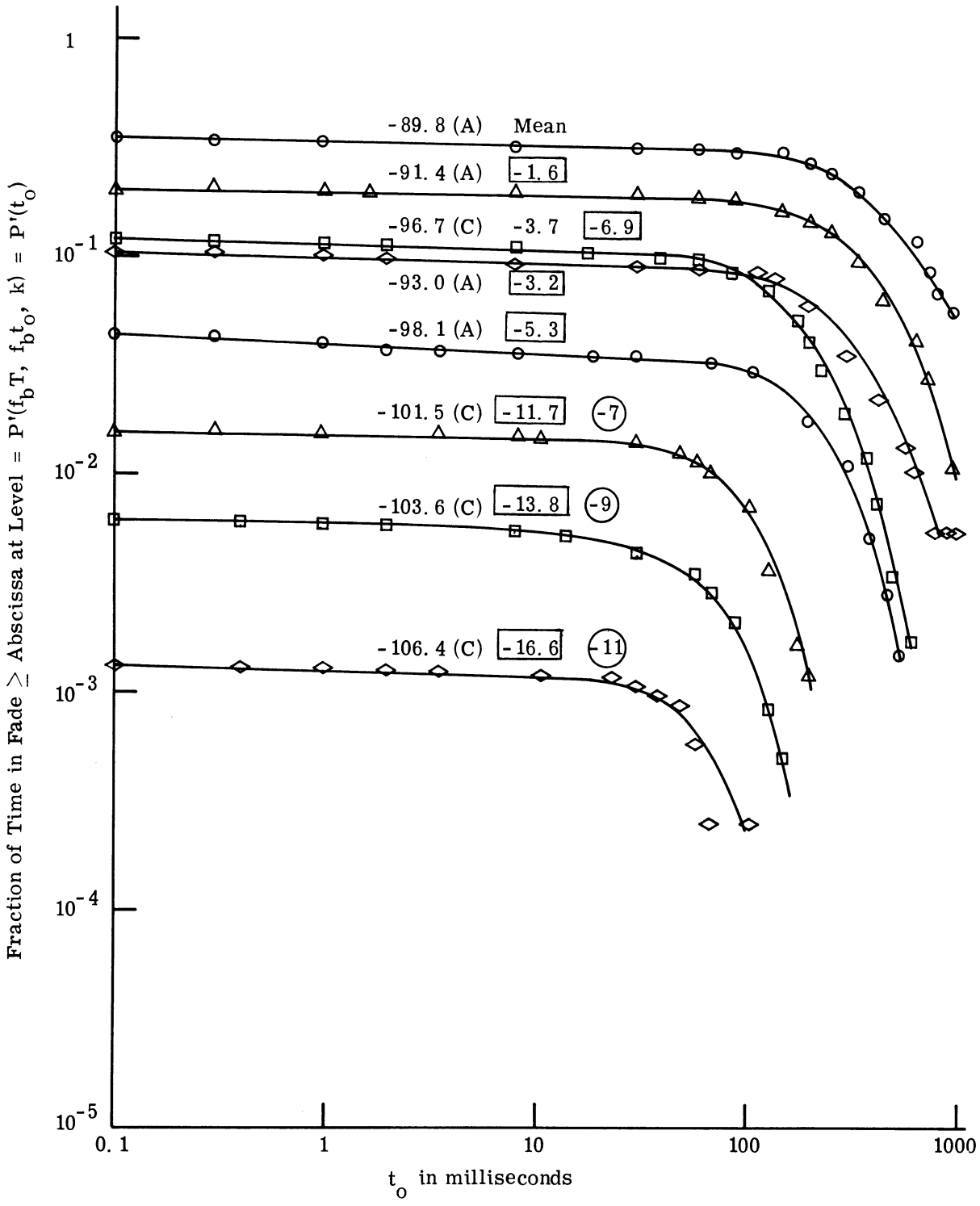


Fig. 6.2. Probability of one or more fades of length greater than or equal to the abscissa, during a 6 minute period for TPN10.

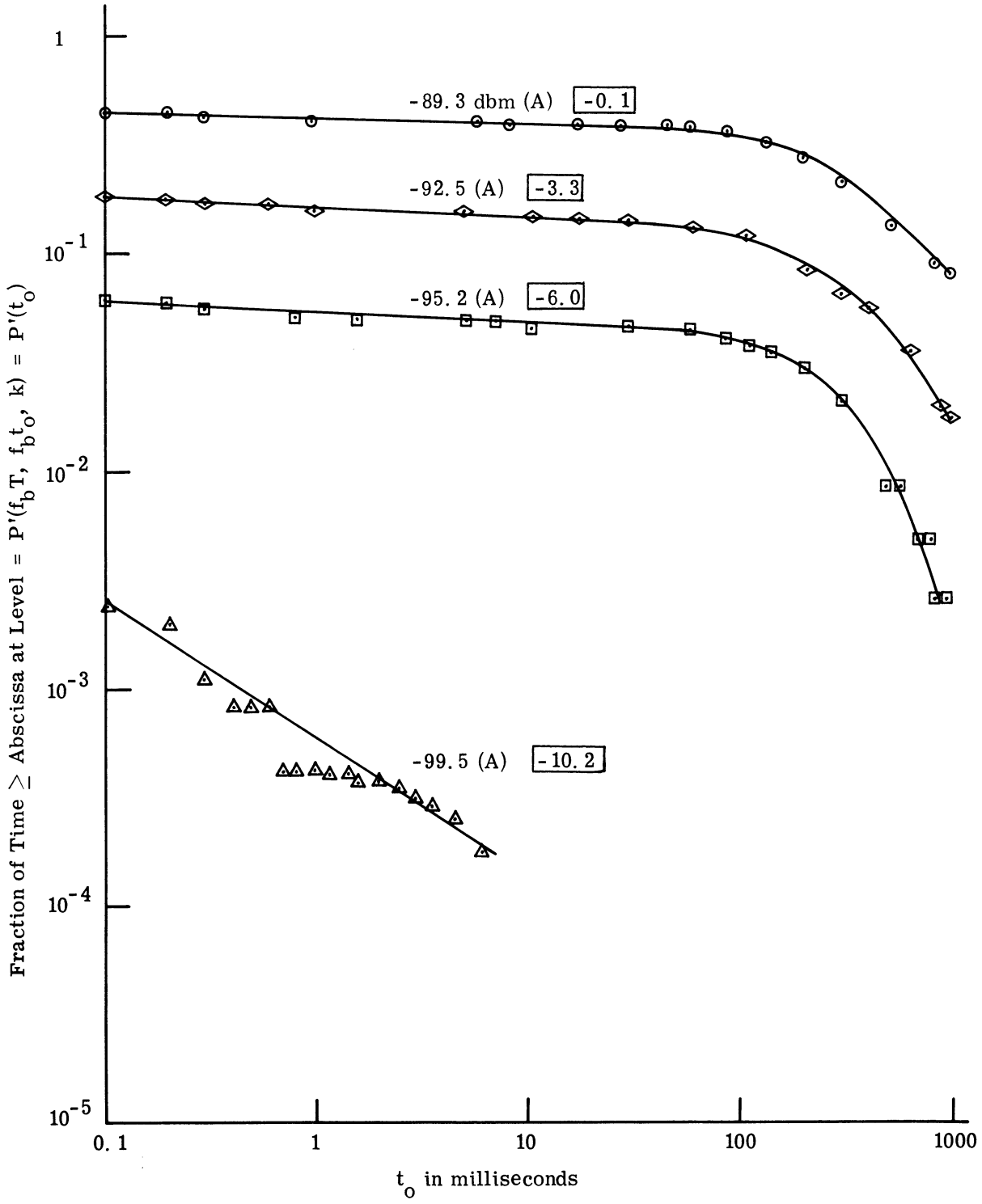


Fig. 6.3. Probability of one or more fades of length greater than or equal to the abscissa, during a 6 minute period for TPN12.

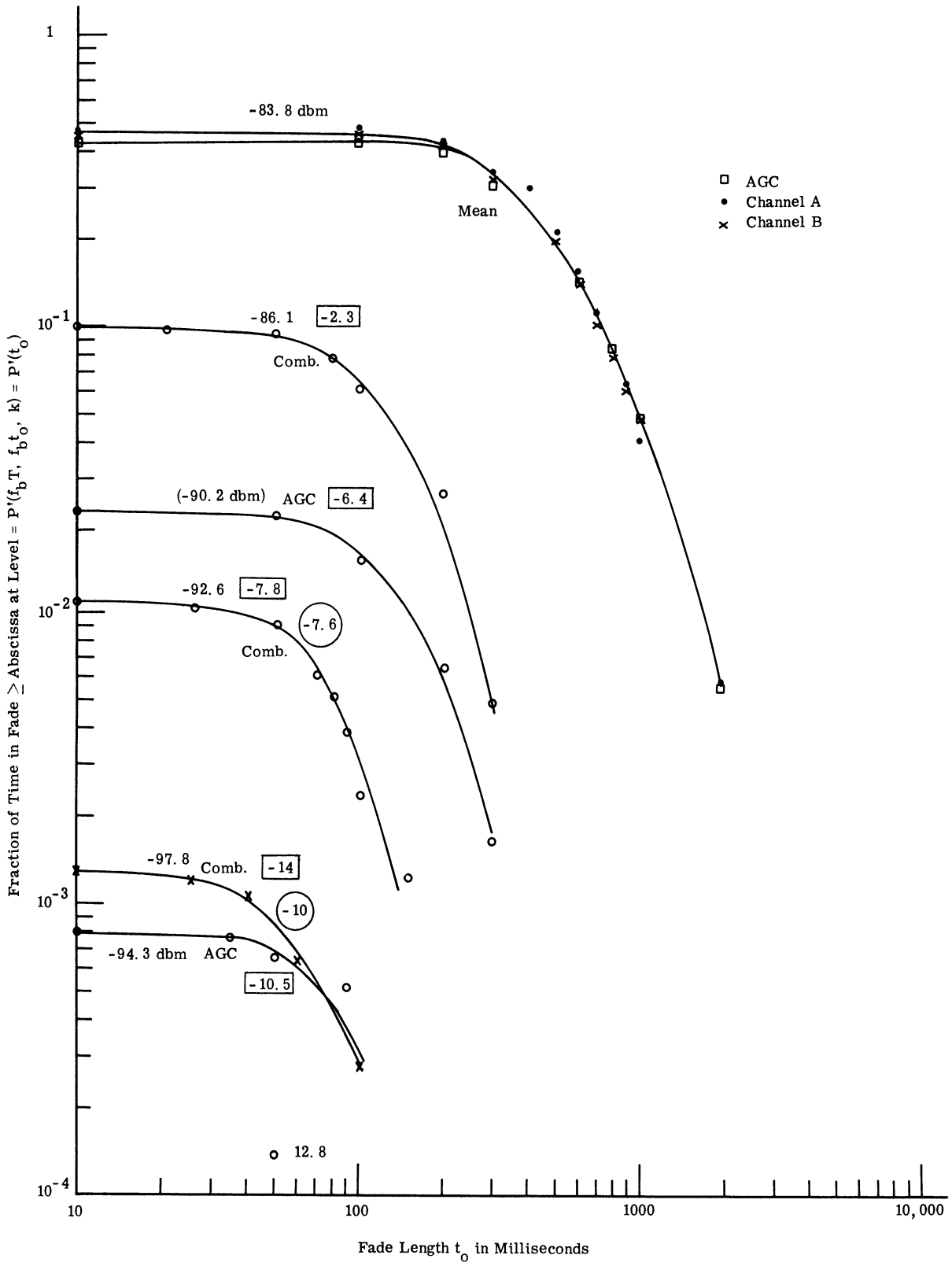


Fig. 6. 4. Probability of one or more fades of length greater than or equal to the abscissa, during a 6 minute period, for TPF8.

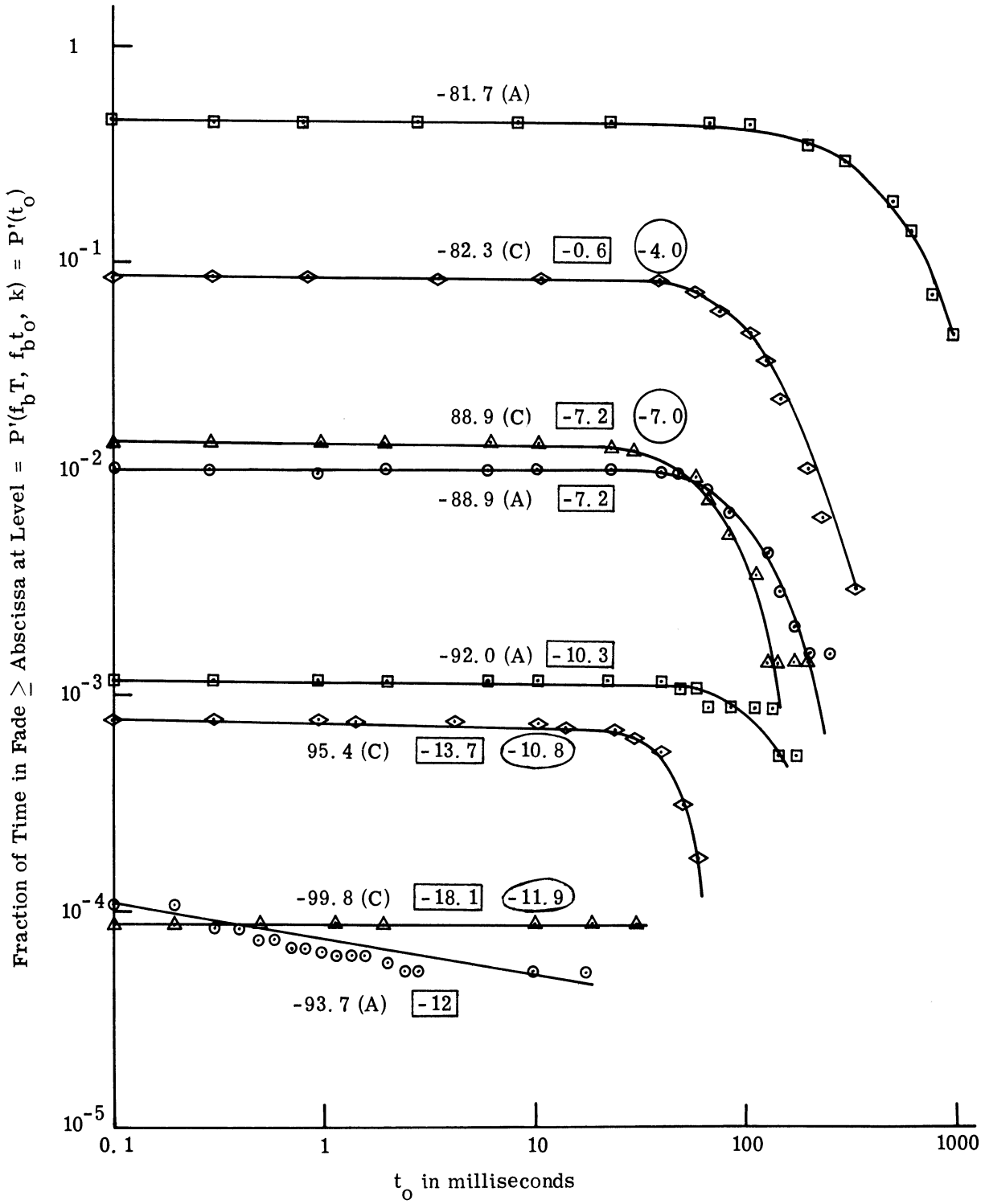


Fig. 6.5. Probability of one or more fades of length greater than or equal to the abscissa, during a 6 minute interval for TPF9.

The next step in finding the level crossing probabilities for any observation time (T) --using the assumptions implied in Eq. 6.3-- is to use the data in Figs. 6.1 to 6.5 and find the $P'_{1,2}(0)$. The resulting plots of $P'_{1,2}(0)$, for all the combiner-curves in Figs. 6.1, 6.2, 6.4, and 6.5, are shown plotted in Fig. 6.6. The $P'_{1,2}(0)$ calculated with Eq. 6.3 is plotted versus the fade length $t_o$ in milliseconds.

It is remembered that we are using the combiner-measured curves for this fade analysis because the AGC saturates at the very low power levels. However, we have used the AGC-generated set to correct (or estimate) the absolute level described by a given curve. This is because we have found that the AGC signal has provided an accurate measure of diversity power, by using the checks described before.

To calculate the $P'_{1,2}(0)$ from the $P'(t_o)$ values, we had to find the fading bandwidth. For this we used the fading bandwidth of the single channel signals. In Ref. 4 it is shown that, for a signal with a Rayleigh distribution and a Gaussian power spectrum with standard deviation $\sigma$, the number of one-way crossings per second is given by

$$N(E) = (8\pi \ell n2)^{\frac{1}{2}} \sigma \left(\frac{E}{E_m}\right) \exp\left[-(\ell n2)\left(\frac{E}{E_m}\right)^2\right] \qquad (6.4)$$

where:

$E$ = the signal level in volts

$E_m$ = the mean signal level in volts

$\sigma$ = the standard deviation of the Gaussian spectrum.

Given the experimental number of one-way crossings at a particular level, Eq. 6.4 can be solved for the standard deviation of the spectrum $\sigma$. Reference 4 notes that the bandwidth $f_b$ of a flat power spectrum equivalent to the Gaussian spectrum with standard deviation $\sigma$ is

$$f_b = \frac{1.25\,\sigma}{2\pi} \qquad (6.5)$$

where $f_b$ is in cycles per second and $\sigma$ is in radians per second. Since our level crossing program found the number of crossings at the mean of channel A and channel B (see Section

3.2), we found that $f_b$ for the various types using the relation (from Eqs. 6.4 and 6.5)

$$f_b = 0.0953\ N(E_m)\ \text{cps} \tag{6.6}$$

where:

$N(E_m)$ = number of one-way crossings at the mean, per second.

Although the fading bandwidths are included in Table 3.5, the short table below summarizes the $f_b$'s used in the calculation of $P'_{1,2}(0)$.

| Tape No. | $f_b$ of Channel A | $f_b$ of Channel B | Estimated $f_b$ |
|---|---|---|---|
| TPN 6 | 2.68 | 2.065 | 2.68 |
| TPN10 | 2.24 | 2.36 | 2.36 |
| TPF 8 | 3.03 | 1.772 | 3.03 |
| TPF 9 | 3.64 | 1.915 | 3.64 |

Table 6.1. Fading bandwidths.

In Fig. 6.6 the numbers on the curves give the values, for each tape, in db below the median. As mentioned previously, the AGC fade curves were used to estimate these values. The curves of Fig. 6.6 also indicate that the November tapes are consistent among themselves, as are the February ones. However these data do show a discernibly different statistical fade behavior between November and February.

Although we have considered the $P'_{1,2}(0)$ of Fig. 6.6 as a means of evaluating the level-crossing probabilities in general (next figure), the curves in Fig. 6.6 indicate some direct conclusions regarding sync. Given that the median signal is fixed by the transmitted power-path loss situation, and the receiver threshold is given in absolute dbm, one can locate the proper curve on a set such as in Fig. 6.6. The nature of the curves indicates that there is a fairly sharp threshold with regard to "tolerable fade lengths." That is, there is little profit in increasing the synchronization tolerable fade lengths until one reaches the knee in Fig. 6.6. Assume that we have a threshold -10 db below the median signal. Then we see that increases in tolerable fade lengths are relatively profitless until 30 to 40 milliseconds.

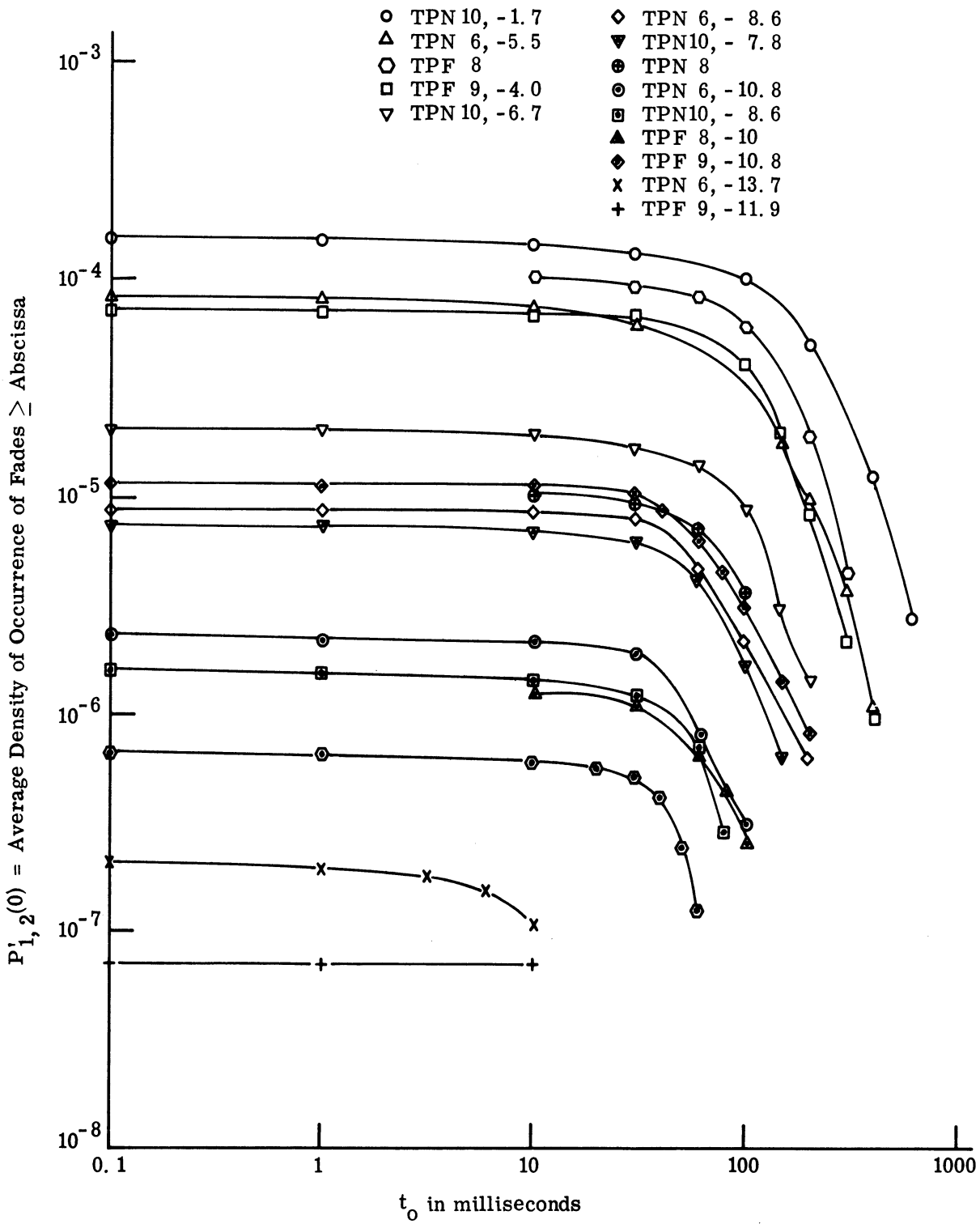


Fig. 6.6. Average time density of occurrence of fades greater than or equal to the abscissa value.

Increases in tolerable fade lengths beyond this point reduce the fade probability by a substantial amount.

Using the $P'_{1,2}(0)$ of Fig. 6.6 and Eq. 6.3, we can now predict the level crossing probabilities for any fading bandwidth and observation time product ($f_b T$). Curve of $P'(t_o)$ versus $f_b T$ are shown in Fig. 6.7 for the November data, and Fig. 6.8 for the February data. For both graphs, the $P'_{1,2}(0)$ value was estimated by grossly averaging the values from the respective two tapes.

It was mentioned earlier that this $P'(t_o)$ versus $f_b T$ was estimated earlier (Refs. 2 and 13) by theoretically predicting the change from a single channel case. Comparing the previous theoretical estimates to the experimental curves here, we find that their probability of fades, in a given time, is far lower here than was previously estimated.

Using Fig. 6.7, let us consider an example. Let us assume that the synchronization threshold of interest is about 10 db below the median, and that we cannot tolerate fades longer than 100 milliseconds. Assume an $f_b$ of 2 cps. From Fig. 6.7 we see that the probability of exceeding such a fade in 500 seconds (about 8.3 minutes) is of the order of $2.5 \times 10^{-4}$. The probability of exceeding this fade in an 8 hour period would be of the order of $1.4 \times 10^{-2}$.

Similar data can be extracted from the February curves in Fig. 6.8.

The curves of Figs. 6.8 and 6.9 are some of the most important results of this data recording and analysis. Using the 6-minute samples of data, and the assumptions inherent with Eq. 6.3, we can predict the probability of exceeding given fade lengths during any period of time. The alternative to this procedure would be to take link data over a very long time, and do a level crossing analysis on the large amount of data.

Finally, Fig. 6.9 shows $P'(t_o)$ as a function of $t_o$ for three different observation times ($f_b T$). This shows, for a given observation time, how the probability of exceeding a given fade length will change with respect to increasing the $t_o$. The data here used the -10 db curve for TPN6 (in Fig. 6.6). It can be seen that not much improvement in the probability is obtained until the tolerable fade length $t_o$ reaches the order of 30 milliseconds. Then the probability drops steeply. Consequently, if one can extend the permissible $t_o$ (or tolerable fade) beyond 100 milliseconds, one can obtain sizeable reductions in the probability of exceeding the critical fade.

Figure 6.10 shows the average fade length versus db below median for three data

tapes. For these plots the AGC level crossing information was used. It was found that the combiner level crossing information gave a rather erratic median fade length versus db below the median. We attribute this to the inaccuracy of the "level" reading for the combiner signal (discussed in Sections 3. 1 and 4. 1). As expected, the average fade length in milliseconds decreases as one goes below the median. The average fade lengths are much smaller than have been predicted for convoluted Rayleigh signals (Ref. 4). We attribute this to the fact that specular fading reduces the fade length, and also to the fact that any "hunting" on the part of the coherent diversity combiner will contribute to shorter diversity signal fades.

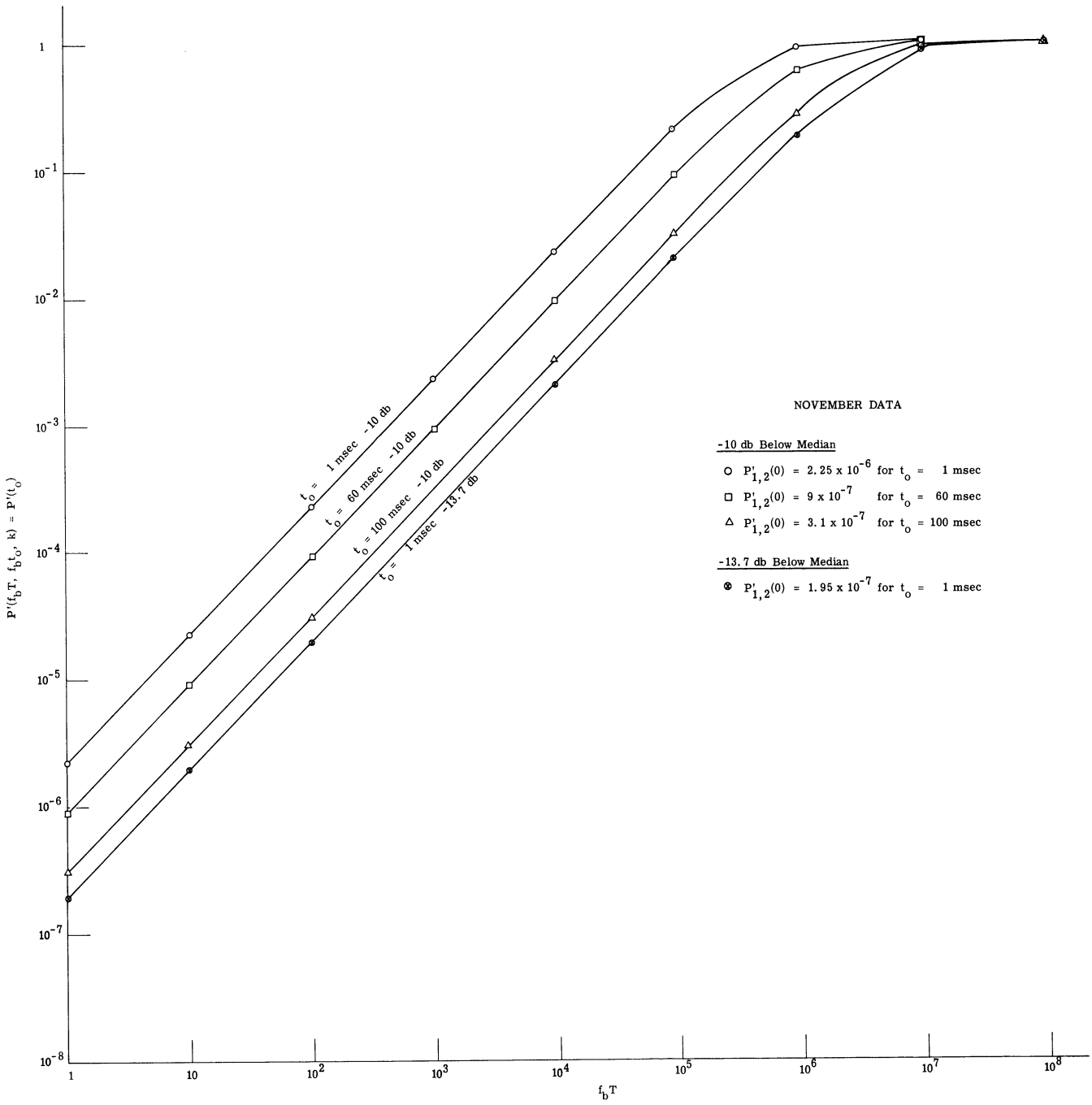


Fig. 6.7. Probability of one or more fades of length greater than or equal to the $t_o$ shown, in a time $f_bT$.

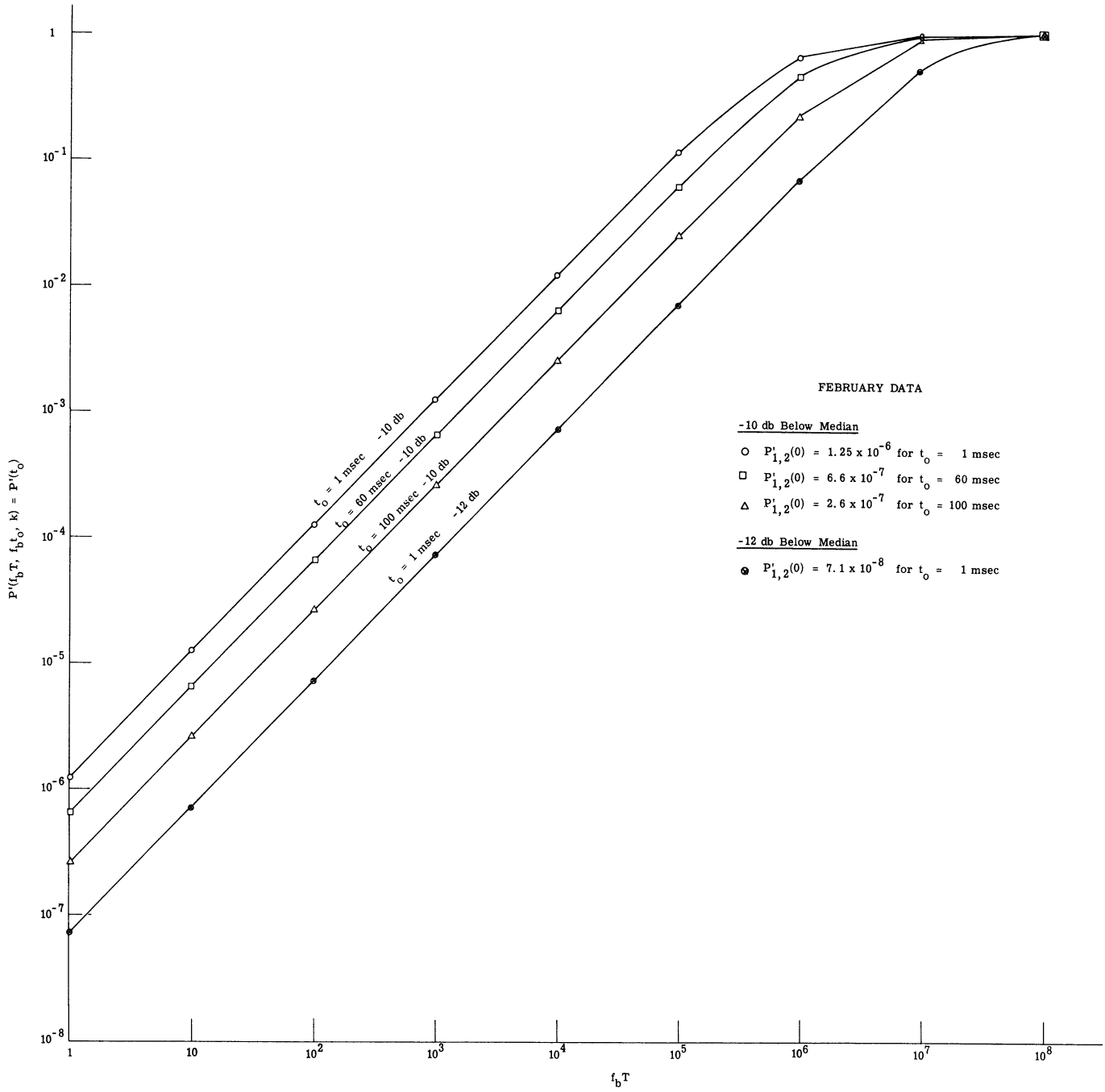


Fig. 6.8. Probability of one or more fades of length greater than or equal to the $t_o$ shown, in a time $f_bT$.

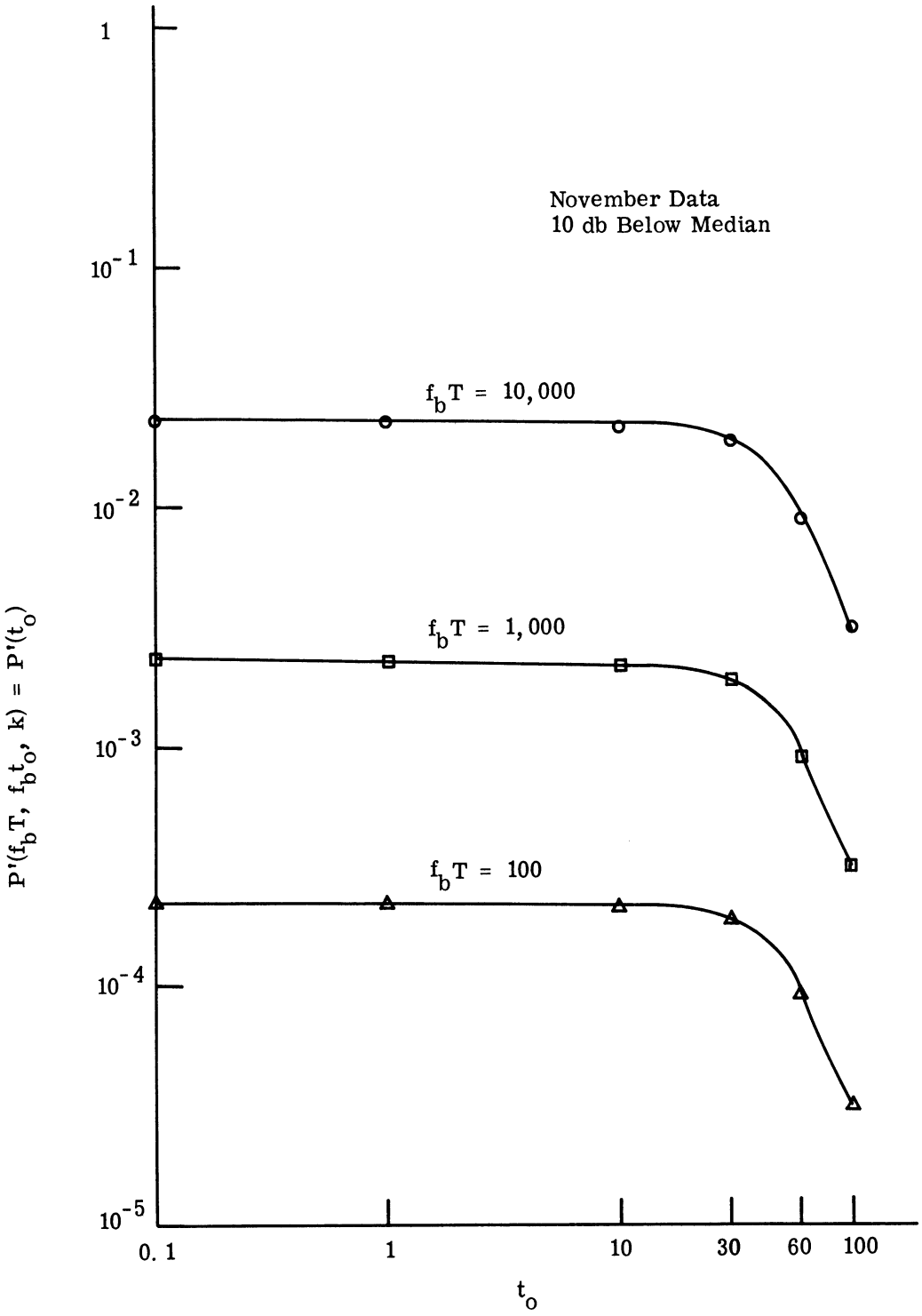


Fig. 6.9. Probability of one or more fades of length $\geq$ abscissa, for three observation times.

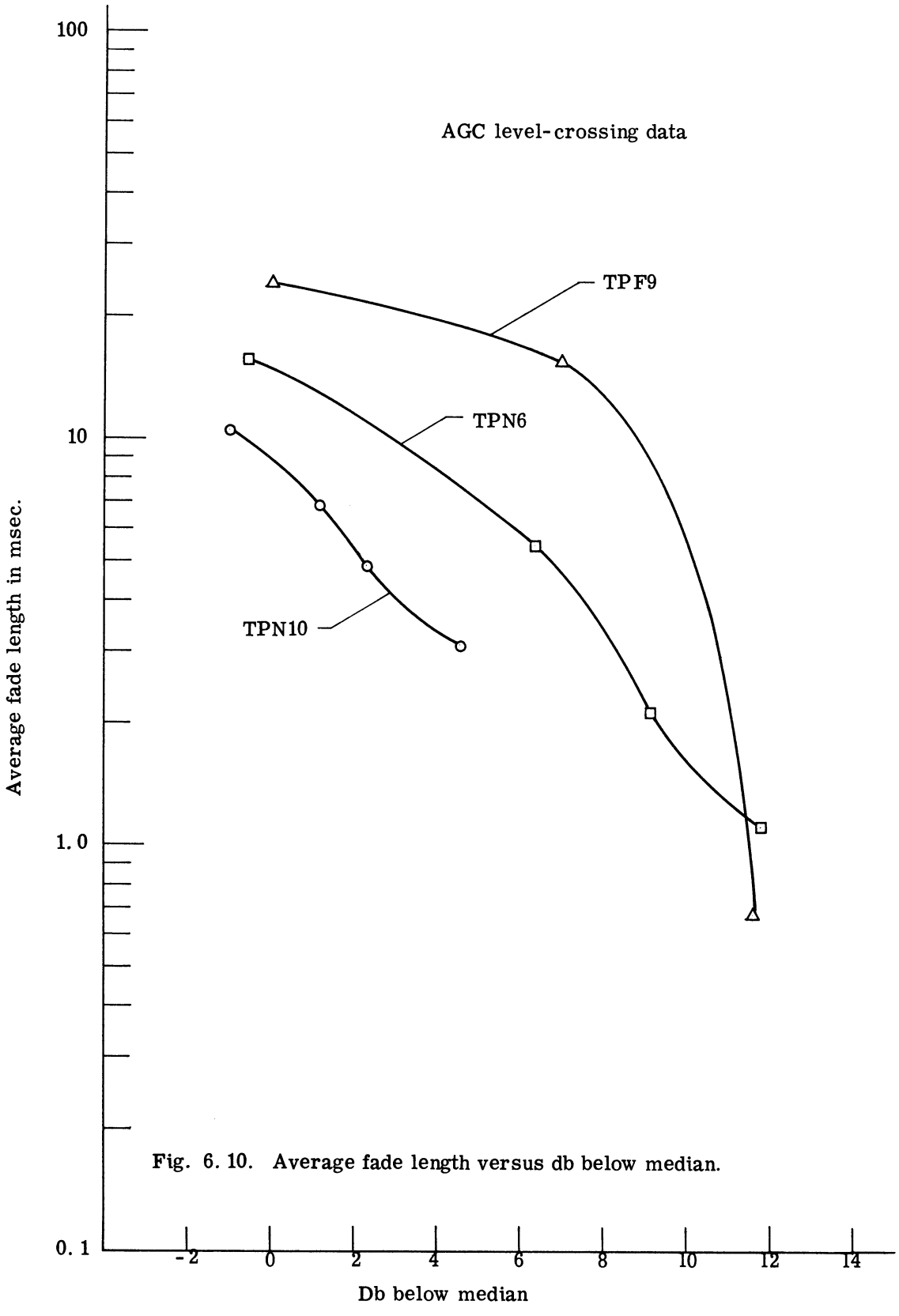


Fig. 6.10. Average fade length versus db below median.

## VII. CONCLUSIONS

The error and signal performance of troposcatter links are a function of three items: natural signal behavior (including fading, weather and seasonal effects), unnatural effects (such as specular fading), and terminal equipment behavior. When viewing any experimental results these three items must be kept in mind.

We will discuss the conclusions in terms of the following six areas:

1. An important conclusion from these data is that the role of specular fading as caused by airplanes must be brought to the forefront in considering tactical troposcatter links. The incidence of such specular fading in a tactical situation is going to be continuously increased. (For a strategic troposcatter link, the airplane specular fading issue will depend on the proximity of the common volume to airplane traffic.) Another reason for emphasizing specular fading is that much of the classical theory and discussion deals with the convoluted Rayleigh fading signals and ignores the specular fading issue.

During specular fading, two major changes occur on the tropo system. First, the specular fading greatly increases the fading rate of the single channel signals. The rate increases from the order of a few cycles per second to the order of 30 to 50 cycles per second (when the airplane is both approaching and receding from the common volume). This will affect the time constants of the synchronization circuits.

Second, the pattern of the error bursts is changed by the specular fading. Without specular fading, the errors tend to occur in single (relatively isolated) bursts. With the specular fading occurring while the airplane is approaching or receding, groups of error bursts tend to occur. When the airplane is in the common volume, of course, the signal is higher than otherwise and there should be no errors during that period.

In general then a major conclusion of these data is that specular fading should be included when designing synchronization circuits, and when performing error predictions.

2. A second conclusion concerns the particular equipment operation encountered here. First, it appears that the equipment, so far as error performance is concerned, could

be modeled by a sharp threshold occurring around -95 to -97 dbm. This is indicated by the $P_E$ versus carrier level curves (Fig. 5.2), and by comparing the fraction of time spent in error run curves (Fig. 5.3a), with the fade probability curves of Figs. 6.1 through 6.5.

A peculiarity of this equipment is that the error runs slightly precede both the combiner signal (dip) and the AGC peak. The error run peaks first, the combiner next, and then the AGC. This is evident from the figures of signal behavior in Section 3.1. This phenomenon also can be seen on the computer table printouts of the error count at each signal level, and from the scatter diagram printout of signal A and signal B during errors (neither of these printouts could sensibly be shown in a report).

The $P_E$ versus carrier level curves of Fig. 5.2 also show this "phase difference." As can be seen in Fig. 5.2, the poorest $P_E$ does not occur at the lowest carrier level encountered. It should be remembered that the $P_E$ behavior is determined by the combination of the selective fading behavior and the equipment response. It would be desirable to have, as auxiliary data, information about mathematical mode descriptions (such as the differential delay) when interpreting the behavior. Any future data should multiplex such data with the type taken here.

The data and pictures suggest that the errors are proportional to the combination of "low carrier level" and "rapidity of carrier change." In any event, it does appear that any such action is because of the manner in which the coherent phase combiner (of the equal-gain combiner) operates.

Finally, we found that the combiner measure of the carrier level was consistently lower than the AGC measure. Since the AGC measure yielded good checks, we relied on the AGC signal as the measure of the carrier level.

3. The error results found here have shown that the longest error run encountered lasted 15 milliseconds (Fig. 5.3b). Also, 90 percent of the error runs are less than 0.4 millisecond in length.

Conversely for the intervening error-free runs, 90 percent of the error-free runs were greater than 30 milliseconds for the poorest $P_E$ encountered ($P_E$ of $1.39 \times 10^{-3}$--Fig. 5.4). For the best $P_E$ encountered in Fig. 5.4, 90 percent of the error-free runs exceeded four seconds.

At the poorest $P_E$ of $1.7 \times 10^{-3}$, the error rate was better than $4 \times 10^{-3}$ for 90 percent of the time (Fig. 5.5). At the best $P_E$ of $3.3 \times 10^{-5}$ the error rate was better than $3 \times 10^{-5}$ for 90 percent of the time. A rule of thumb appears to be that the locally averaged $P_E$ rate will be exceeded approximately 90 percent of the time.

4. For the diversity signal fade behavior it was found, under the given assumptions, that the probability of achieving a fade 10 db below the median for a time greater than 100 milliseconds in an interval of 8 hours is about $1.4 \times 10^{-2}$ (Fig. 6.7). This indicates that fading margins of 10 to 15 db and tolerable fade lengths of 100 milliseconds or greater should result in successful synchronization.

For any given fade margin, it has been shown that increases in tolerable fade length are not profitable until one reaches the area of 30 to 50 milliseconds (Fig. 6.6). Increases in tolerable fade lengths beyond 30 to 50 milliseconds sharply reduce the probability of encountering such fades.

5. We saw that the single channel curves have essentially a Rayleigh distribution, perturbed in the expected manner by specular fading.

6. With regard to seasons, our data have not shown any substantial variation from season to season. Rather the data here are most strictly correlated with the total error rate. Although we did see discernible differences in the cumulative behavior of the signal (between November and February), the error performance does not show any appreciable change with season. This is probably because such random variables as specular fading and weather conditions cover up small changes in error behavior. Therefore, we are led to the conclusion that the major error behavior can be predicted simply by knowing the mean or median, and dealing with the relative db.

## APPENDIX A

## THE EXPERIMENTAL EQUIPMENT

E. P. Gould

The basic experimental block diagram is shown in Fig. 2. 2 of Section 2 in the text. The material here expands, where necessary, on that description.

The way in which the error count is formed, and the timing with which this error count is sampled along with the other signals is shown in Fig. A. 1. This figure shows the interface equipment between the tropo receiver and our multiplexer. From the tropo receiver, we obtain the three outputs for the amplitude samples of the three signals. In addition, the two error signals from the terminal equipment are:

1) an indication a bit error has occurred,

2) a clock signal which indicates when a bit has arrived.

The occurrence of a bit error is indicated by a negative pulse output formed by using digital logic on signals internal to the error detection circuitry. A basic 288-kc positive pulse clock with a one-one correspondence with every two incoming data bits is provided by a second test point of the terminal equipment. The basic idea behind processing these two signals to form an analog waveform whose height is proportional to the number of bit errors per frame is as follows:

(1) The 288-kc clock pulses are counted down in a special flip-flop count-down circuit. This circuit puts out pulses corresponding to each frame (whether 14, 28, or 56 bits) and a basic clock pulse of 41, 142-kc to drive the A-D/tape unit. The pulses corresponding to each frame are used to transfer data to a flip-flop buffer and to reset the bit error counter.

(2) The bit error pulses are counted in a basic flip-flop counter. This counter can be reset by a frame pulse in 0. 5 microsecond so that no bit error pulses are dropped at the end of a frame. At the end of each frame, the contents of each stage of the counter are read out into a flip-flop buffer. The contents of this buffer are automatically transferred to a D-A unit which converts the input bits to a voltage level proportional to the number of errors

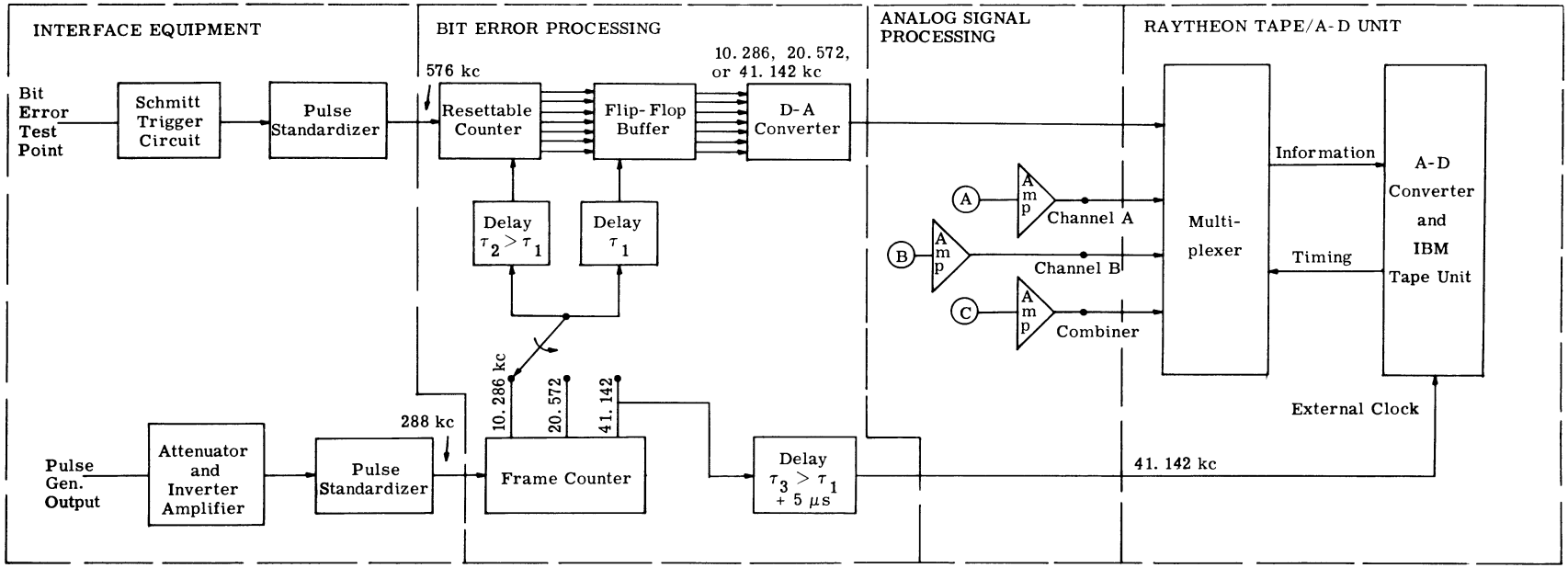


NOTE: The D-A and multiplexer timing is independent of the resettable counter because of the flip-flop buffer. The criterion on the delay $\tau_3$ is determined by the amount the auxiliary analog signals are sampled in time behind the actual bit error per frame count.

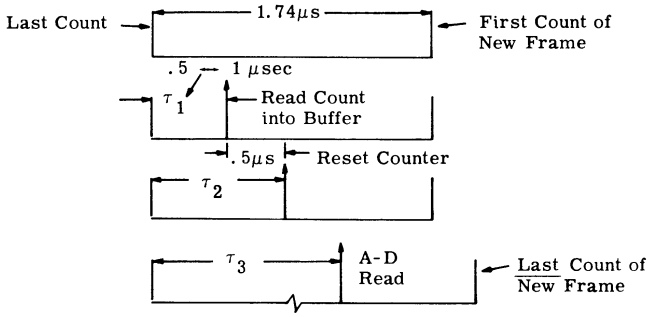


Timing Diagram

Fig. A. 1. Timing system and frame error counter.

counted in the frame.

The proper transfer of bits necessitates the use of delays of the proper magnitude, as indicated by the timing diagram of Fig. A. 1. A more detailed discussion of the original circuitry is contained in Appendix A of Ref. 13. Since the basic equipment was described in detail in that predecessor report, here we need only describe the modifications made since the reporting time of Ref. 13. These modifications were made both to increase the reliability of the equipment and to improve its performance.

## A. 1 The Test Equipment

A block diagram of the entire system was presented in Fig. A. 1. Referring to this block diagram, we can divide the system into the following sections:

1) Error detector circuit
2) Inverter amplifier
3) Pulse standardizer
4) Resettable bit error counter
5) Flip-flop buffer
6) Frame counter
7) Delay units
8) D-A converter unit
9) Analog amplifiers
10) Multiplexer A-D conversion equipment, and IBM tape deck.

Of these units, differences from the equipment described in Ref. 13 exist only in units 1, 6, and 9. Only these three equipment units are described in this appendix. A description of the remaining units can be found in Appendix A of Ref. 13.

A. 1. 1 Error Detection Circuit. A completely new interface circuit between the RCA data processing equipment (Ref. 7) and the Cooley Electronics Laboratory data processing equipment was developed. Internal circuit points of the error detection chassis, instead of the bit error pulse output previously used, were used as inputs to an interface circuit.

Inputs to the new interface circuit were taken from test points 3 and 4 of the error detection chassis. Test point 4 provides a locally generated 576-kc reference pulse train synchronized with the incoming information bits. Test point 3 provides the output of a multivibrator which fires every time there is no error. These signals were combined to provide a negative-going pulse from zero volts to -6 volts each time an error occurred. These error

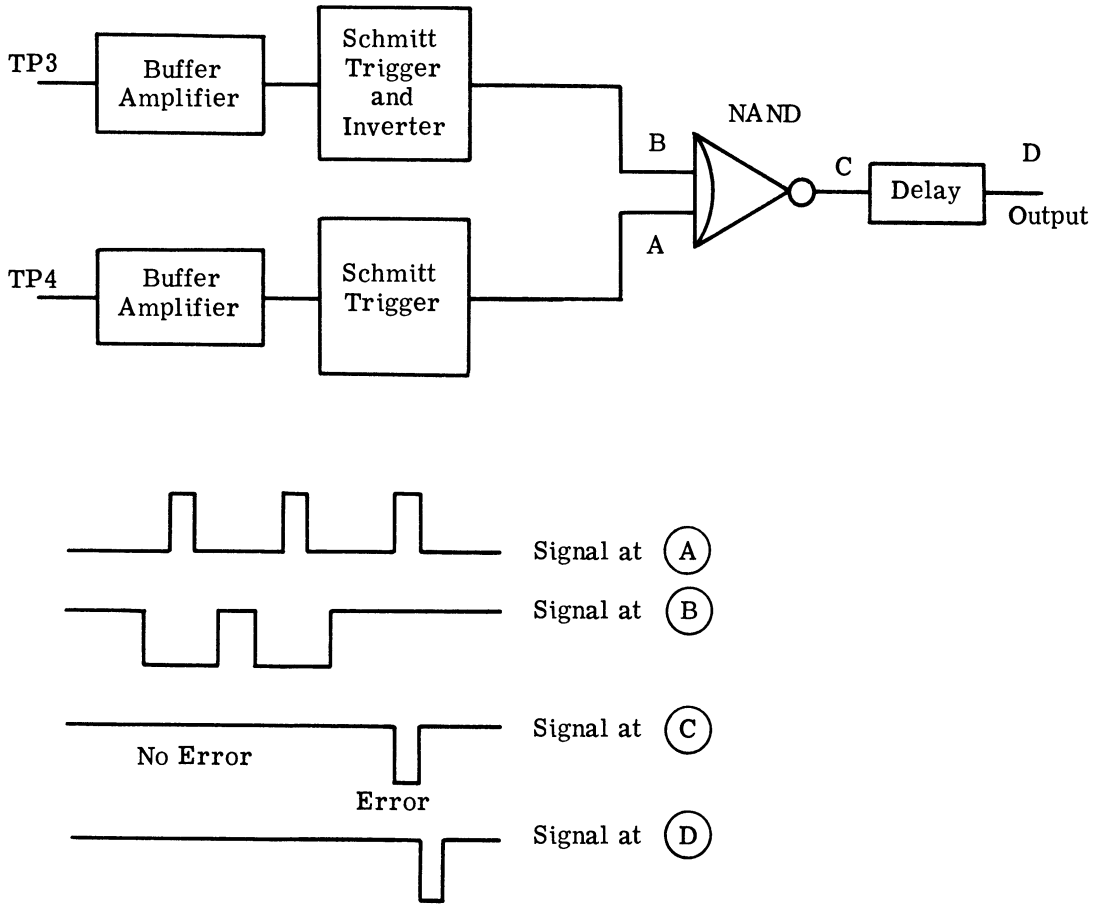


Fig. A. 2. Logic diagram and waveforms of interface circuit.

pulses were then fed into the data processing equipment. A logic diagram of the circuitry that was used is shown in Fig. A. 2. The final output pulse, which corresponds directly to an error, was used to drive the Cooley system and also a counter. The counts on this counter were compared directly with the counter tied to the error detection chasses. During the tests, it was found the counter agreed exactly on almost all runs. This indicated that the RCA and Cooley systems operating in parallel were receiving the same data.

The buffer amplifiers (Figs. A. 2 and A. 3) that were used to interface with test points 3 and 4 were designed and built by R. Lillie of Cooley Electronics Laboratory. The remainder of the logic was Raytheon digital logic cards.

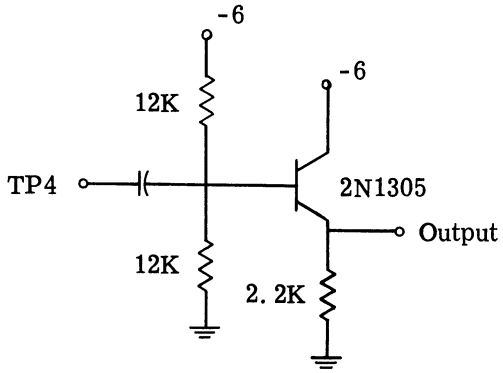


Buffer amplifier for reference pulses

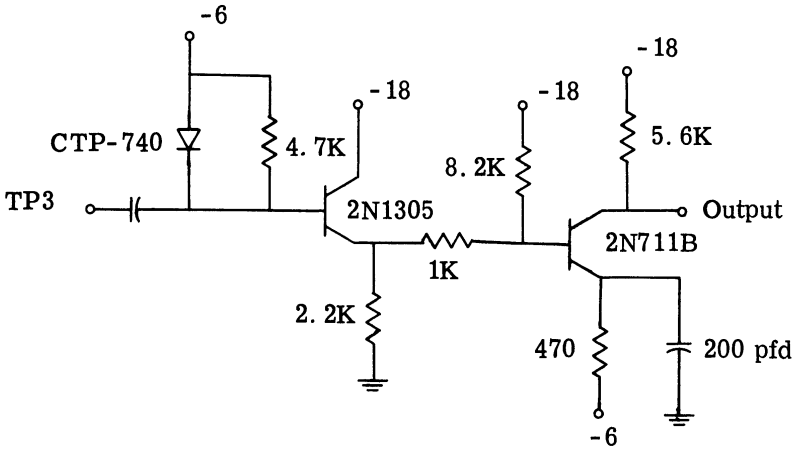


Buffer amplifier for multivibrator waveform

Fig. A. 3. Buffer amplifier for multivibrator waveform and reference pulses.

The Schmitt trigger circuits with internal inverter stage were Raytheon ST-23 digital logic cards. These were used to shape the signals from the buffer amplifier giving sharp rise time square pulses for the following NAND circuit, a Raytheon NA-2 logic card. The delay circuit was used to make the bit error pulses coincident in time with the timing pulses generated from the incoming video signal. The delay circuit was a Raytheon one-shot, OS-23, digital logic card which was fired off the trailing edge of the bit error pulse forming the same polarity of pulse with a width that was adjustable by external capacitors. The 0 to -6 volt output pulses were directly connected into the input of a pulse standardizer.

A. 1. 2 Frame Counter.[1] This circuit is used to subdivide the basic 288-kc clock of the tropo system to derive clock pulses at the frame rates of either 41. 142, 20. 571, or 10. 285 kc. These frequencies correspond to frame sizes of 56, 28, and 14 bits per frame. One output of this circuit, the 41, 142-kc clock, is always used to clock the A-D tape unit. This output and the other outputs, depending on the frame size being used, are used to reset the bit error counter and to transfer the data from the bit error counter to the flip-flop buffer at the end of each frame. This circuit was built from Harvey-Wells Digital Data Blocs. These blocs are versatile front, patch-wired units. The wiring diagram of the frame counter (Fig. A. 4) indicates the wiring of the Harvey-Wells packages. The digital logic requires 0 or -4 volt input and gives a 0 or -4 volt output. A logical "one" is 0 volts and a logical "zero" is -4 volts. This frame counter circuit is composed of a four-stage binary counter package (of which only 3 stages are used), and a two-stage binary counter built from flip-flops. By some associated digital logic, the three-stage binary counter can be used as a divide-by-seven circuit. The first stage of the two-stage binary counter can be a divide-by-two circuit, and the output of the second stage of the counter can be a divide-by-four circuit with respect to the input clock of the binary counter. Thus, beginning with the 288-kc clock frequency from the tropo terminal equipment, the output of the divide-by-seven circuit is 288/7 or 41. 142 kc, the output of the first stage of the binary countdown circuit is 41. 142/2 or 20. 571 kc and the output of the second stage of the binary countdown circuit is 20. 571/2 or 10. 285 kc.

The divide-by-seven circuit uses a NAND circuit, an inverter, and two gated pulse amplifiers in addition to the four-stage binary counter previously mentioned. The counter unit can be reset at any time to an all zero state by applying a pulse to a reset terminal. The counter changes state with the application of a pulse to the input terminal. The input to this circuit is the 288-kc pulse train. This pulse train is fed into two different gated pulse amplifiers. The output of one pulse amplifier which goes to the counter reset terminal is also the divide-by-seven pulse output. The output of the other pulse amplifier goes to the counter input terminal. At any one time, pulses will be present at only one pulse amplifier output because of the NAND and inverter logic used for the gating levels. It is easiest to explain the

[1]The frame counter used before was a 3-stage shift register. This was improved by using a binary counter circuit described here. The basic counting idea is still the same as in Appendix A of Ref. 13.

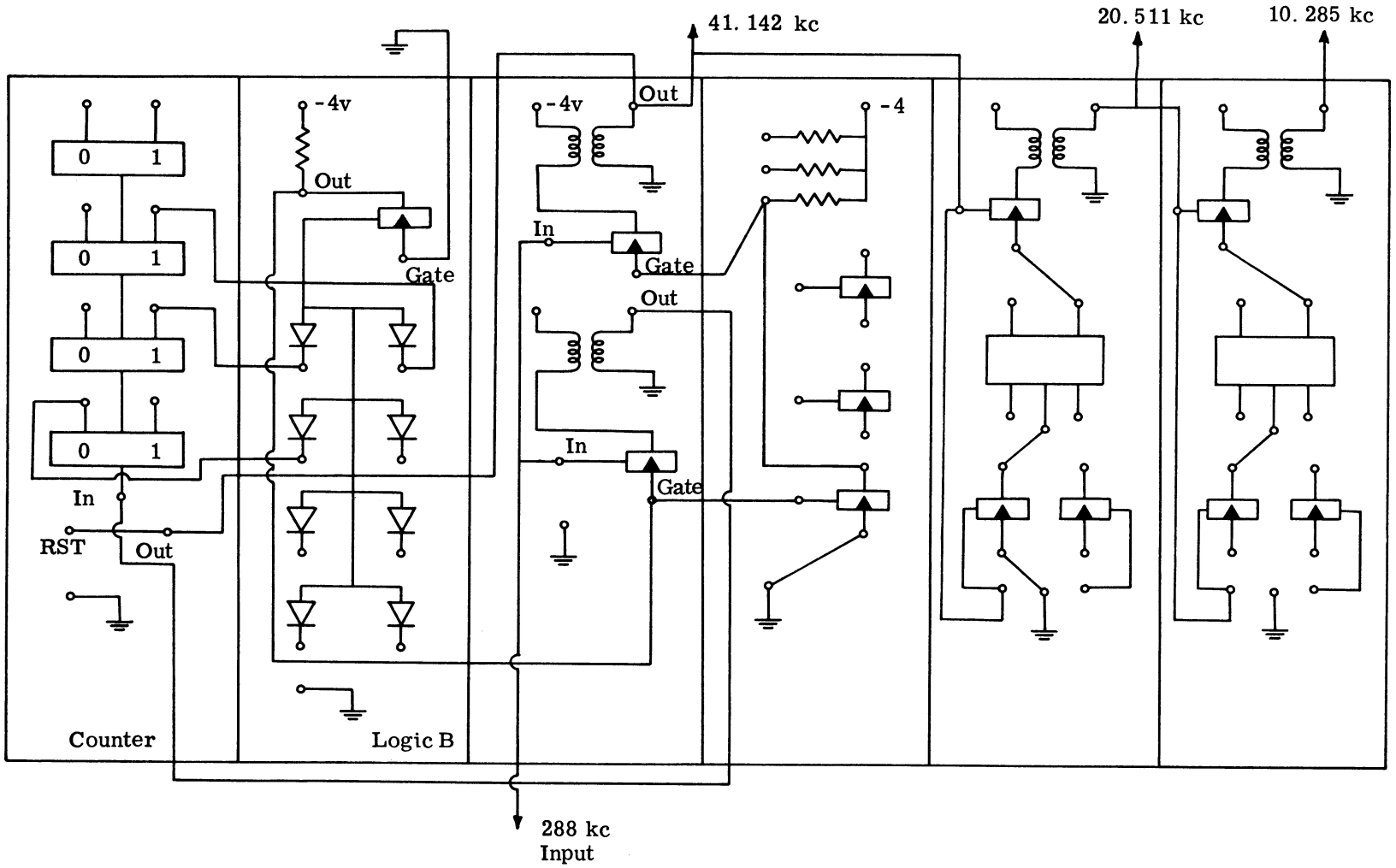


Fig. A. 4. Wiring diagram of frame counter.

operation of this circuit by assuming the counter to be in the binary zero state. In this state, the gating levels allow the next pulse from the 288-kc pulse train to pass through the pulse amplifier to the input of the counter advancing the counter to the binary-one state. This action is repeated until the counter is in the binary-six state. The NAND circuit recognizes this state by changing voltage level which in turn changes the gating levels. The next pulse from the 288-kc pulse train is steered to the reset terminal, resetting the counter to the zero state. With this type of operation, one out of every seven pulses from the 288-kc pulse train is used to reset the binary counter and thus provides the 288/7 = 41. 142-kc pulse train. This 41. 142-kc pulse train is then used as the input clock to the two-stage binary counter circuit. This operation of a binary counter circuit of this type has previously been described in Section A. 1. 3. 2 of Ref. 13. The outputs of the two-stage binary counter are 20. 571 and 10. 285-kc pulse trains.

A. 1. 3 Analog Amplifiers. To help eliminate spurious 60-cycle noise on the analog signals, a special 60-cps notch filter was inserted before the input of each analog amplifier. Also, to help eliminate spurious 1500-cps noise, an RC filter was placed in the feedback path of the feedback amplifier. This produced a 6-db per octave roll-off characteristic. The combined filter characteristics are shown in Fig. A. 5.

An additional operational (Philbrick) amplifier was wired as a cathode follower buffer between the output of the D-A converter and the multiplexer. This, plus the use of twisted pair-wires instead of coaxial cable, reduced the capacitive and resistive load on the D-A converter. This allowed the D-A converter output voltage to change levels without a noticeable RC charge curve transition between levels. It increased the reliability that at the time of sampling the D-A output had reached a final, quiescent value and the proper number of errors per frame was recorded on the digital magnetic tape.

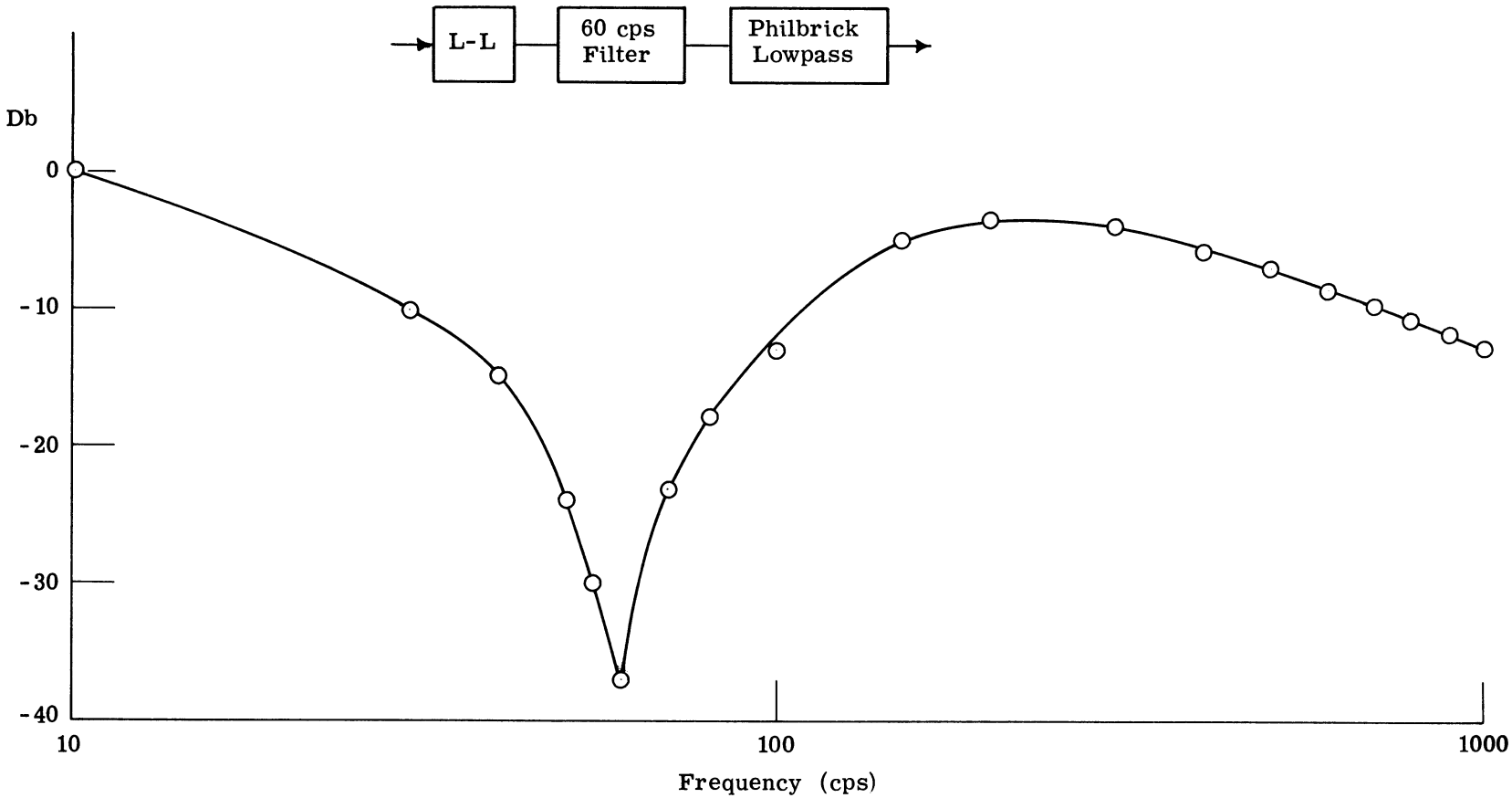


Fig. A. 5. Log-linear filter characteristics for November and February test series.

## APPENDIX B

## DESCRIPTION OF COMPUTER PROGRAMS FOR THE ANALYSIS OF TROPOSPHERIC SCATTER

E. P. Gould and A. M. Collins

The programs to be described have been written in two languages, MAD (Michigan Algorithm Decoder) and UMAP (University of Michigan Assembly Program), and have been processed on an IBM 7090 digital computer at The University of Michigan with the Michigan Executive System. Some subroutines used in the programs for printing and tape handling are unique to this system. MAD, a compiler language similar to FORTRAN, has been employed for all parts of programs which do not consume extensive computer time. UMAP (an adaptation of the Bell Telephone Laboratory assembly program) has been used where repetition makes optimal programming worth the additional cost in programming and debugging. Tape reading time is minimized by buffering, so that while one record is being unpacked and processed on tape, the next record is being read into core storage.

### B. 1 Computer Programs for Data Analysis

The analysis of tropo tapes has been divided into two parts: a general analysis program for all tapes, and then a level crossing program for tapes selected for further analysis from the results gained from the general analysis program. These two programs will be discussed separately in the next two sections.

B. 1. 1 Tropo Analysis Program. Two different computer programs have been written for analysis of the tropo tapes produced: one program for 2 channel tapes, and one program for either 4 or 5 channel tapes. As was discussed in Section 2. 2. 1, the 2-channel case multiplexed an error count with one signal level; the 4-channel case multiplexed both individual signal levels, either the AGC signal or the combined signal level, and the error count; and the 5-channel case multiplexed both individual channels, the combined channel, the AGC channel, and the error count.

In each case, there is a main program written in the MAD language which sets up storage; calls the subroutines to read, unpack, and store the data for each record; and finally, sets up and prints out the information. In addition, there are two UMAP subroutines. One subroutine reads in a 4001 word record from tape into core storage. The other unpacks the data and counts the occurrences of the various events needed to compute the distributions printed at the end of the main program.

Each input frame for a channel is in a six-bit mode. For the signal channels, the voltage level can be one of $2^6$ (or 64) different levels coded as 0-63 in the two programs. The error channel, the count of the number of samples in error in each frame, has a maximum of 28 for the 2-channel case, and 56 for the 4- and 5-channel case. In the programs the two signal channels are labeled A and B, the combined signal channel C, the error channel D, and the AGC channel E. In all cases, each computer word read in from tape contains 6 frames of 6 bits each (or 36 bits). The 2-channel case includes both D and A channels, and each word contains 3 frames arranged D-A|D-A|D-A. The 4-channel case has 3 frames packed into each 2 computer words as follows: either, 1) D-C-A-B|D-C, 2) A-B|D-C-A-B, or, 1) D-E-A-B|D-E, 2) A-B|D-E-A-B. The 5-channel case has two formats. For the November 1964 test series, the 5-channel case has 6 frames packed into each 4 computer words as follows: 1) D-C-A-B|D-E, 2) A-B|D-C-A-B, 3) D-E-A-B|D-C, 4) A-B|D-E-A-B. For the February 1965 test series, the 5-channel case has 6 frames packed into each 4 computer words as follows: 1) D-E-A-B|D-C, 2) A-B|D-E-A-B, 3) D-C-A-B|D-E, 4) A-B|D-E-A-B. In each record of data the multiplexer must start with the D channel as shown, for the programs assume this in unpacking each record of data.

B. 1. 1. 1 The UMAP Tape Reading Subroutine RDTAPE. RDTAPE is buffered tape routine which reads data records of 4001-words into the computer core. The first computer word in each record is treated as a record identification word resulting in 4000 data words being read at one time. The record length is based on space limitations in storage for the 5-channel case. The troposcatter tape has up to 600 records (the exact number to be processed is specified by input data) in one file, with a file mark at the beginning and two file marks at the end of the data file. The routine has the following two entries:

(1) SETRD sets initial addresses and reads the first record into the lower half of

the buffer. If two records in a row at the beginning of tape have parity errors, the program halts.

(2) RDTAPE initiates a read into the other half of the buffer after checking that the previous record has been read correctly. If an end-of-file or a parity error is found in the previous record, the next record is read over the record in error and the program waits until the new record is read in. If there are two end-of-files in succession, the program assumes it is at the end of tape and transfers to the print out read of the main program. The tape reading will also stop after a preset number of records (input data), if the record number specified is less than the total number of records on tape.

RDTAPE is a buffered routine which always reads one record ahead of the data record being processed. This buffered action reduces the tape processing time considerably.

B. 1. 1. 2 The UMAP Unpacking and Processing Subroutine. While RDTAPE reads into one-half of the buffer another UMAP routine unpacks and processes the data in the other half. Separate routines are used for the 2 channel (STORE) and 4 and 5 channel tapes. Two routines exist for the 4 and 5 channel tape: one routine, STOR-4, is used for the TPN data series; and STOR-1 is used for the TPA, F, J series. These routines all work in a similar fashion with only slight differences because of the different data formats and the statistics needed. A special difference exists in the STOR-4 routine. To eliminate errors in recording, 4 errors were added to each error frame at the time of recording. These falacious 4 errors are subtracted out in the STOR-4 routine. STORE unpacks one frame at a time finding the values for D and A and then makes appropriate entries in tables, before handling the next frame. STOR-4 and STOR-1 unpack 4 computer words at a time and then make appropriate entries in tables before unpacking the next 4 computer words. The STOR-4 and STOR-1 programs are altered at running time to use either the 4 or 5 channel format by reading an input data card which specifies whether the tape being processed is a 4 or 5 channel tape.

A description of the tables prepared for each case follows. Most of the following tables are constructed by increasing a counter for each frame that has a particular value in some channel(s). Hence, a linear or two-dimensional array is formed for the entire tape, with each entry containing the count of the number of frames with that value. Some tables, however, are based on runs of frames. These tables are carried over from record to record, even though some frames are lost during record gaps in preparing the tapes. The data

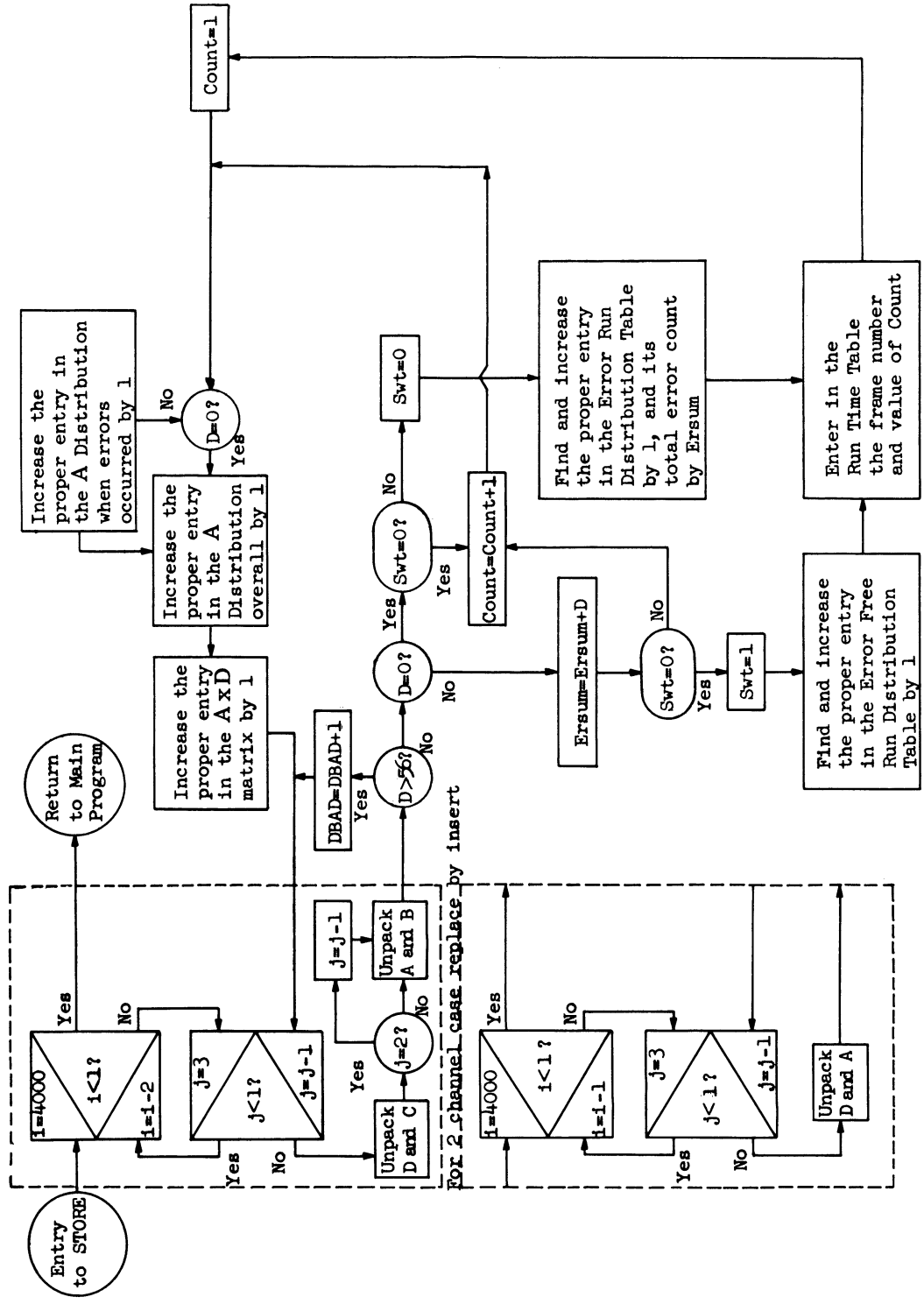


Fig. B. 1. STORE routine for the 2- and 4-channel cases.

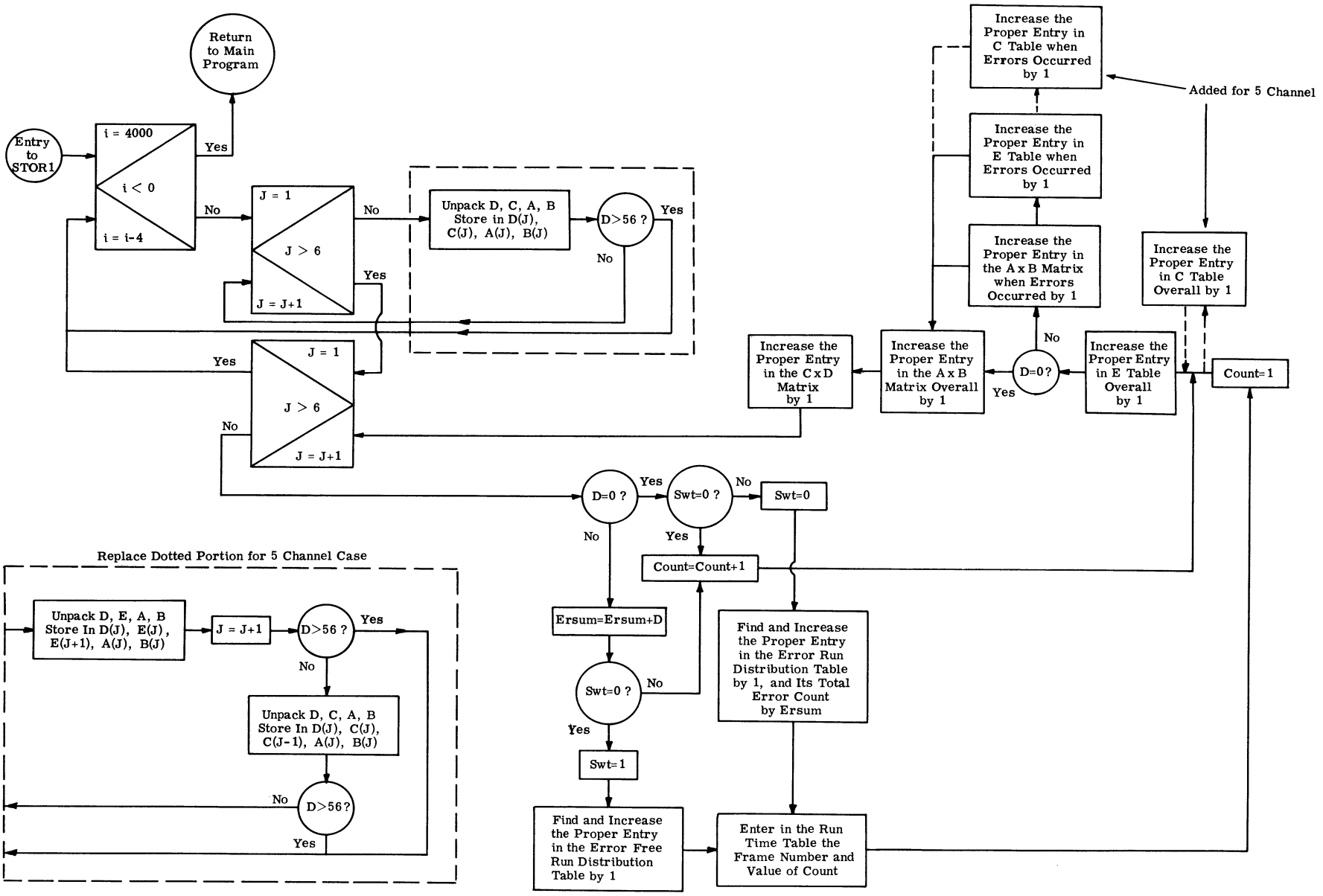


Fig. B. 2. STOR1 routine for the 4 and 5 channel case.
Four channel for AGC signal as fourth channel.

are treated as though the first frame after the record gap actually occurred adjacent to the last frame of the previous record. Figure B. 1 shows the STORE routine for the 2-channel case. Figure B. 2 shows the STOR-4 and STOR-1 routine for the 4 and 5 channel cases.

B. 1. 1. 2. 1 Two Channel Tables.

(1) A distribution of the total number of frames in each entry of an A x D matrix (signal level vs. number of errors).

(2) A run-time table is formed listing in order each error run and each error-free run and its length. For example, two frames in a row without an error are called an error-free run of length 2. This table has limited storage and is compiled only until that storage is exhausted.

(3) Distributions of the total number of error-free runs and error runs of different lengths during the entire tape. For this table, the lengths of runs are grouped to show, for example, the total number of runs between 20 and 50 frames in length (the size of the length groupings is approximately logarithmic).

(4) Distributions of the total number of frames with each signal level (A), both when errors occurred and overall.

B. 1. 1. 2. 2 Four Channel Tables.

(1) As in the 2-channel case, but the entries are in either a C x D matrix (combined signal vs. number of errors) or an E x D matrix (AGC vs. number of errors) depending on which signal has been used on the tape.

(2) and (3) As in the 2-channel case.

(4) As in the 2-channel case, but for either the combined signal (C) or AGC signal (E).

(5) Distribution of the total number of frames in each entry of an A x B matrix both when errors occurred and overall.

B. 1. 1. 2. 3 Five Channel Tables.

(1) A distribution of the total number of frames in each entry of an E x D matrix (signal level vs. number of errors).

(2) and (3) As in 2-channel case.

(4) As in the 2-channel case but for both the combined Signal C and AGC signal E.

(5) As in the 4-channel case.

B. 1. 1. 3 The Main Program. There are two versions of the main program: one for the 2 channel tapes and one for the 4- and 5-channel tapes. The differences exist because of the different tables computed for the different tapes. The main program (Fig. B. 3) contains a short loop that reads in and processes each record individually. This loop contains the calls to RDTAPE and one of the three STORE routines. All the records are processed before any printing is started. When the loop is completed, the main program terminates the final error and error-free runs in the run table of (2) and (3) described in Section B. 1. 1. 2. 1. The remainder of the program for the 2-channel and 4- and 5-channel cases consists of setting up and printing the following:

(1) Error Statistics

a) Overall probability of a bit error and frame error.

b) Distribution of probability of bit errors and frame errors vs. signal level. Channel A for 2-channel, either combiner or AGC for 4-channel, and AGC for 5-channel.

c) Distribution of length of error runs and error-free runs.

d) Distribution of time spent in error runs.

e) Run time table (described in Section B. 1. 1. 2. 1, part (2).

f) Distribution of average number of errors per frame vs. frame size.

(2) Signal Statistics

a) Mean variance and standard deviation of signal levels both when errors occurred and overall. Channel A for 2-channel; channels A, B either combined or AGC, and linear sum of A and B for 4-channel; channel A, B, AGC, combined and linear sum of channels A and B for 5-channel.

b) Distribution of signal levels both when errors occurred and overall. These tables correspond to statistics of part a).

c) Distribution of channel A vs. channel B when errors occurred.

As noted, the voltage levels received have been compressed into 64 levels for digital analysis.

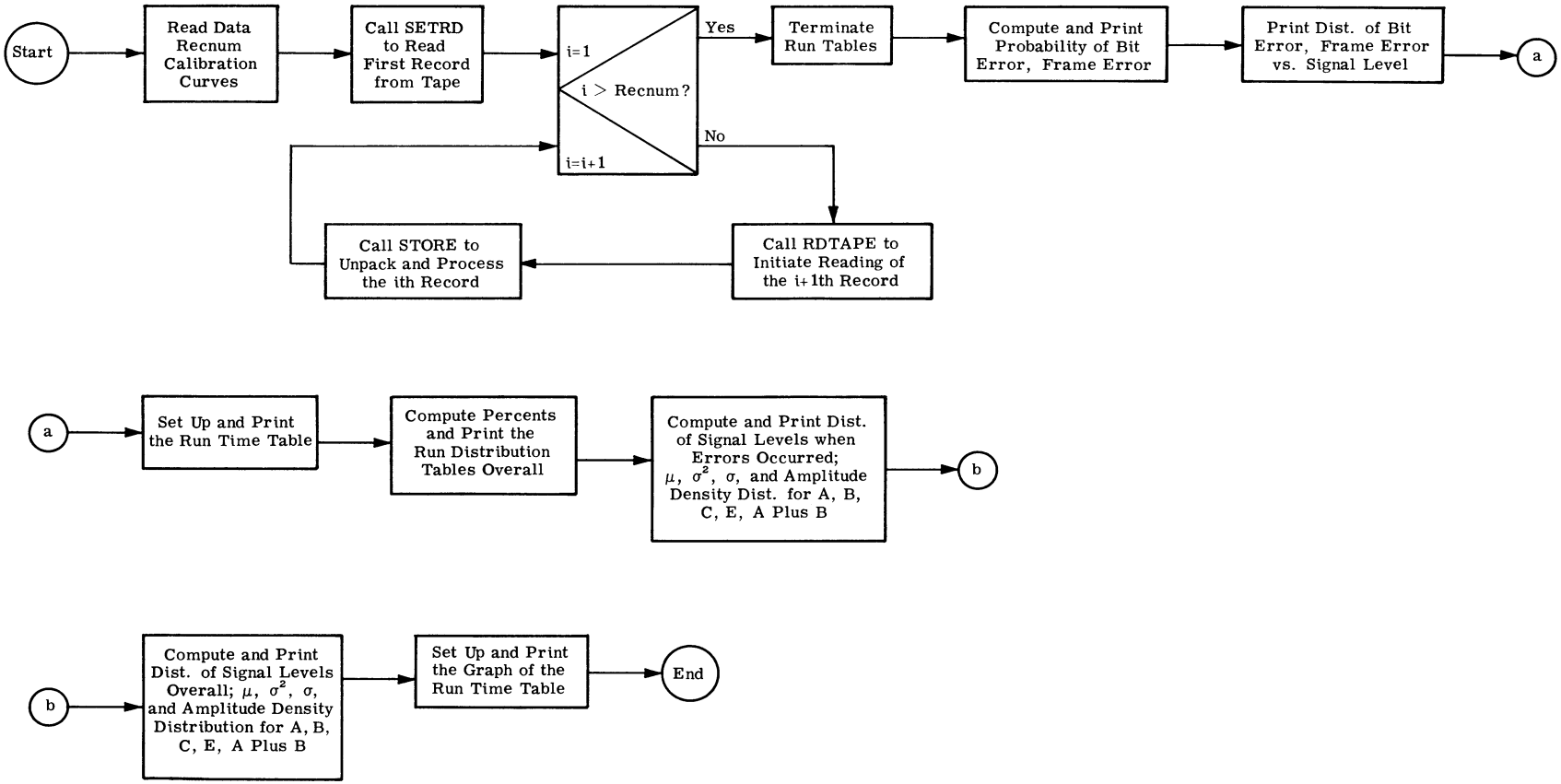


Fig. B. 3. Flow chart of 5-channel main program.

For the signal statistics, means, variance, and standard deviations are determined in db units as well as in the compressed levels. Db units are obtained by reading in calibration curves as input data to the program. The calibration curves are derived from calibration data taken at the same time the data are recorded.

B. 1. 2 Level Crossing Analysis Program. The level crossing analysis program is used to calculate a family of curves denoting the cumulative probability of the signal fades below a predetermined arbitrary signal level for a time greater than or equal to $t_o$ (Fig. B. 4). The strength of the signal in db below the signal mean is used as the parameter of the curves.

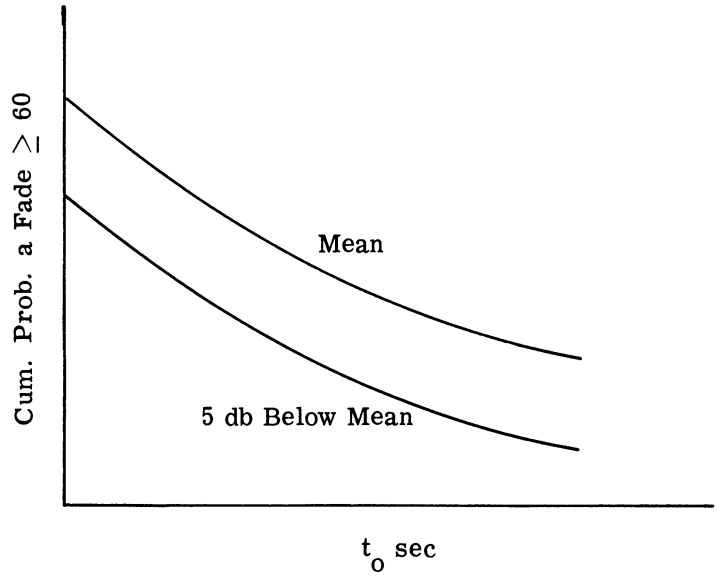


Fig. B. 4. Output of level crossing program.

Level crossing curves can be calculated for channel A and B, the AGC, combiner, and the linear sum of the A and B signals. The program can be used to calculate a variable number of curves for each channel. The individual fade lengths are determined and then grouped into standardized fade lengths for easier data processing.

Inputs needed by the program are:

(1) The number of records to be read on the input tape.

(2) The values of the vector which contain the time quantization levels into which the fade data are to be quantized.

(3) The number of quantization slots minus one.

(4) The values of the various thresholds in computer levels from 1 to 63.

(5) The values of the thresholds in db below the mean as a decimal number.

(6) The calibration tables for channel A and channel B from computer levels to dbm. These are the same tables as were used in the main tropo analysis program.

Outputs of the program are:

(1) The input calibration curves of channel A and channel B, that are being used for the particular tape being run, are printed out.

(2) The number of tape records read and the number of bad records, if any, are printed out.

(3) The results of the fade program are read out with the following results given:

a) The threshold value in computer level used in the fade program.

b) The threshold value in db below the mean used in the fade program.

c) The total number of fades at this threshold level.

d) A table giving the number of fades and the cumulative probability of a fade length greater than or equal to the quantization fade lengths used.

There is an output of (3) for each fade curve being calculated.

The program has three main parts: a main program called MLEVC written in the MAD language, and two subroutines written in UMAP. One subroutine called RDTAPE reads the binary input tape into the computer core, while the second subroutine called LEVCRX determines the fade curves. The subroutine RDTAPE is the same binary tape reading routine used for the main tropo analysis program. A write-up of the operation of this routine was given in Section B. 1. 1.

Both the main program and the subroutine LEVCRX are organized in such a way that changes in the total number of fade curves and the particular signals used in calculating the fade curve can easily be changed. This is accomplished in the main program by having the printout organized as an internal function so that the only change needed to add or subtract a fade curve is to add or delete a call for the internal function. The subroutine LEVCRX uses several macros. The only change needed to add or subtract a fade curve is to add or delete a call for the fade macro. Since the number of quantization levels and their values are

read in as input data, it is easy to change the quantization levels used. The present program is written only for 5-channel tropo tapes. Because of the special format used on the 5-channel TPN tapes, a special UMAP routine LVXTPN must be used in place of LEVCRX. Only three statements differ between the two programs.

B. 1. 2. 1 The Main Program. The main program written in MAD is used for eight distinct functions. These are:

(1) to set up storage locations for the tables needed by the program.

(2) to read in the input data.

(3) to calculate a table used to calculate the linear sum of channel A and channel B.

(4) to call the test program which can be called if a test of the program is desired.

(5) to zero out all the tables that are used.

(6) to call the UMAP subroutines.

(7) to calculate the total number of fades and the cumulative probability of a fade.

(8) to print out the results.

In this program, the vast majority of the variables are stored in common to facilitate the use of the data by both the main program and the UMAP subroutine. A block diagram of the main program is shown in Fig. B. 5. The programming used to calculate a table for the linear sum of channel A and channel B is of enough importance to warrant more detailed discussion.

Linear Sum of A and B

To keep the fade routines of LEVCRX the same for all data channels, it is necessary to convert the linear sum of channels A and B in dbm to one of 64 integers ranging from 0 to 63. The method used for doing this is the following: First, a table is set up where in a

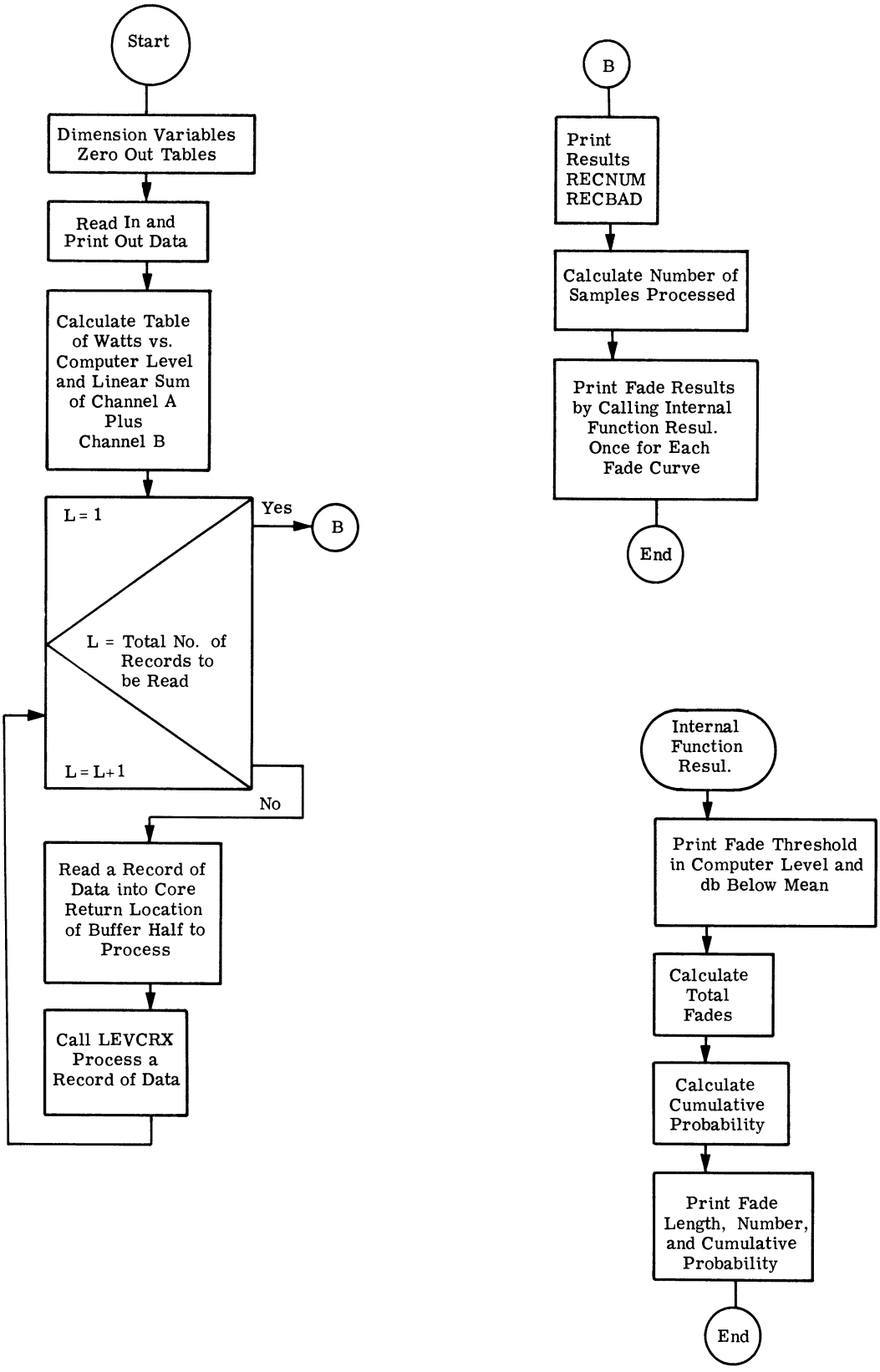


Fig. B. 5. Block diagram of main program.

vector ARCOMF of 64 locations ranging from 0 to 63 is stored a table of values of dbm ranging downward in 1 dbm steps from 57 in location ARCOMF(63) to 120 in ARCOMF(0), that is,

$$\begin{aligned} \text{ARCOMF}\ (63) &= 57 \\ \text{ARCOMF}\ (62) &= 58 \\ &\vdots \\ \text{ARCOMF}\ (1) &= 119 \\ \text{ARCOMF}\ (0) &= 120 \end{aligned}$$

The values of dbm are absolute values since we are actually concerned with minus dbms in the true experiment. The computer program considers all signals as being positive dbm for convenience. Second, a table (WVCOM) of values of the linear sum of channels A and B is prepared. This table is a matrix 64 x 64 corresponding to all combinations of the 64 possible values of channel A and the 64 values of channel B. This table is a floating point table and the values of the linear sum are decimal numbers not necessarily integers. This table of numbers is now quantized to integers lying between 57 and 120 by comparing the values of the WVCOM table with the vector ARCOMF. Instead of storing the integer quantized number, however, the location of the quantized number in the ARDOMF vector (which ranges from 0 to 63) is stored in IWVCOM (an integer table stored in the same location as WVCOM). The result of this sequence of programming is a matrix 64 x 64 which contains numbers ranging from 0 to 63 which have a one-to-one correspondence to the values of the linear sum of channels A and B to the nearest dbm. Each time a sample pair of values of channel A and channel B is encountered the IWVCOM table is consulted to bring back a number from 0 to 63 which corresponds directly with the dbm value of the linear sum of channel A plus channel B.

B. 1. 2. 2 Subroutine LEVCRX. This UMAP subroutine has three functions:

1) Unpacking the experimental multiplexed data.

2) Using the computer levels of channels A and B, calculating a number used by the matrix IWVCOM to find the effective value of the linear sum of channels A and B.

3) Calculating the fade tables.

The subroutine uses 5 macros which are called many times to generate the majority of the program. Because of this organization into macros, it is relatively easy to make changes

in the program. In this program, the value of the number of errors in a frame is not needed, so in unpacking this channel it is discarded. A block diagram of the subroutine LEVCRX is shown in Fig. B. 6. This subroutine has been designed with efficiency of operation as a primary concern rather than efficiency of storage locations to reduce the running time to a minimum.

The entire sequence of instructions used to calculate whether a signal is in a fade; and if so, of what duration is the fade if contained in the macro FADE which is called with different arguments depending on the signal being processed. The sample under consideration is compared with the threshold being used. If the signal is in a fade, a counter is updated by one. If the signal is not in a fade, a check is made to see whether this sample denotes the end of a fade. If this sample is the end of a fade, a routine is entered to store the length of the fade in the proper fade table location. If the sample is just one of many samples above the fade threshold, an exit is made from the routine. If for some reason a fade length is large enough to exceed the maximum size of the fade table, the length of the fade is printed out on-line. It is very unlikely that any on-line printouts will occur since the final entry in the fade table was made extremely large to avoid on-line printouts.

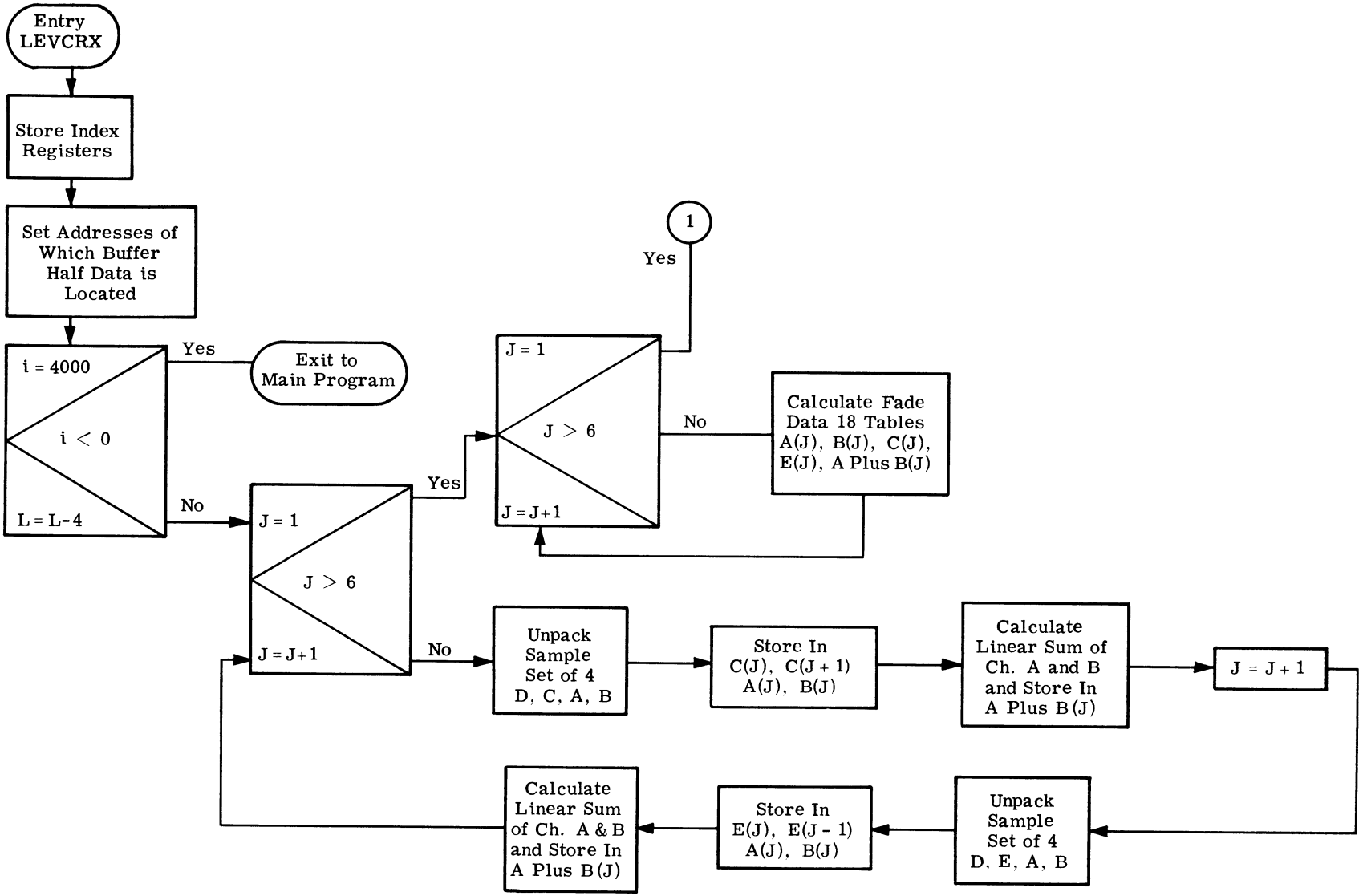


Fig. B. 6. Block diagram of subroutine LEVCRX.

## APPENDIX C

## CUMULATIVE FADE CURVES FOR A + B SIGNAL

The curves, C. 1 through C. 5 depict the "fraction of time in fade for a time greater than the abscissa value" for the linear sum signal A + B. As described in Section 3. 2. 3, this signal was formed during the computer analysis to permit comparison to the actual diversity achieved by the system.

These curves may be compared, respectively, to those in Figs. 6. 1 through 6. 5.

To be consistent with the levels on Figs. 6. 1 through 6. 5 the levels here are expressed in terms of "single channel." To accomplish this, 3 db was subtracted from the experimentally found values of each level of A + B. Thus if the actual level of A + B read 80. 2 dbm, this is equivalent to 83. 2 dbm on a single channel basis.

Comparison of the figures here to those of Figs. 6. 1 through 6. 5 shows that the corresponding fade levels are grossly comparable, using the technique described in Section 5. 5 for estimating the fade levels.

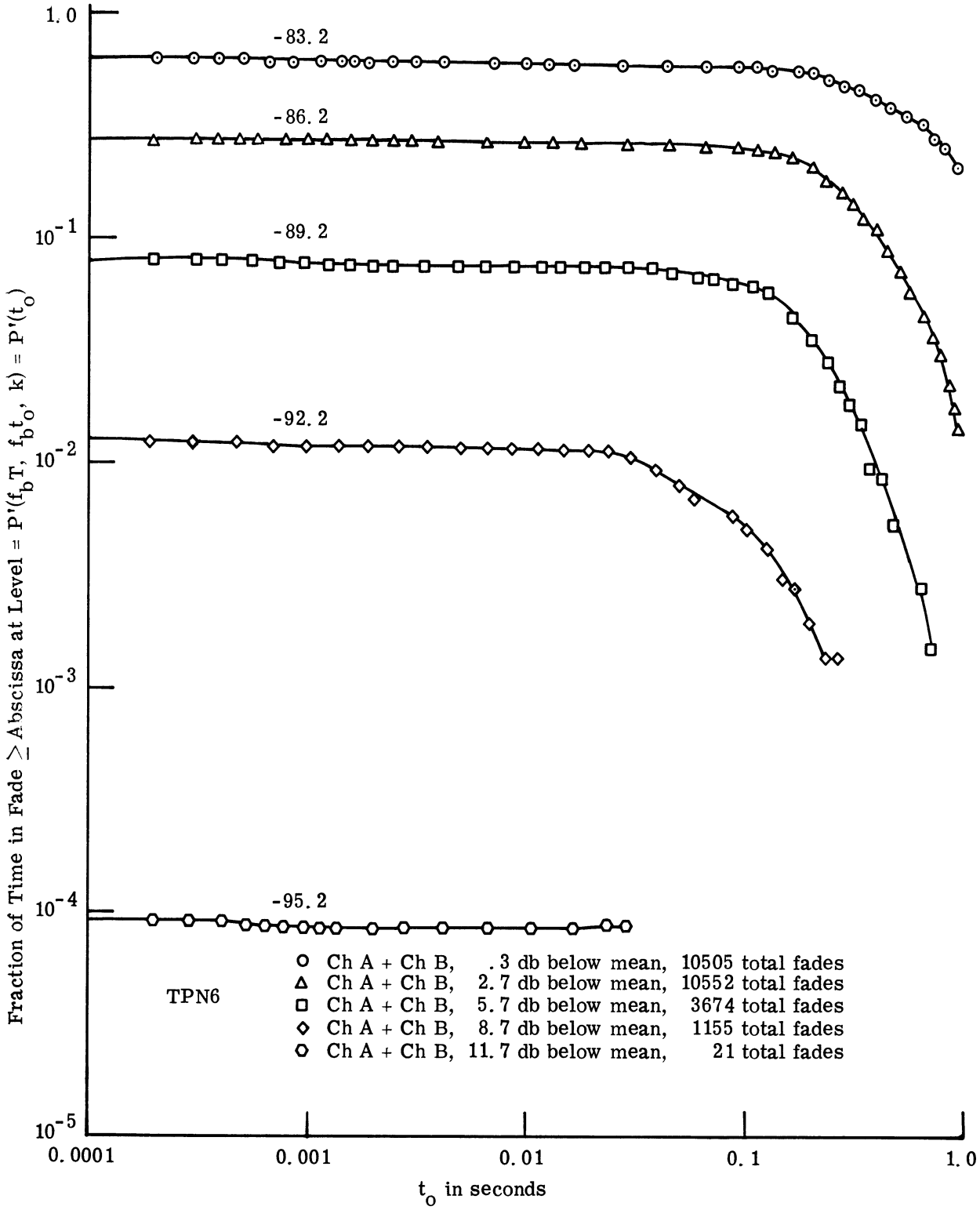


Fig. C. 1. Probability of one or more fades of length greater than or equal to the abscissa, during a period (T) of 6 minutes, for TPN6.

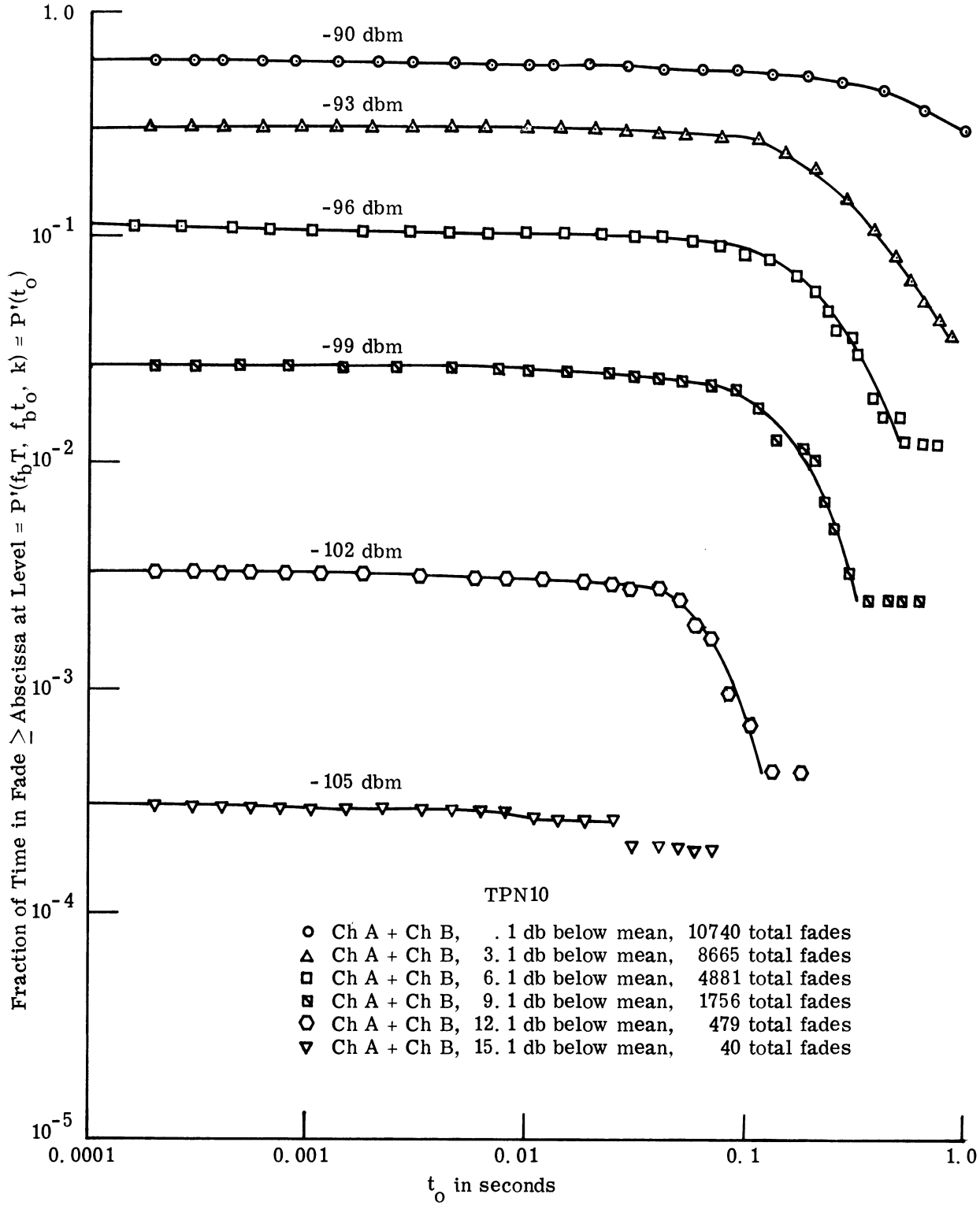


Fig. C. 2. Probability of one or more fades of length greater than or equal to the abscissa, during a 6 minute period for TPN10.

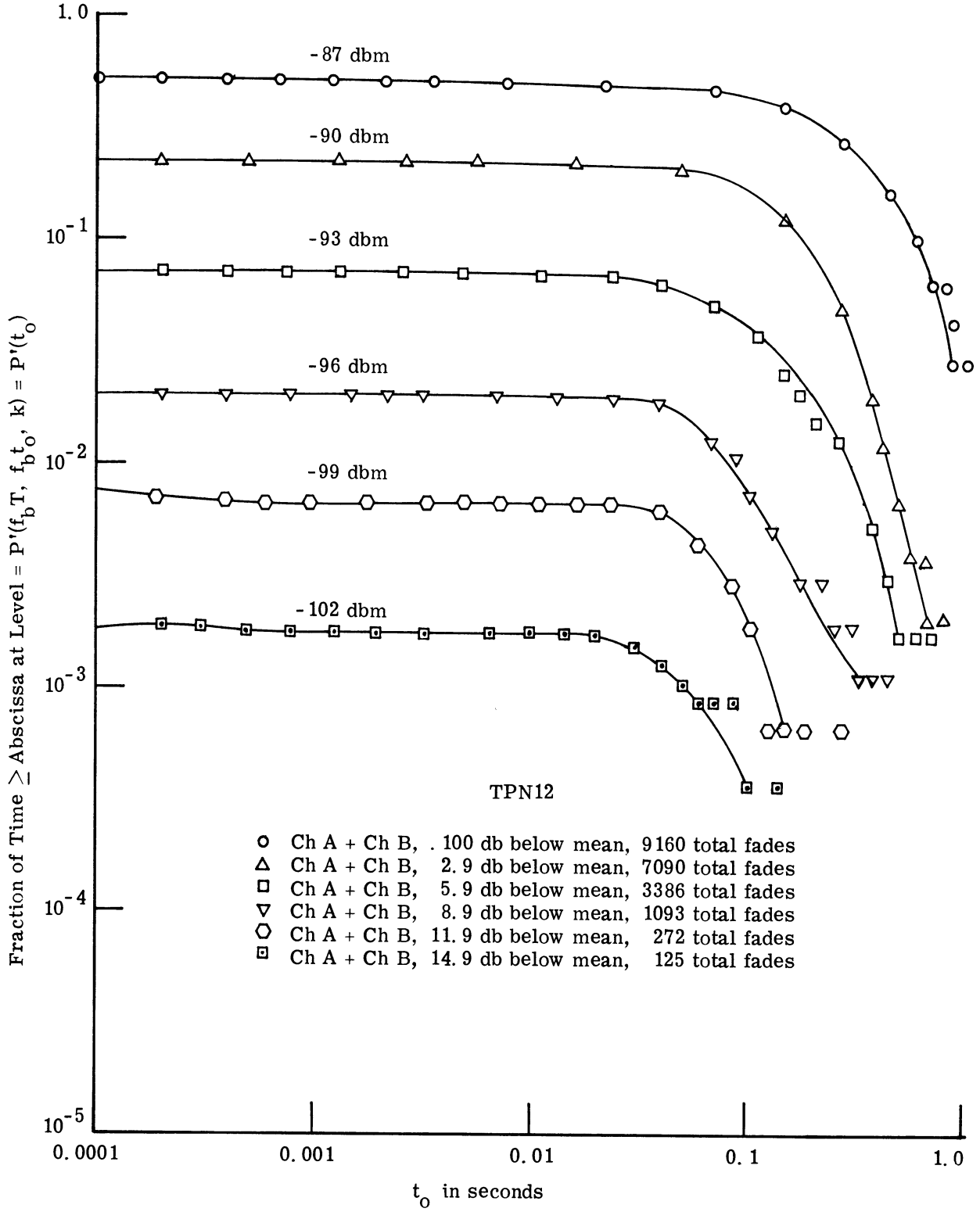


Fig. C. 3. Probability of one or more fades of length greater than or equal to the abscissa, during a 6 minute period for TPN12.

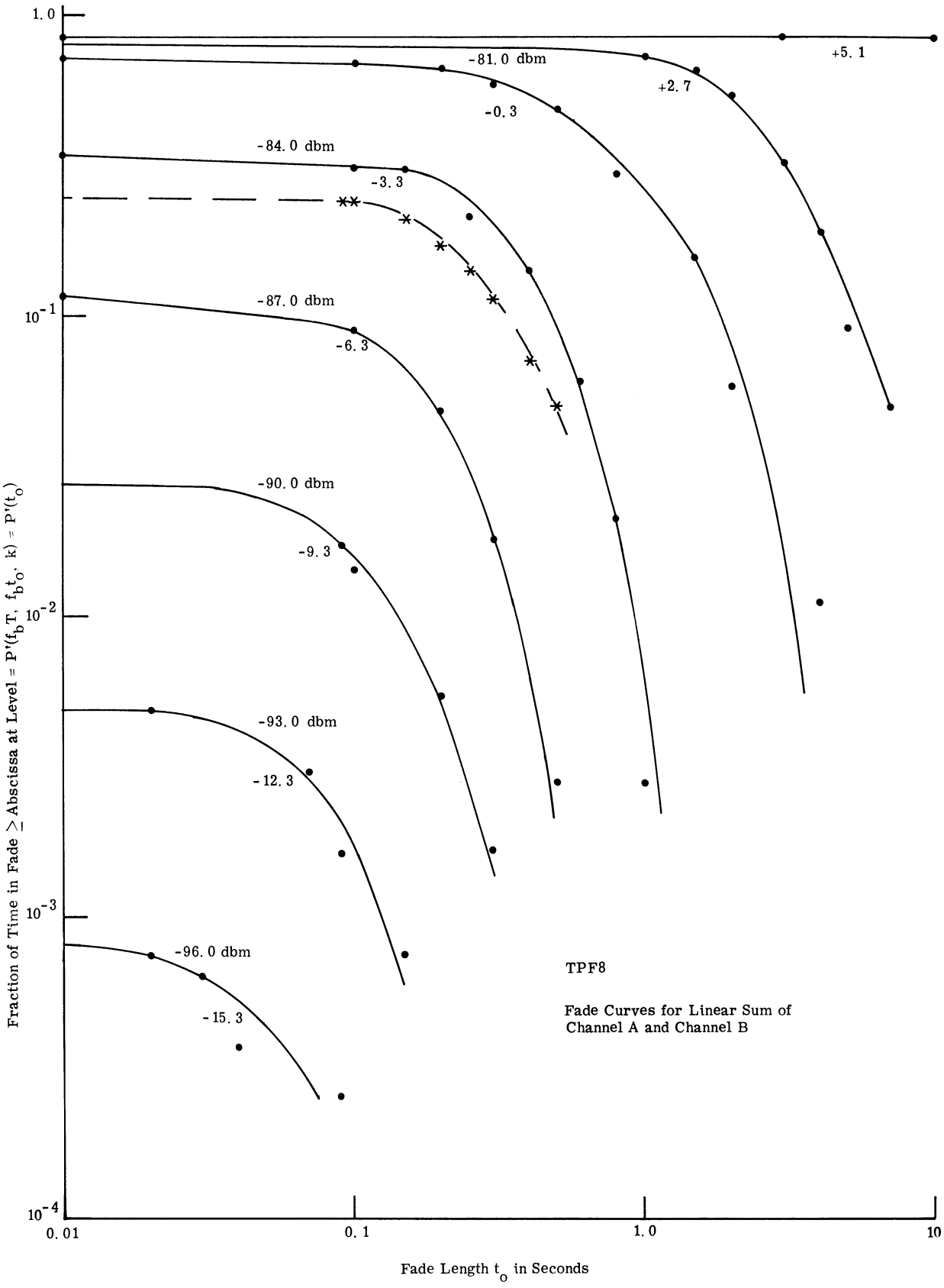


Fig. C. 4. Probability of one or more fades of length greater than or equal to the abscissa, during a 6 minute period, for TPF8.

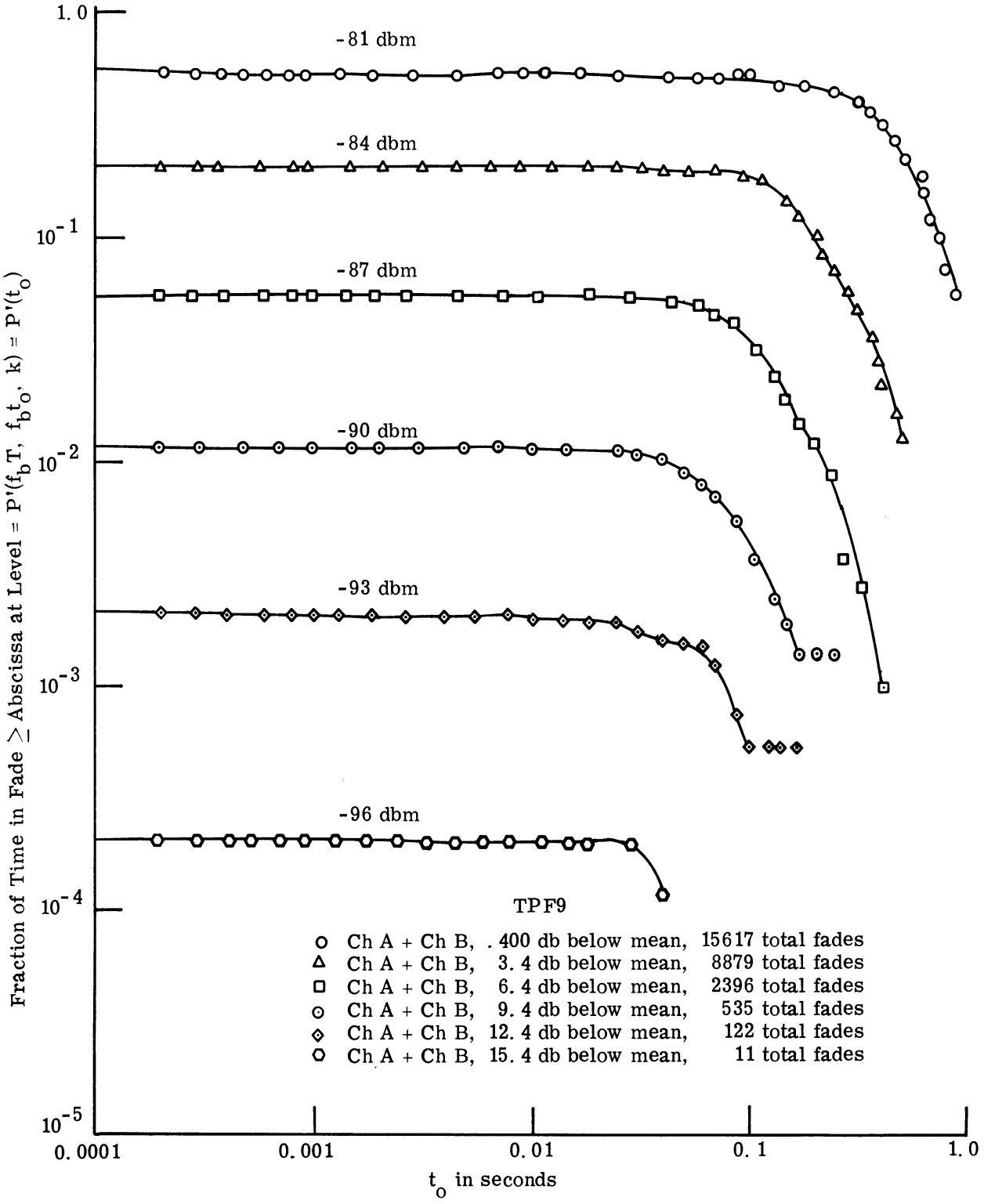


Fig. C. 5. Probability of one or more fades of length greater than or equal to the abscissa, during a 6 minute interval for TPF9.

## REFERENCES


1. Joint Technical Advisory Committee Report II, "Long Range Tropospheric Transmission," Proc. IRE, Vol. 48, January 1960, pp. 30-44.

2. M. P. Ristenbatt and K. A. Haines, Digital Communication Studies, Cooley Electronics Laboratory Technical Report No. 143, The University of Michigan, Ann Arbor, Michigan, August 1963.

3. Ground Telecommunication Performance Standards, Tropospheric Systems, National Bureau of Standards Report 6767, June 15, 1961.

4. A. B. Crawford, et al., "Studies in Troposcpheric Propagation beyond the Horizon," Bell Systems Technical Journal, Vol. 38, No. 5, September 1959, p. 1067.

5. E. D. Sunde, "Digital Troposcatter Transmission and Modulation Theory," Bell Systems Technical Journal, Vol. 43, No. 1, January 1964, p. 143.

6. Private communication with I. Kullback of Radio Relay Branch, Communications Dept., USAEL.

7. A. Tepfer, PCM Troposcatter Error Instrumentation System, RCA Report No. CR-61-419-11, New York 13, New York, April 28, 1961.

8. Tropospheric Scatter, Principles and Applications, Collins Radio Company, Task Report No. 45-56-0024, Fort Huachuca, Arizona, March 1960.

9. R. R. Favreau, et al., "Evaluation of Complex Statistical Functions by an Analog Computer," IRE National Convention Record, Computers, 1956, pp. 31-37.

10. S. W. Rice, "Distribution of the Duration of Fades in Radio Transmission: Gaussian Noise Model," Bell Systems Technical Journal, Vol. 37, No. 3, May 1958, pp. 581-635.

11. W. B. Davenport, Jr. and W. L. Root, Random Signals and Noise, McGraw-Hill, New York, 1958.

12. J. S. Bendat, Principles and Applications of Random Noise Theory, John Wiley and Sons, New York, 1958.

13. M. P. Ristenbatt and E. P. Gould, Experimental Signal and Error Data from Troposcatter Digital Communication Link, Cooley Electronics Laboratory Technical Report No. 157, The University of Michigan, Ann Arbor, Michigan, November 1964.

14. Data from Radio Relay Branch of USAEL, called "Simulated PCM Bit Error Rate," (private letter), 1963.

15. P. A. Bello and D. B. Nelin, "The Effect of Frequency Selective Fading on the Binary Error Probability of Incoherent and Differentially Coherent Matched Filter Receivers," IEEE Trans. on Communication Systems, Vol. CS-11, No. 2, June 1963, pp. 170-186.

16. J. A. Bradshaw, "Some Implications of Aircraft Interference Patterns in Troposcatter Reception," Journal of Research of the National Bureau of Standards--D. Radio Propagation, Vol. 67D, No. 4, July-August 1963, pp. 405-415.

DISTRIBUTION LIST

| | No. of Copies |
|---|---|
| Office of the Assistant Secretary of Defense<br>(Research and Engineering)<br>ATTN: Technical Library, Room 3E1065<br>Washington, D. C. 20301 | 1 |
| Chief of Research and Development<br>Department of the Army<br>Washington, D. C. 20315 | 1 |
| Commanding General<br>U. S. Army Materiel Command<br>ATTN: R and D Directorate<br>Washington 25, D. C. | 1 |
| Commanding General<br>U. S. Army Electronics Command<br>ATTN: AMSEL-AD<br>Fort Monmouth, New Jersey | 1 |
| Commander<br>Defense Documentation Center<br>Cameron Station<br>Alexandria, Virginia | 20 |
| Commanding General<br>USA Combat Developments Command<br>ATTN: CDCMR-E<br>Fort Belvoir, Virginia 22060 | 1 |
| Deputy Commander<br>U. S. Army Combat Developments Command<br>Communications-Electronics Agency<br>Fort Huachuca, Arizona 85613 | 1 |
| Commanding General<br>U. S. Army Electronics Proving Ground<br>ATTN: Technical Library<br>Fort Huachuca, Arizona 85613 | 1 |
| Chief<br>U. S. Army Security Agency<br>ATTN: AC of S, G4 (Technical Library)<br>Arlington Hall Station<br>Arlington 12, Virginia | 1 |
| Deputy President<br>U. S. Army Security Agency Board<br>Arlington Hall Station<br>Arlington, Virginia 22207 | 1 |

DISTRIBUTION LIST (Cont.)

| | No. of Copies |
|---|---|
| Director, U. S. Naval Research Laboratory<br>ATTN: Code 2027<br>Washington, D. C. 20390 | 1 |
| Air Force Cambridge Research Laboratories<br>ATTN: CRXL-R<br>L. G. Hanscom Field<br>Bedford, Massachusetts | 1 |
| Director<br>U. S. Navy Electronics Laboratory<br>ATTN: Library<br>San Diego, California 92101 | 1 |
| Rome Air Development Center<br>ATTN: EMLAL-1<br>Griffiss Air Force Base, New York 13442 | 1 |
| U. S. National Bureau of Standards<br>Boulder Laboratories<br>ATTN: Library<br>Boulder, Colorado | 1 |
| AFSC Scientific/Technical Liaison Office<br>U. S. Army Electronic Laboratories<br>ATTN: AMSEL-RD-LNA<br>Fort Monmouth, New Jersey | 1 |
| Commanding Officer<br>U. S. Army Electronics Laboratories<br>ATTN: Logistics Division (Mr. A. Boniello, AMSEL-NL-E-1)<br>Fort Monmouth, New Jersey | 10 |
| Commanding Officer<br>U. S. Army Electronics Laboratories<br>ATTN: Director of Engineering<br>Fort Monmouth, New Jersey | 1 |
| Commanding Officer<br>U. S. Army Electronics Laboratories<br>ATTN: AMSEL-NL-R-2<br>NL-R-5<br>NL-R-4<br>NL-A-1<br>NL-P-3<br>NL-S<br>Fort Monmouth, New Jersey | 1<br>1<br>1<br>1<br>1<br>1 |
| Commanding Officer<br>U. S. Army Electronics Laboratories<br>ATTN: Technical Documents Center<br>Fort Monmouth, New Jersey | 1 |

DISTRIBUTION LIST (Cont.)

| | No. of Copies |
|---|---|
| Director, National Security Agency<br>ATTN: R12 (M. Klein)<br>Fort George Meade, Maryland | 1 |
| Commanding General<br>U. S. Army Electronics Command<br>ATTN: AMSEL-I0-T<br>Fort Monmouth, New Jersey 07703 | 1 |
| Dr. T. W. Butler, Jr., Director<br>Cooley Electronics Laboratory<br>The University of Michigan<br>Ann Arbor, Michigan | 1 |
| Cooley Electronics Laboratory<br>The University of Michigan<br>Ann Arbor, Michigan | 20 |

UNCL

Security Classification

**DOCUMENT CONTROL DATA - R&D**

*(Security classification of title, body of abstract and indexing annotation must be entered when the overall report is classified)*

1. ORIGINATING ACTIVITY *(Corporate author)*

University of Michigan, Cooley Electronics Laboratory, Ann Arbor, Michigan

2a. REPORT SECURITY CLASSIFICATION

UNCLASSIFIED

2b. GROUP

3. REPORT TITLE

Experimental Error and Signal Data from High Bit Rate Tactical Troposcatter Digital Communication Link

4. DESCRIPTIVE NOTES *(Type of report and inclusive dates)*

Final Report

5. AUTHOR(S) *(Last name, first name, initial)*

Ristenbatt, M. P.
Gould, E. P.

| 6. REPORT DATE | 7a. TOTAL NO. OF PAGES | 7b. NO. OF REFS |
|---|---|---|
| April 1966 | | 16 |

| 8a. CONTRACT OR GRANT NO. | 9a. ORIGINATOR'S REPORT NUMBER(S) |
|---|---|
| DA-36-039 sc-89168 | 4951-5-F |
| b. PROJECT NO. 4951 | |
| c. | 9b. OTHER REPORT NO(S) *(Any other numbers that may be assigned this report)* |
| d. | Technical Report No. 174 |

10. AVAILABILITY/LIMITATION NOTICES

Unlimited Distribution

| 11. SUPPLEMENTARY NOTES | 12. SPONSORING MILITARY ACTIVITY |
|---|---|
| | U. S. Army Electronics Command<br>Fort Monmouth, N. J. 07703 |

13. ABSTRACT

This report describes experimental error and signal data from a 100 mile troposcatter digital communication link at a bit rate of 576 kc. A repetitive one-zero pattern with binary FM was used at 4.8 kMc. Data were taken in each of the four seasons, recording 10 to 15 six-minute tapes per season.

The objective was a detailed computer analysis of error behavior, including analysis of instantaneous signal behavior so as to describe system conditions during errors. Five signals were sampled and multiplexed directly onto a digital tape: AGC, Combiner, Channel A, Channel B, and local Error Count.

From the equipment point of view, increases in tolerable fade length do not appear profitable until one exceeds 30 to 50 milliseconds. Further increases sharply reduce the probability of encountering such fades.

Finally, the results verified that there is little signal variation from season to season except varying median level.

In general, the data analyzed here permit determining the requirements for synchronization circuits of the fading link. In addition, the data here serve an indicator of what can be expected with 100 mile troposcatter links at a bit rate of 576 kc.

DD FORM 1 JAN 64 1473

UNCL

Security Classification

UNCLASSIFIED
Security Classification

| 14. KEY WORDS | LINK A | | LINK B | | LINK C | |
|---|---|---|---|---|---|---|
| | ROLE | WT | ROLE | WT | ROLE | WT |
| Communication Error Data<br>Computer Analysis<br>Digital Data<br>Digital Error Probabilities<br>Diversity Fade Behavior<br>Experimental Troposcatter Data<br>Fading Data<br>High Bit Rate Digital Data<br>Signal Level Distributions<br>Synchronization<br>Tactical Troposcatter Link | | | | | | |

## INSTRUCTIONS

1. ORIGINATING ACTIVITY: Enter the name and address of the contractor, subcontractor, grantee, Department of Defense activity or other organization *(corporate author)* issuing the report.

2*a*. REPORT SECURITY CLASSIFICATION: Enter the overall security classification of the report. Indicate whether "Restricted Data" is included. Marking is to be in accordance with appropriate security regulations.

2*b*. GROUP: Automatic downgrading is specified in DoD Directive 5200.10 and Armed Forces Industrial Manual. Enter the group number. Also, when applicable, show that optional markings have been used for Group 3 and Group 4 as authorized.

3. REPORT TITLE: Enter the complete report title in all capital letters. Titles in all cases should be unclassified. If a meaningful title cannot be selected without classification, show title classification in all capitals in parenthesis immediately following the title.

4. DESCRIPTIVE NOTES: If appropriate, enter the type of report, e.g., interim, progress, summary, annual, or final. Give the inclusive dates when a specific reporting period is covered.

5. AUTHOR(S): Enter the name(s) of author(s) as shown on or in the report. Enter last name, first name, middle initial. If military, show rank and branch of service. The name of the principal author is an absolute minimum requirement.

6. REPORT DATE: Enter the date of the report as day, month, year; or month, year. If more than one date appears on the report, use date of publication.

7*a*. TOTAL NUMBER OF PAGES: The total page count should follow normal pagination procedures, i.e., enter the number of pages containing information.

7*b*. NUMBER OF REFERENCES: Enter the total number of references cited in the report.

8*a*. CONTRACT OR GRANT NUMBER: If appropriate, enter the applicable number of the contract or grant under which the report was written.

8*b*, 8*c*, & 8*d*. PROJECT NUMBER: Enter the appropriate military department identification, such as project number, subproject number, system numbers, task number, etc.

9*a*. ORIGINATOR'S REPORT NUMBER(S): Enter the official report number by which the document will be identified and controlled by the originating activity. This number must be unique to this report.

9*b*. OTHER REPORT NUMBER(S): If the report has been assigned any other report numbers *(either by the originator or by the sponsor)*, also enter this number(s).

10. AVAILABILITY/LIMITATION NOTICES: Enter any limitations on further dissemination of the report, other than those imposed by security classification, using standard statements such as:

(1) "Qualified requesters may obtain copies of this report from DDC."

(2) "Foreign announcement and dissemination of this report by DDC is not authorized."

(3) "U. S. Government agencies may obtain copies of this report directly from DDC. Other qualified DDC users shall request through

_____."

(4) "U. S. military agencies may obtain copies of this report directly from DDC. Other qualified users shall request through

_____."

(5) "All distribution of this report is controlled. Qualified DDC users shall request through

_____."

If the report has been furnished to the Office of Technical Services, Department of Commerce, for sale to the public, indicate this fact and enter the price, if known.

11. SUPPLEMENTARY NOTES: Use for additional explanatory notes.

12. SPONSORING MILITARY ACTIVITY: Enter the name of the departmental project office or laboratory sponsoring *(paying for)* the research and development. Include address.

13. ABSTRACT: Enter an abstract giving a brief and factual summary of the document indicative of the report, even though it may also appear elsewhere in the body of the technical report. If additional space is required, a continuation sheet shall be attached.

It is highly desirable that the abstract of classified reports be unclassified. Each paragraph of the abstract shall end with an indication of the military security classification of the information in the paragraph, represented as *(TS)*, *(S)*, *(C)*, or *(U)*.

There is no limitation on the length of the abstract. However, the suggested length is from 150 to 225 words.

14. KEY WORDS: Key words are technically meaningful terms or short phrases that characterize a report and may be used as index entries for cataloging the report. Key words must be selected so that no security classification is required. Identifiers, such as equipment model designation, trade name, military project code name, geographic location, may be used as key words but will be followed by an indication of technical context. The assignment of links, rules, and weights is optional.

UNCLASSIFIED
Security Classification